BOSE-EINSTEIN CONDENSATES IN LOW DIMENSIONAL OPTICAL LATTICES: NOVEL QUANTUM PHASES AND NON-EQUILIBRIUM PHENOMENA

A Dissertation

Presented to the Faculty of the Graduate School

of Cornell University

in Partial Fulfillment of the Requirements for the Degree of

Doctor of Philosophy

by

Sayan Choudhury

August 2017

BOSE-EINSTEIN CONDENSATES IN LOW DIMENSIONAL OPTICAL LATTICES: NOVEL QUANTUM PHASES AND NON-EQUILIBRIUM PHENOMENA

Sayan Choudhury, Ph.D.

Cornell University 2017

Cold atoms trapped in optical lattices (crystals of light) provide a pristine platform for exploring quantum many body physics. Motivated by several recent experiments, this thesis examines the equilibrium and non-equilibrium dynamics of a Bose-Einstein condensate (BEC) loaded in a low dimensional optical lattice in order to realize novel quantum phases.

There are two main research directions in this thesis. The first one involves the possibility that exotic order spontaneously forms when two-component bosons are trapped in a honeycomb lattice. My studies on this theme is motivated by the observation of a "twisted superfluid" state in Prof. Klaus Sengstock's group at Hamburg (*Soltan-Panahi et al.*, Nat. Phys. 8, 71 (2012)). A twisted superfluid involves Bose-Einstein condensation into a state whose order parameter has a spatially varying phase. In chapter 3, I study the stability of a Bose-Einstein condensate towards forming a twisted superfluid within the framework of mean field theory. Despite a exhaustive numerical search I do not find a parameter regime with a twisted superfluid. This search involved all experimentally relevant parameter regimes and therefore mean field theory predicted that the experimentalists should not observe a twisted superfluid. I conclude that the experimental observations were either a manifestation of counter

superfluidity or due to interactions during time-of-flight. Subsequent experiments showed that the observations were an artifact of the measurement process.

The second research direction in this thesis is an exploration of the stability of periodically driven quantum systems (also known as Floquet systems). Floquet systems can be used to realize exotic non-equilibrium quantum phases which do not have a counterpart in static systems. However, the driving can cause these systems to heat up which presents a major obstacle to creating exotic states. To explore this issue in a concrete example, I model an experiment (Parker, Ha, and Chin, Nat. Phys. 9, 769 (2013)) where a Bose-Einstein condensate loaded in an optical lattice is subjected to periodic shaking. I investigate the stability of this Floquet BEC to interactions. This research direction consists of 3 studies. In chapter 4, I first do this analysis for a purely one-dimensional system and identify a large parameter regime where the BEC is stable. In the next two chapters, I go beyond 1D and consider the role of transverse degrees of freedom. This is because the shaken lattice experiments that I model involves a 1D array of pancakes. I find that this geometry leads to much more dissipation than a purely 1D system. This extra dissipation arises because interactions can transfer energy between different directions. In chapter 5, I consider the extreme case where there is no transverse confinement. I find that in the absence of transverse confinement, a one-dimensional Floquet BEC is generically unstable. Finally, in chapter 6, I consider harmonic transverse confinement modeling the crossover between chapters 4 and 5. I find that as the transverse confinement is made stronger, the atom loss rate initially increases, but beyond a critical transverse confinement, the atom loss disappears due to unavailability of

phase space for scattering. I also predict that if the transverse confinement is tuned to the vicinity of certain magic values, the heating rate exhibits a sharp drop. I perform similar analyses for a shaken square lattice and find that generically a low-dimensional Floquet BEC can be stabilized by suitably designing the transverse confinement.

BIOGRAPHICAL SKETCH

Sayan Choudhury was born in the small industrial city of Asansol, India. He completed his schooling in Asansol and thereafter moved to the Indian Institute of Science, Education and Research (IISER), Kolkata in 2006. He obtained his M.S. in Physics from IISER in 2011 with a thesis on the dynamics of one-dimensional Bose-Einstein Condensates. In the Fall of 2011, Sayan joined the PhD program in Physics at Cornell University. At Cornell, he worked on the theory of degenerate quantum gases under the tutelage of Prof. Erich Mueller. He will be joining Prof. Qi Zhou's group at Purdue University for a postdoctoral position in the fall of 2017.

Sayan is an avid reader. He loves traveling to new places and trying new food. He enjoys drinking coffee and taking long walks in the woods with his wife, Esha.

To Esha, for giving me shelter from the storm

ACKNOWLEDGEMENTS

As I look back on my 6 years at Cornell, I am filled with gratitude towards everyone who made this thesis possible.

First and foremost, I want to thank my advisor Prof. Erich Mueller. Erich has been a great source of inspiration and encouragement throughout my stay at Cornell. He has been extremely patient with me, teaching me cool mathematical tricks, nitty-gritty details of Mathematica, and strategies for making effective presentations. I have benefited greatly from his deep knowledge of theoretical techniques as well as his familiarity with the minute details of experiments. Moreover, he has granted me a lot of freedom in pursuing different ideas. I have really cherished working with him and learning from him. Erich has been the ideal advisor and someday I hope I can live up to the example set by him.

I want to thank Prof. Mukund Vengalattore and Prof. Jim Sethna for serving on my committee. A lot of my knowledge of cold atoms comes from a wonderful course taught by Mukund in the Fall of 2011. My interest in non-equilibrium physics grew out of a term paper that I did for that course. I learnt a lot of fun stuff in Jims Stat Mech II course (including a little bit of conformal field theory!). I also enjoyed his module on Sloppy models and I ended up working on a small sloppy models project with an economics graduate student for fun. In recent years, an A exam question posed by him on periodically driven classical systems, has taken on a life of its own and I have learnt a lot by talking to him and his group member, Archishman.

The physics department at Cornell provided a stimulating environment. All the Professors here have been extremely supportive. In particular, I thank the late Prof. Chris Henley for teaching me all about condensed matter physics and for providing some amazing lecture notes. I would also like to thank all

the administrative staff: Kacey, Deb, Douglas, Caroline, Becky, Judy, John and Craig for taking care of all the administrative hassles and letting me concentrate on physics.

I was very lucky to have been part of an amazing group which worked on an eclectic array of projects. I learnt a lot from talking to Matthew, Shovan, Ran, Yariv,Bhuvanesh, Natu, Junjun, and Nur. I thank them all. I also want to thank Yogesh for telling me about all the interesting experiments going on in the Vengalattore group.

Outside of Cornell, I would like to first thank Prof. Kaden Hazzard. My stay had not overlapped with Kadens during his time in the Mueller group. However, I met him regularly at conferences and, at the last DAMOP, I started a very productive collaboration with him. He has been a great sounding board for ideas and like Erich, he has been a very hands-on collaborator. Last December, he flew me out to Rice where we discussed a lot of physics (and drank a lot of coffee!). Thank you Kaden for being so awesome! I would also like to thank Prof. Cheng Chin and his group members, Harry and Logan for generously sharing their experimental data. Chapter 5 of this thesis grew out a suggestion made by Prof. Wolfgang Ketterle and I thank him for his insight.

Outside of physics, I have been very lucky to have a very supportive group of friends. Jishnu was my first friend in Ithaca and I have enjoyed my discussions with him and cooking with him. I have been very lucky to have Ujani and Anshul as my neighbors during the last year. They are my friends from IISER and I have really enjoyed reliving old hostel days with them. Outside of Ithaca, I had several friends in Collge Park, MD (thanks to Esha being there). Tanvir has been a brother more than a friend. Saad took me on road trips in Rural Virginia and the Adirondacks and helped build my bed. Ibraheem took me to

Afghan Bistro and gave me a lot of tea. Souvik and Piyana have been extremely close friends who I could rely on for anything. Last but not the least, I owe a big thank you to Auyon bhai and Saara Apu for the board game nights, the coffee, the trips, and most importantly their friendship. Thank you all, for being so amazing!

My family has been a pillar of support and strength for me. I have been very lucky to have been brought up by my grandparents who have always encouraged me to pursue my dreams. I can never thank them enough for everything that they have done, and all the sacrifices that they have made, for me. I am extremely thankful to my parents for their unwavering faith in me. Eshas parents have been always been very supportive. I especially thank Maa for redesigning my wardrobe, taking me to exotic places, feeding me at Michelin star restaurants, and generally being awesome always.

Finally, I would like to thank the most important person in my life: Esha. She has filled my life with happiness. Thank you for always being there for me through the good and bad times. With you, I have seen the sun come up in Ocean City, hiked the Appalachians in Harpers Ferry, walked the cliff in Newport and seen the sun go down in La Jolla. With you, I have experienced life in all its flavors. Quoting the words of Tagore "Tomarei Koriachi Jibonero Dhrubotara", (I have made you the pole star of my life). I can never thank you enough!

TABLE OF CONTENTS

LIST OF FIGURES

CHAPTER 1

INTRODUCTION

The reductionist hypothesis does not by any means imply a "constructionist" one: The ability to reduce everything to simple fundamental laws does not imply the ability to start from those laws and reconstruct the universe. - P. W. Anderson

1.1 Overview

Most of our everyday experiences are built around objects which have a very large number of constituent atoms ($\sim 10^{23}$). It is rather fascinating that several common physical phenomena can't be explained merely by understanding the properties of their constituent atoms. For instance, a single gold atom does not glitter, but a gold pendant does! This leads to an intriguing question: how does the properties of a particular material (rigidity, conductivity etc.) emerge from the interactions between its constituent atoms. The branch of physics dedicated to the study of such emergent phenomena is called "many-body physics". Cold neutral atoms loaded in optical lattices present a very pristine setting for studying many body physics in quantum systems.

The many body problem is a hard problem in general. It is easy enough to write down a Hamiltonian that describes a collection of interacting particles, but it is generally impossible to solve the Schrödinger equation for that Hamiltonian. Thus, the first step in understanding the behavior of many body system usually involves writing down a minimal model that is believed to retain the

relevant phenomenology. However, exactly solving even the minimal model is impossible in general. This is where cold atoms come in. They provide a very versatile platform for realizing a variety of many-body models and probing their dynamics. I study one such model in this thesis: the Bose-Hubbard model.

The Bose-Hubbard model is realized experimentally by first cooling bosonic alkali atoms to quantum degeneracy and then trapping them in an optical lattice. Atoms loaded in optical lattices experience a periodic potential analogous to that experienced by electrons in solids. Thus, cold atoms can be used to realize models related to those describing solid state materials.

A big difference between cold atoms and electronic systems they emulate is their energy scales. Typically atoms are 10^4 times heavier than electrons. Moreover the spacing between atoms is of the order of microns (for electrons in solids, this is of the order of angstroms). Quantum effects start dominating the physics when the thermal de Broglie wavelength is of the order of the spacing between the atoms. Thus, the temperature at which quantum effects become important is:

$$T = \frac{h^2 n^{2/3}}{2\pi m k_B} \tag{1.1}$$

For atoms, this condition is satisfied when the temperatures of order 500 nK (in traditional solids, this temperature is of the order of hundreds of Kelvin and for superfluid ^{4}He, this temperature is about 5 K). Cooling dilute atomic gases down to such temperatures requires extremely specialized cooling techniques. Once cooled however, these atomic systems provide several advantages for probing. In particular, the dynamics of atoms can be followed on the timescales of miliseconds! In the next section, I give an overview of how experimentalists cool

atoms, load them in optical lattices and probe their state.

1.2 Cooling atoms, loading them in optical lattices and probing their state

1.2.1 Cooling Atoms

At first glance, cooling down 10^6 atoms to nanokelvin temperatures looks like an impossible task. However, over the past two and a half decades, experimentalists have mastered the techniques to achieve this [1]. In this subsection, I will discuss a set of cooling techniques which are commonly used to create a Bose-Einstein condensate.

The first step is to produce an atomic beam by evaporating a metal in an oven. The oven temperatures can vary a lot by atomic species (about 600 K for ^{23}Na to about 333 K for ^{133}Cs[3]). The atomic beam is then collimated and put inside a Zeeman slower. The Zeeman slower comprises a cylindrical tube in which the atomic beam is irradiated by a counter-propagating laser beam whose frequency is tuned to be resonant with an atomic transition. When an atom absorbs a photon of momentum k, it transitions to an excited state and its velocity reduces by $\frac{\hbar k}{m}$. The atoms can return to their ground state by the spontaneous emission of a photon. This photon is emitted in a random direction and thus on average, the atom slows down. Once an atom is back to its ground state, it can absorb another photon with momentum k and the cooling cycle continues.

A major bottleneck to the cooling atoms in a Zeeman slower is caused by the fact different atoms in the atomic beam have different atomic transition frequencies due to the Doppler effect. In order to overcome this challenge, experimentalists harness the spin of the atoms. In particular, by cleverly designing a spatially varying magnetic field, the Zeeman and Doppler effects can be made to cancel resulting in efficient cooling of the atoms. At this stage, atoms exhibit a huge drop in temperature (^{23}Na atoms are cooled to 1K [2] and ^{133}Cs atoms are cooled to 40μK [3] at this stage).

After coming out of the Zeeman slower, the atoms are trapped in a magneto-optical trap (MOT) and cooled by laser cooling. Laser cooling is carried out by subjecting the the atoms to a laser beam which is red detuned from an atomic transition. Atoms moving towards the laser experience a relativistic Doppler shift which puts the laser beam in resonance with the atomic transition. Thus, the atom can absorb a photon and thereby lose momentum. This cools atoms down further (^{133}Cs atoms cool down to a temperatures of 10μK [3] and ^{23}Na atoms cool down to a temperature of 100μK[2])

After about $10^7 - 10^{10}$ atoms have been trapped in the MOT, the laser beams are turned off and atoms are trapped in a purely magnetic trap. The magnetic trap can localize the weak field seeking states near its minima. This trap compresses the cloud and sets the stage for evaporative cooling of the gas.

Evaporative cooling is achieved by first allowing the gas to thermalize in the trap. The highest energy atoms are removed by lowering the trap depth. When the remaining atoms thermalize again, but this time the atoms thermalize to a lower temperature. Evaporative cooling relies crucially on the role of elastic collisions ("good collisions") between atoms which causes the atoms to rether-

malize. The rethermalization time is given by $\tau \sim 1/(n\sigma v)$ where n is the density of the atoms, σ is the collision cross section and v is the average velocity of the atoms. During the evaporative cooling stage, atoms also suffer from inelastic collisions ("bad collisions") which can lead to heating of the gas. For evaporative cooling to be successful, the ratio of "good collisions" to "bad collisions" must be 100:1 [4]. This is indeed the case for alkali atoms like ^{23}Na and ^{87}Rb. However, evaporatively cooling ^{133}Cs can be substantially more difficult. This is because the magnetically trappable state of ^{133}Cs ($|F = 3, m_F = -3\rangle$) suffers from a lot of two-body inelastic collisions that change the spin angular momentum of the atoms. These collisions cause the atoms to transition to a state that is not magnetically trappable, leading to massive atom loss from the trap[4]. The collision cross section for ^{133}Cs atoms is about 1000 times greater than that that of ^{87}Rb atoms. Thus, while in ^{87}Rb, each atom undergoes several oscillations before colliding with another atom, ^{133}Cs atoms experience multiple collisions during one oscillation period. This leads to quick local thermalization, but the sample as a whole rethermalizes on the timescale of one trap oscillation period. In this regime the ratio of "good" to "bad" collisions scale inversely with the density. Thus, as the density of atoms in the trap rises, the evaporation process becomes more and more inefficient [4]. Two body inelastic scattering can be suppressed completely if the atom is cooled to its lowest energy state ($|F = 3, m_F = 3\rangle$) [3, 5]. This state however is not magnetically trappable. Thus, in order to create a BEC of ^{133}Cs atoms, the atoms are spin polarized to the $|F = 3, m_F = 3\rangle$ and then trapped in a purely optical trap. These atoms can then be evaporatively cooled successfully[3, 5].

The cooling steps involving the Zeeman slower and MOT are independent of quantum statistics and are also used to cool fermions. However, evapora-

tively cooling fermions is very difficult unless the atom has multiple hyperfine states that can be magnetically trapped. This is because collisions between spin-polarized fermions are highly suppressed at low temperatures and collisions are crucial for evaporative cooling[6]. ^{40}K has two magnetically trappable states and hence a gas of ^{40}K atoms has been cooled to quantum degeneracy using evaporative cooling[7]. However, ^{40}K is very scarce in nature. ^{6}Li on the other hand is widely available fermionic atom making it the atom of choice for a lot of quantum gas experiments. However, ^{6}Li does not have two magnetically trappable states and has to be either cooled sympathetically using another atomic species as a bath[8, 9] or by using purely optical traps [10] (analogous to the case of ^{133}Cs). In order to engineer more exotic states of matter (like quantum antiferromagnets), experimentalists have developed further sophisticated cooling techniques [11, 12].

1.2.2 Loading atoms in an optical lattice

Once the atoms have been cooled, then these atoms are loaded in an optical lattice[13]. An optical lattice is a crystal of light created by interfering laser beams. The oscillating electric field of a laser $\mathbf{E}$ induces a dipole moment, $\mathbf{d}$ in the atom which interacts with the field, $E(\mathbf{r})$ in the following way:

$$V(\mathbf{r}) = -\mathbf{d} \cdot \mathbf{E}(\mathbf{r}), \tag{1.2}$$

where $\mathbf{E} = \epsilon(\mathbf{r}) \exp(-i\omega t) + \epsilon^*(\mathbf{r}) \exp(-i\omega t)$. In linear response, the dipole moment $\mathbf{d}$ can be written as:

$$d_i^{\pm} = \sum_j \alpha_{ij}(\omega) E_j^{\pm} \tag{1.3}$$

where $\alpha(\omega)$ is the polarizability of the atom, ω is the laser wavelength and $E^+(E^-)$ corresponds to the positive(negative) frequency component of $\mathbf{E}$. Similarly, $d^+(d^-)$ corresponds to the positive(negative) frequency component of $\mathbf{d}$. The polarizability of the atom depends on the energies of the excited states of the atom and the laser wavelength ω. In particular, the maximum contribution to the polarizability comes from the excited state whose energy, E_e has the lowest detuning, $\Delta = E_e - \hbar\omega$. The shift in the energy of the ground state, ΔE is equal to:

$$\Delta E = -2Re(\sum_{i,j} \alpha_{ij} E_i^+ E_j^-) \tag{1.4}$$

When the polarizability is scalar $\alpha_{ij} = \alpha\delta_{ij}$, then the energy shift (AC stark shift) is:

$$\Delta E = -2Re(\alpha)|\mathbf{E}(\mathbf{r})|^2 \propto \frac{I(\mathbf{r})}{\Delta} \tag{1.5}$$

Thus the atoms experience a potential which is proportional to the intensity of the laser field. A periodic potential is readily created by interfering lasers.

1.2.3 Probes of Cold atoms

The most commonly used technique to probe the state of a trapped cold gas is *time-of-flight* imaging. The basic idea behind this method is to turn off all external potentials, allow the gas to expand and finally image the atom cloud. If the gas is allowed to expand for a sufficiently long time, then the time-of-flight images can be used to reconstruct the momentum space wave function of the trapped gas. I sketch out the rationale for this method below. The interested reader can find a a more thorough analysis in refs.[14, 15].

When all the external potentials are turned off, interaction effects become

unimportant after the first few moments and the gas expands ballistically [16]. This means that the Hamiltonian governing the time of flight expansion of a cold gas is :

$$H = \sum_k \frac{\hbar^2 k^2}{2m} \Psi_k^\dagger \Psi_k \tag{1.6}$$

where $\Psi(k)$ is the annihilation operator for a particle of momentum k. The density distribution after a time t is :

$$\begin{aligned} n_{\mathrm{TOF}}(r,t) &= \langle \Psi(r)^\dagger \Psi(r) \rangle \\ &= \int d^3k d^3k' \langle \Psi(k,t)^\dagger \Psi(k',t) \rangle \exp(ikr) \exp(-ik'r) \\ &= \int d^3k d^3k' \langle \Psi(k,0)^\dagger \Psi(k',0) \rangle \exp(-i\frac{\hbar^2 k^2}{2m}t) \exp(ikr) \exp(-ik'r) \exp(i\frac{\hbar^2 k'^2}{2m}t) \\ &\approx (\frac{m}{\hbar t})^3 \langle \Psi(k = \frac{mr}{\hbar t}, 0)^\dagger \Psi(k = \frac{mr}{\hbar t}, 0) \rangle = (\frac{m}{\hbar t})^3 \langle n_{\mathrm{trap}}(k) \rangle \end{aligned} \tag{1.7}$$

Thus, the density distribution in time-of-flight can be used to probe the quantum state of the trapped gas. In this analysis, I have ignored the initial size of the atomic cloud, which is a very good approximation for long times[14, 15].

The imaging procedure in a TOF protocol involves shining a laser on a cloud of gas and then measuring the light transmitted on a CCD. Within a ray optics picture, the transmitted light's intensity profile is given by:

$$I(x,y) = I_0 \exp(-iN(x,y)\sigma) \tag{1.8}$$

where $N(x,y) = \int dz n(x,y,z)$ is the cross-sectional density of the atoms and σ is the photon absorption cross-section. This technique measures the shadow of the gas.

1.3 This Thesis

1.3.1 Frontiers of cold atoms research

There are several frontiers in cold atoms research. This thesis focuses on two broad areas:

- **Hamiltonian Engineering and State Control** : One of the main directions of research in cold atoms physics is the quantum simulation of interacting many body systems. In order to quantitatively emulate models of interest, a lot of effort has been directed towards devising protocols to engineer Hamiltonians which are expected to host exotic ground states. A complimentary approach is to devise protocols to create highly correlated states. Both of these avenues of research has been very fruitful in realizing novel quantum phases of matter.
- **Non-equilibrium Dynamics**: Apart from the special case of non-interacting systems, it is notoriously difficult to simulate quantum dynamics. Cold atom setups provide a perfect place to observe non-equilibrium dynamics of closed quantum systems. This provides a platform for answering fundamental questions in statistical mechanics (like how do quantum systems equilibrate) and also engineer exotic non-equilibrium quantum states (like Floquet topological insulators).

1.3.2 Structure of the thesis

In this thesis, I explore many body physics using Bose-Einstein condensates loaded in one and two dimensional optical lattices. I show these systems can be used to study exotic phases and non-equilibrium dynamics. I also discuss how non-equilibrium protocols like periodic driving can be used for creating exotic states. This thesis is divided into 7 chapters. Each chapter is followed by the relevant bibliography.

In chapter 2, I lay out the central mathematical framework used in this thesis. I start off by deriving the Hamiltonian describing the dynamics of interacting bosons. Specializing to the case of a BEC, I go on to derive the Gross-Pitaevskii functional which models the free energy of a BEC. Finally, in the case of bosons loaded in an optical lattice, I map the continuum Hamiltonian to a tight binding model: the Bose-Hubbard model. I finish the chapter with a brief discussion on interpreting time-of-flight images of bosons released from an optical lattice.

In chapter 3, motivated by the reported observation of an exotic "twisted superfluid phase"[17], I study the stability of a two-component BEC loaded in a spin-dependent honeycomb lattice towards forming a twisted superfluid. My exhaustive numerical search fails to find this phase, pointing to two possible scenarios: the experimental observations were either a manifestation of non-mean field physics or due to interactions during time-of-flight. Subsequent experimental studies have revealed that the data in that paper was misinterpreted confirming our results[18].

In Chapters 4,5, and 6, I explore the stability of driven quantum systems.

First, in chapter 4, I analyze the stability of a BEC in a one-dimensional lattice

subjected to periodic shaking. My work is motivated by an experiment in Prof. Cheng Chin's group [19]. In such a system there is no thermodynamic ground state, but there may be a long-lived steady-state, described as an eigenstate of a "Floquet Hamiltonian". I calculate how scattering processes lead to a decay of the Floquet state. I map out the phase diagram of the system and find regions where the BEC is stable and regions where the BEC is unstable against atomic collisions.

Then, in chapter 5, I analyze the stability of a three-dimensional BEC loaded in a periodically driven one-dimensional optical lattice. I explore collisional instabilities of the Floquet ground state which transfer energy into the transverse modes. I calculate decay rates, finding that the lifetime scales as the inverse square of the scattering length and inverse of the peak three dimensional density. These rates can be controlled by adding additional transverse potentials.

In chapter 6, I explore the effect of transverse confinement on the stability of a BEC loaded in a shaken one-dimensional or two-dimensional square lattice. I calculate the decay rate from two-particle collisions. I predict that if the transverse confinement exceeds a critical value, then, for appropriate shaking frequencies, the condensate is stable against scattering into transverse directions. I explore the confinement dependence of the loss rate, explaining the rich structure in terms of resonances. This chapter concludes my investigation of the stability of driven quantum systems.

In chapter 7, I conclude my thesis with directions for future work.

BIBLIOGRAPHY

[1] W. D. Phillips, Reviews of Modern Physics, **70**, 721 (1998)

[2] C. J. Pethick and H. Smith, "BoseEinstein Condensation in Dilute Gases" 2nd Edition, *Cambridge University Press* (2008).

[3] C-L. Hung, PhD Thesis, University of Chicago, 2011.

[4] A. M. Thomas, PhD Thesis, University of Oxford, 2004.

[5] T. Weber, J. Herbig, M. Mark, H-C Nägerl, and R. Grimm, Science, **299**, 232, 2003.

[6] Z. Hadzibabic, PhD Thesis, Massachusetts Institute of Technology, 2003.

[7] B. DeMarco and D. S. Jin, Science **285**, 1703 (1999).

[8] A. G. Truscott, K. E. Strecker, W. I. McAlexander, G. B. Partridge, and R. G. Hulet, Science **291** 2570 (2001).

[9] Z. Hadzibabic, C. A. Stan, K. Dieckmann, S. Gupta, M. W. Zwierlein, A. Gorlitz, and W. Ketterle, Phys. Rev. Lett. **88**, 160401 (2002).

[10] S. Jochim, M. Bartenstein, A. Altmeyer, C. Hendl, S. Riedl, C. Chin, J. Hecker-Denschlag and R. Grimm Science **302**, 2101 (2003).

[11] R. A. Hart, P. M. Duarte, T-L Yang, X. Liu, T. Paiva, E. Khatami, R. T. Scalettar, N. Trivedi, D. A. Huse, and R. G. Hulet, Nature **519**, 211-214 (2015)

[12] A. Mazurenko, C. S. Chiu, G. Ji, M. F. Parsons, M. Kanász-Nagy, R.Schmidt, F. Grusdt, E. Demler, D. Greif, and M. Greiner, arXiv: 1612.08436

[13] I. Bloch, Nature Physics, **1**, 23-30, (2005).

[14] P. Pedri, L. Pitaevskii, S. Stringari,C. Fort,S. Burger,F. S. Cataliotti,P. Maddaloni,F. Minardi, and M. Inguscio, Phys. Rev. Lett. **87**, 220401 (2001)

[15] F. Gerbier, S. Trotzky, S. Fölling, U. Schnorrberger, J. D. Thompson, A. Widera, I. Bloch, L. Pollet, M. Troyer, B. Capogrosso-Sansone, N. V. Prokofev,and B. V. Svistunov, Phys. Rev. Lett. **101**, 155303 (2008)

[16] J. N. Kupferschmidt and E. J. Mueller, Phys. Rev. A **82**, 023618 (2010).

[17] P. Soltan-Panahi, D.-S. Lühmann, J. Struck, P. Windpassinger and K. Sengstock, Nature Physics **8**, 71-75 (2012).

[18] M. Weinberg, O. Jürgensen, C. Ölschlger, D-S Lühmann, K. Sengstock, and Juliette Simonet Phys. Rev. A **93**, 033625 (2016).

[19] C. V. Parker, L-C. Ha and C. Chin, Nature Phys. **9**,769 (2013).

CHAPTER 2

BOSONS IN OPTICAL LATTICES

2.1 Overview

In this chapter, I introduce the mathematical framework for modeling a Bose-Einstein condensate (BEC) loaded in an optical lattice. In section 2.2, I describe the interactions between bosons in a dilute quantum gas. In section 2.3, I derive the Gross-Pitaevskii energy functional which describes the properties of a BEC. In section 2.4, show that bosons loaded in an optical lattice can emulate the Bose-Hubbard model. Finally, in section 2.5, derive an expression for the distribution of atoms in time-of-flight after they have been released from an optical lattice.

2.2 Interactions between atoms

In this section, I consider the interactions between neutral alkali atoms. The interaction between the atoms is often approximated by a Lennard-Jones potential, $U(r)$ of the form:

$$U(r) = \frac{A}{r^{12}} - \frac{B}{r^6} \tag{2.1}$$

The $\frac{1}{r^{12}}$ part of the potential models the repulsion at short distances while the $\frac{1}{r^6}$ part of the potential models the van der Walls attraction between the atoms at larger distances. The ground state of an ensemble of alkali atoms is a solid. However, for the dilute atomic vapors present in cold atom experiments, scientists can produce a metastable BEC. In order to model the BEC, I will use a pseudo-potential, $U_{\text{pseudo}}(r)$ which is repulsive at short distances, has no bound

states and correctly reproduces the long range, low energy physics when treated in the Born approximation. The common choice of the pseudo-potential used in modeling quantum gases is:

$$U_{\text{pseudo}}(r) = g\delta^3(r). \tag{2.2}$$

In the rest of this section, I solve the two-body scattering problem for $U(r)$ and and show that low-energy scattering can be described in terms of a single number: the scattering length, a. I will then show how the parameter g in eqn.(2.2) is related to a within the Born approximation.

The two-particle scattering problem is described by the Hamiltonian :

$$\begin{aligned} H &= \frac{\hbar^2 k_1^2}{2m} + \frac{\hbar^2 k_1^2}{2m} + U(r) \\ &= \frac{\hbar^2 k_{\text{com}}^2}{4m} + \frac{\hbar^2 k_{\text{rel}}^2}{m} + U(r) \end{aligned} \tag{2.3}$$

Thus, in the center-of-mass frame, the two-particle scattering problem reduces to a one-particle problem of a quantum particle of mass $m/2$ in a potential $V(r)$. The Schrödinger equation for this system is given by:

$$\left(-\frac{\hbar^2\nabla^2}{m} + U(r)\right)\psi(r) = E\psi(r) \tag{2.4}$$

The solution to the scattering problem is of the form:

$$\psi = \exp(i\ \mathbf{k}\cdot\mathbf{r}) + \psi_{\text{sc}}(\mathbf{r}) \tag{2.5}$$

At large distances, the scattered wave is a spherical wave of the form $f(\mathbf{k}')\exp(i\mathbf{k}\cdot\mathbf{r})/r$. Thus, at large r, the wavefunction ψ is of the form

$$\psi = \exp(ikz) + f(\mathbf{k}')\frac{\exp(ikr)}{r}, \tag{2.6}$$

where I have chosen z to be the direction of $\mathbf{k}$ and $|\mathbf{k}'| = k$. The interaction between alkali atomis is spherically symmetric. This means that $f(\mathbf{k}')$ can be

written as $f(\theta)$. At low energies, only the s-wave channel contributes. Thus $f(\theta)$ can be considered to be a constant at large distances. Labelling that constant as $-a$, the wavefunction ψ can be written as:

$$\psi = \exp(ikz) - \frac{a}{r}\exp(ikr). \tag{2.7}$$

For s-wave scattering, a is defined to be the scattering length in the limit of large distances ($k = 0$).

I am interested in formulating a theory which only involves the long wavelength and low energy degrees of freedom. To do this, I Fourier transform the wavefunction ψ given in eqn.(2.5) to obtain

$$\psi(k') = (2\pi)^3\delta^3(k' - k) + \psi_{\rm sc}(k') \tag{2.8}$$

This wave-function satisfies the Schrödinger equation

$$\left(\frac{\hbar^2k^2}{2m} - \frac{\hbar^2k'^2}{2m}\right)\psi_{\rm sc}(k') = U(k' - k) + \frac{1}{V}\sum_{k''} U(k' - k'')\psi_{\rm sc}(k'') \tag{2.9}$$

The scattered wave-function can be written down as:

$$\begin{aligned}\psi_{\rm sc}(k') &= \left(\frac{\hbar^2k^2}{2m} - \frac{\hbar^2k'^2}{2m} + i\delta\right)^{-1}\left(U(k' - k) + \frac{1}{V}\sum_{k''} U(k' - k'')\psi_{\rm sc}(k'')\right) \\ &= \left(\frac{\hbar^2k^2}{2m} - \frac{\hbar^2k'^2}{2m} + i\delta\right)^{-1} T(k', k; E = \frac{\hbar^2k^2}{2m})\end{aligned} \tag{2.10}$$

and the T-matrix satisfies the relation:

$$T(k', k; E) = U(k' - k) + \frac{1}{V}\sum_{k''} U(k' - k'')\left(E - \frac{\hbar^2k''^2}{2m} + i\delta\right)^{-1} T(k'', k; E) \tag{2.11}$$

At long distances and low energies ($E = k = 0$), the scattered wave takes the form:

$$\psi_{\rm sc} = -\frac{mT(0, 0; 0)}{4\pi\hbar^2 r} \tag{2.12}$$

From the definition of the scattering length in eqn.(2.7), I obtain

$$a = \frac{m}{4\pi\hbar^2} T(0,0;0) \tag{2.13}$$

Now, for a contact interaction, $U(k',k) = g$ and thus the the T matrix becomes:

$$T(k',k;E) = g + \frac{g}{V}\sum_{k''}\left(E - \frac{\hbar^2 k''^2}{2m} + i\delta\right)^{-1} T(k'',k;E) \tag{2.14}$$

Since, I am only interested in the asymptotic nature of the scattered wave, I can $T(k',k;E)$ approximate to be just a function of the energy E. Thus, one gets:

$$T(k',k;E) = \frac{g}{1 - \frac{g}{V}\sum_{k''}\left(E - \frac{\hbar^2 k''^2}{2m} + i\delta\right)^{-1}} \tag{2.15}$$

This means

$$T(0,0,0) = \frac{4\pi\hbar^2 a}{m} = \frac{g}{1 - \frac{g}{V}\sum_{k''}\left(-\frac{\hbar^2 k''^2}{2m} + i\delta\right)^{-1}} \tag{2.16}$$

For a particular measured value of a and a high momentum cutoff Λ, this equation yields a particular value of g. The Born approximation amounts to taking the cut-off $\Lambda = 0$ yielding:

$$g = \frac{4\pi\hbar^2 a}{m}. \tag{2.17}$$

The scattering lengths, of alkali atoms that are typically used in cold atom experiments is about 5 nm while the typical inter-particle spacing is about 500 nm. Thus, these gases are dilute in the sense $na^3 \ll 1$, where n is the density of the atoms. The Born approximation is sufficient to accurately calculate the low energy properties of such dilute quantum gases [1]. Hence, throughout this thesis, I use an effective interaction of the form:

$$U(r - r') = \frac{4\pi\hbar^2 a}{m}\delta(r - r') \tag{2.18}$$

2.3 Gross-Pitaevskii Energy Functional

With the pseudopotental from eq.(2.18), the Hamiltonian describing a system of interacting trapped bosons is given by:

$$H = \int d^3r\ \Psi^\dagger(r)\left(-\frac{\hbar^2\nabla^2}{2m} + V_{\text{ext}}(r) + \frac{g}{2}\Psi^\dagger(r)\Psi(r)\right)\Psi(r), \tag{2.19}$$

where $\Psi(r)$ is the annihilation operator for a boson at position r. The operators Ψ and $\Psi^\dagger$ obey the usual bosonic commutation relation:

$$\begin{aligned}\left[\Psi(r), \Psi^\dagger(r')\right] &= \delta^3(r - r') \\ [\Psi(r)\ , \Psi(r')] &= \left[\Psi^\dagger(r), \Psi^\dagger(r')\right] = 0\end{aligned} \tag{2.20}$$

In describing a BEC, I assume that all the bosons macroscopically occupy the same quantum state $\phi(r)$. Thus the wavefunction is given by :

$$\psi(r_1, r_2, \ldots, r_N) = \Pi_{i=1}^N \phi(r_i) \tag{2.21}$$

where $\int d^3r|\phi(r)|^2 = 1$. Thus, in this mean-field approach, the energy of the condensate is given by:

$$E[\phi] = N\int d^3r\ \phi^*(r)\left(-\frac{\hbar^2\nabla^2}{2m} + V_{\text{ext}}(r) + \frac{g}{2}|\phi(r)|^2\right)\phi(r). \tag{2.22}$$

In order to variationally minimizing the energy functional $E[\phi]$ while keeping the number of particles constant, I have to minimize the functional:

$$F[\phi] = E[\phi] - \mu N\int d^3r\ |\phi(r)|^2, \tag{2.23}$$

where N is the number of particles and μ is the chemical potential. The functional $F[\phi]$ is minimized by setting $\frac{\delta F}{\delta\phi^*} = 0$. This condition leads to the time-independent Gross-Pitaevskii equation

$$\left(-\frac{\hbar^2}{2m}\nabla^2 + V_{\text{ext}}(r) + g|\psi(r)|^2\right)\psi(r) = \mu\psi(r) \tag{2.24}$$

where $\psi(r) = N^{1/2}\phi(r)$.

2.4 Bose-Hubbard Model

In this section, I show that bosons loaded in an optical lattice emulates the Bose-Hubbard model. This analysis follows Jaksch *et al.* [2].

My starting point is the Hamiltonian in eqn.(2.19) where $V_{\text{ext}}(\mathbf{r})$ is a periodic potential:

$$V_{\text{ext}}(\mathbf{r}) = V_0 \sin(\mathbf{k} \cdot \mathbf{r}). \tag{2.25}$$

Following Bloch's theorem[3], I can write down the eigenfunctions of the single particle Hamiltonian can be written down in the form:

$$\psi_{n,k}(\mathbf{r}) = u_{n,k}(\mathbf{r}) e^{i\,\mathbf{k}\cdot\mathbf{r}} \tag{2.26}$$

where $u_{n,k}(\mathbf{r}) = u_{n,k}(\mathbf{r} + \mathbf{R})$, n is the band-index and k is the crystal momentum. Using these Bloch functions, I construct a basis of Wannier functions, $w_\alpha(r, R)$ where R is a bravais lattice vector:

$$w_\alpha(r, R) = \sum_k \psi_{\alpha,k}(\mathbf{r}) \exp(-i\ \mathbf{k} \cdot \mathbf{R}) = \sum_k u_{\alpha,k}(\mathbf{r}) \exp(-i\ \mathbf{k} \cdot (\mathbf{r} - \mathbf{R})). \tag{2.27}$$

The Wannier function only depends on $\mathbf{r} - \mathbf{R}$. The creation and annihilation operators can now be expanded in the basis of the Wannier states:

$$\psi(r) = \sum_i a_{n,i} w_n(r - R_i). \tag{2.28}$$

I now expand the Hamiltonian in eqn.(2.19) to obtain a tight binding model:

$$H = \sum_{i,j} \left(-J^n_{ij} a^\dagger_{n,i} a_{n,j} + \frac{1}{2} \sum_{m,n,m',n'} \sum_{i,j,i',j'} U^{m,n,m',n'}_{i,j,i',j'} a^\dagger_{m,i} a^\dagger_{n,j} a_{m',i'} a_{n',j'} \right), \tag{2.29}$$

where

$$\begin{aligned} J^n_{ij} &= \int d^3r\ w^*_n(r - R_i) \left(-\frac{\hbar^2 \nabla^2}{2m} + V_0 \sin(\mathbf{k} \cdot \mathbf{r}) \right) w_n(r - R_j) \\ U^{m,n,m',n'}_{i,j,i',j'} &= \int d^3r\ g \left(w^*_n(r - R_i) w^*_m(r - R_i) w_{m'}(r - R'_i) w_{n'}(r - R'_i) \right). \end{aligned} \tag{2.30}$$

As has been shown in ref.[4], if only the lowest band is considered, the the on-site interaction term U is about two orders of magnitude greater than the other interaction terms. Thus, the tight-Binding Hamiltonian takes a much simpler form when only the lowest band is considered, :

$$H - \sum_{i,j}\left(-J_{ij}a_i^\dagger a_j + \frac{U}{2}\sum_i a_i^\dagger a_i^\dagger a_i a_i\right) \tag{2.31}$$

Moreover, for typical cold atom experiments, the nearest neighbor hopping term is sufficient to describe the single-particle physics in the lowest band [4]. Thus, the model in eq.(2.31) takes the form:

$$H - \sum_{\langle i,j\rangle}\left(-ta_i^\dagger a_j + \frac{U}{2}\sum_i a_i^\dagger a_i^\dagger a_i a_i\right), \tag{2.32}$$

where $\langle i, j\rangle$ means that only tunneling between nearest neighbor sites is allowed. This is the Bose-Hubbard model and it can be used to study both the superfluid and Mott insulator phases of bosons.

2.5 Time-of-flight images

In this section, I derive an expression for the density distribution of an expanding cloud of atoms after all the external potentials are turned off. This density distribution can be used to interpret time-of-flight images which in turn can be used to reconstruct the momentum space distribution of the trapped gas. For bosons loaded in an optical lattice, the momentum space distribution of the trapped atoms is given by:

$$n_{\text{trap}}(\mathbf{k}) = \int d^3r d^3r' \exp(-i\ \mathbf{k}\cdot(\mathbf{r}-\mathbf{r}')\langle\psi^\dagger(r)\psi(r')\rangle. \tag{2.33}$$

From the expansion given in eq.(2.28), I obtain:

$$n_{\text{trap}}(\mathbf{k}) = \left(\frac{m}{\hbar t}\right)^3 |w(\mathbf{k})|^2 \sum_{i,j} \exp(i\ \mathbf{k}\cdot(\mathbf{r_i} - \mathbf{r_j}))\langle a_i^\dagger a_j\rangle. \tag{2.34}$$

Thus after switching off all external potentials and waiting for time t, the density of atoms at a position, $n_{\text{TOF}}(\mathbf{r})$ is proportional to $n_{\text{trap}}(\frac{m\mathbf{r}}{\hbar t})$:

$$n_{\text{TOF}}(\mathbf{r}) = |w(\frac{m\mathbf{r}}{\hbar t})|^2 n(\mathbf{k} = \frac{m\mathbf{r}}{\hbar t}), \tag{2.35}$$

where $n(\mathbf{k} = \frac{m\mathbf{r}}{\hbar t}) = \sum_{i,j} \exp(i\ \mathbf{k}\cdot(\mathbf{r_i} - \mathbf{r_j}))\langle a_i^\dagger a_j\rangle$ is the momentum space structure factor of the trapped gas [5, 6]. All the experiments that I model in this thesis have used time-of-flight imaging to probe the condensate wavefunction.

BIBLIOGRAPHY

[1] C. J. Pethick and H. Smith, "BoseEinstein Condensation in Dilute Gases" 2nd Edition, *Cambridge University Press* (2008).

[2] D. Jaksch, C. Bruder, J. I. Cirac, C. W. Gardiner, and P. Zoller, Phys. Rev. Lett. **81**, 3108 (1998).

[3] N. W. Ashcroft, and N. D. Mermin, "Solid Sate Physics" Holt-Saunders, Philadelphia (1976).

[4] Y. Yanay, PhD thesis, Cornell University, 2015.

[5] Y. Kato, Q. Zhou, N. Kawashima, and N. Trivedi, Nature Physics, **4**, 617-621, (2008)

[6] F. Gerbier, A. Widera, S. Fölling, O. Mandel, T. Gericke, and I. Bloch, Phys. Rev. A. **72**, 053606 (2005).

CHAPTER 3

ABSENCE OF THE TWISTED SUPERFLUID STATE IN A MEAN FIELD MODEL OF BOSONS ON A HONEYCOMB LATTICE

This chapter is adapted from the paper from "Absence of the Twisted Superfluid State in a mean field model of bosons on a Honeycomb Lattice" by Sayan Choudhury and Erich J Mueller, published in Physical Review A **87**, *033621 (2013).*

3.1 Overview

Motivated by recent observations [Soltan-Panahi *et al.*, Nat. Phys. 8, 71 (2012)], I study the stability of a Bose-Einstein condensate within a spin-dependent honeycomb lattice towards forming a twisted superfluid state. My exhaustive numerical search fails to find this phase. The experimental results are the either a manifestation of non-mean-field physics or due to interaction effects during time of flight. I also discuss a recent experiment which has shown that the observations were an artifact of the measurement process, thus validating my conclusion.

3.2 Introduction

3.2.1 Background

Recently, the Hamburg group found evidence of a zero quasi-momentum "Twisted Superfluid" state of a two-component Bose-Einstein condensate (BEC)

trapped in a spin-dependent honeycomb lattice [1]. A twisted superfluid is characterized by Bose-Einstein condensation into a state whose order parameter (a macroscopically occupied single particle wavefunction) has a spatially varying phase. The simplest example is condensation at finite momentum. Alternatively, in a non-Bravais lattice where the unit cell involves multiple sites, one can have a twisted superfluid at zero quasi-momentum if the phase of the order parameter varies throughout the unit cell. In this chapter, I model Soltan-Panahi *et al.*'s experiment [1] with a mean field Gross-Pitaevskii functional. I find that the twisted superfluid state is absent within mean field theory thus suggesting that the observations are either due to non-mean field effects or due to interactions during time-of-flight.

Twisted Superfluids are quite exotic; the phase twists of the order parameter are naturally associated with microscopic currents. Moreover, the present example involves spontaneous symmetry breaking, and provides a setting for studying phase transition physics. Analogous physics can be found in magnetic systems [2] and in the excited states of lattice bosons [3, 4].

3.2.2 Experimental Evidence for a Twisted Superfluid

In their experiment [1], Soltan-Panahi *et al.* created a two component Bose-Einstein condensate (BEC) of ^{87}Rb atoms in a spin-dependent honeycomb lattice. Soltan-Panahi *et al.* find evidence for the Twisted Superfluid state in two cases: a BEC of ^{87}Rb atoms in the $|F = 1, m_F = -1\rangle$ and $|F = 1, m_F = 1\rangle$ state and a BEC of ^{87}Rb atoms in the $|F = 2, m_F = -2\rangle$ and $|F = 1, m_F = -1\rangle$ state. In both of

these cases, the two spin states form out-of-phase charge density waves in this spin dependent lattice. In Figure 3.1, I show a cartoon of the density of atoms in one of the two spin states. For the rest of this chapter, I focus on the case where the two spin states are $|F = 1, m_F = -1\rangle$ and $|F = 1, m_F = 1\rangle$.

The main experimental evidence for non-trivial phases of the superfluid order parameter comes from time-of-flight expansion, a technique where all trapping fields are removed and the atomic ensemble falls freely under gravity. Neglecting interactions [5], the long-time real space density profile is simply the initial density in momentum space. For the special case of a BEC, the momentum space density, n_k is the Fourier transform of the order parameter : $n_k = |\psi(\mathbf{k})|^2 = |\int \exp(+i\mathbf{k}.\mathbf{r})\psi(\mathbf{r})|^2$, where $\psi(\mathbf{r})$ is the order parameter of the BEC. As schematically illustrated in Figure 3.2, if $\psi(\mathbf{r})$ is real, and has the symmetry of the honeycomb lattice, its Fourier transform (and consequently the time-of-flight pattern) is six fold symmetric. This six-fold symmetry persists even if the densities on the two sub-lattices differ, forming a three-fold symmetric charge density wave as illustrated in Figure 3.1. Mathematically, this six-fold rotational symmetry of the time-of-flight pattern is a consequence the point group symmetry of the lattice (C_{3v}) and the relation $\psi(-\mathbf{k}) = \psi^*(\mathbf{k})$, which holds for real $\psi(\mathbf{r})$. Therefore, a time-of-flight pattern without inversion symmetry ($\psi(-\mathbf{k}) \neq \psi^*(\mathbf{k})$) is direct evidence of a complex wavefunction (i.e. a twisted superfluid state). The experimentalists see exactly this signature.

From the time-of-flight images obtained in [1], a breakdown of the six-fold rotational symmetry in momentum space is observed for lattice depths V_{lat} rang-

ing from about 1 to 4 E_{R}, where $E_{\mathrm{R}} = \frac{\hbar^2}{2m\lambda_L^2}$, λ_L is the wavelength of the lasers forming the lattice, m is the mass of ^{87}Rb atoms and V_{lat} is precisely defined by Eq.(3.6). Figure 3.2 illustrates this structure in which the amplitudes of the first order time-of-flight peaks (denoted by $|t|$ and $|z|$) have different values for this range of lattice depths. An important aspect of their experiment was that this rotational symmetry breaking arises only if both species of atoms are present. Moreover, the symmetry breaking was opposite for the two species (i.e $\frac{|t_1|}{|z_1|} = \frac{|z_2|}{|t_2|}$). The order parameter (OP) for the twisted superfluid state is given by:

$$O = |\frac{|\mathrm{z}|^2 - |\mathrm{t}|^2}{|\mathrm{z}|^2 + |\mathrm{t}|^2}| \tag{3.1}$$

By construction, *OP* has a non-zero value in the twisted superfluid and is zero for a uniform condensate. Soltan-Panahi *et al.* measure this quantity.

The experimental evidence suggests that the order parameter is uniform on each of the triangular sub-lattices of the honeycomb lattice, but that there is a relative phase δ between them.

$$|z|^2 = n_+ + n_- + 2\sqrt{n_+ n_-}\sin(\delta) \quad \text{and} \tag{3.2}$$

$$|t|^2 = n_+ + n_- - 2\sqrt{n_+ n_-}\sin(\delta), \tag{3.3}$$

where the n_+ and n_- denote the density of atoms on the two distinct sub-lattices. Thus, the order parameter is :

$$OP = \frac{2\sqrt{n_+ n_-}|\sin(\delta)|}{n_+ + n_-}. \tag{3.4}$$

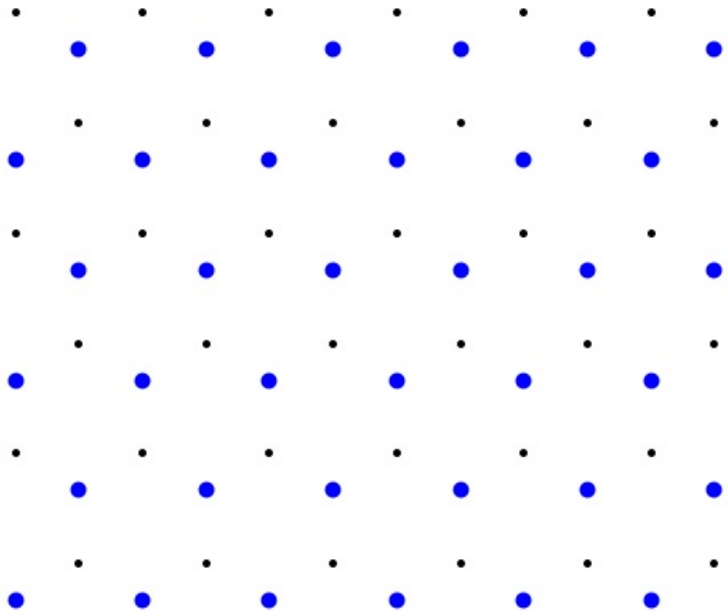

Figure 3.1: The density wave formed in a honeycomb lattice for the $m_F = 1$ atoms. The points represent lattice sites. Larger points indicate a site filled with more atoms. This pattern is periodically repeated. A complementary density wave is formed by $m_F = -1$ atoms. This density wave does not lead to a 6-fold symmetry breaking in time-of-flight unless additional phases appear on the sites.

3.3 The Model

Within a mean field model, I will investigate the relative stability of twisted or ordinary superfluids. The energy of a two component BEC, described by macroscopic wavefunctions ψ_1 and ψ_2 is :

$$E_{3D} = \int d^3\mathbf{r} \sum_{\sigma=1,2} \left(\frac{\hbar^2}{2m} |\nabla\psi_\sigma(\mathbf{r})|^2 + V_\sigma(\mathbf{r})|\psi_\sigma(\mathbf{r})|^2 + V_{\text{conf}}(\mathbf{r})(|\psi_1(\mathbf{r})|^2 + |\psi_2(\mathbf{r})|^2) + \frac{U^\sigma_{3D}}{2}|\psi_\sigma(\mathbf{r})|^4 \right) + W_{3D}|\psi_1(\mathbf{r})|^2|\psi_2(\mathbf{r})|^2 \quad (3.5)$$

Here, $U^\sigma_{3D} = \frac{4\pi\hbar^2 a_\sigma}{m}$ is the intra-species interaction energy (a_σ is the intra-species scattering length for species σ), while $W_{3D} = \frac{4\pi\hbar^2 a_{12}}{m}$ is the inter-species

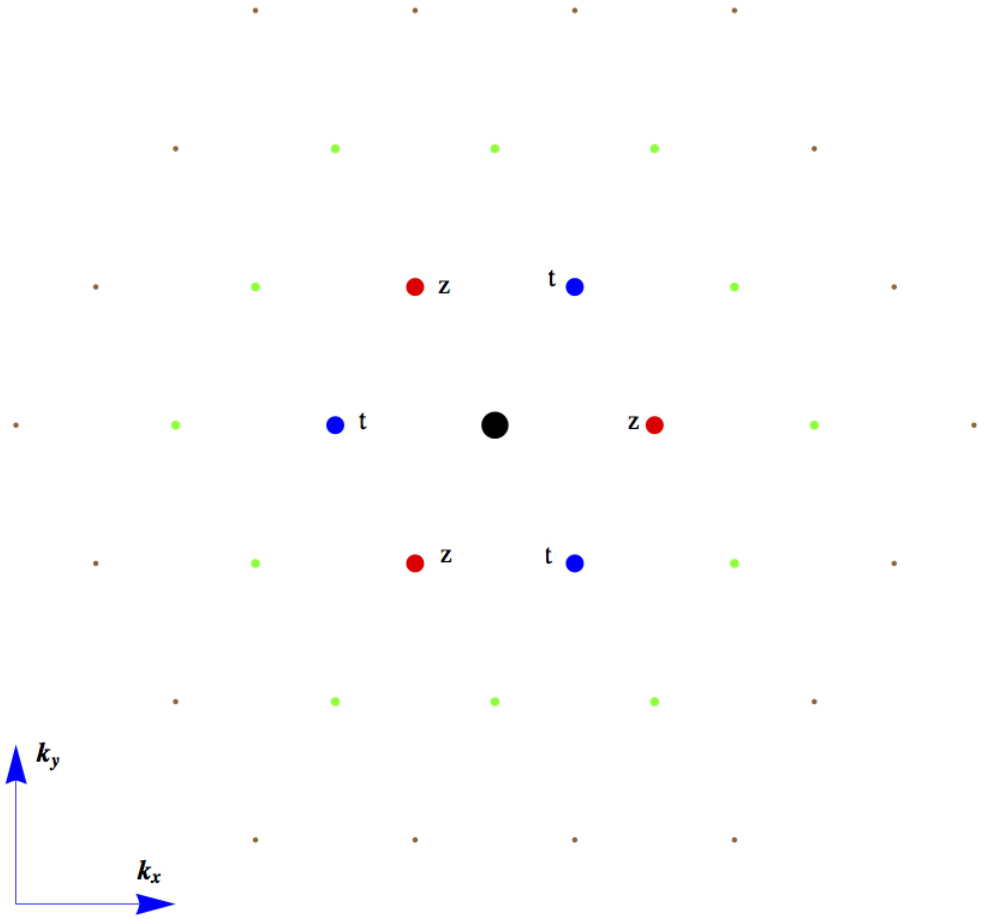

Figure 3.2: Schematic of the Time-of-Flight pattern for a superfluid in a 2D honeycomb lattice. Larger darker dots correspond to more particles with a given momentum. The complex numbers |t| and |z| represent the amplitudes of the Fourier transform of the condensate wavefunction at $k = (\frac{\pi}{a}, 0)$ and $k = (\frac{\sqrt{3}\pi}{2a}, \frac{\pi}{2a})$ (see text). The twisted superfluid is described by $|t| \neq |z|$.

interaction energy (a_{12} is the inter-species scattering length). As already mentioned in Section 3.2.2, I focus on the case in [1], where the states 1 (described by ψ_1) and 2 (described by ψ_2) are the $|F = 1, m_F = 1\rangle$ and $|F = 1, m_F = -1\rangle$ states of ^{87}Rb. For these two hyperfine states of ^{87}Rb atoms, U^1_{3D},$U^2_{3D}$and W_{3D} are almost equal ($a \approx 100a_0$ where a_0 is the Bohr radius). In principle collisions can connect these hyperfine states to others (for example $|F = 1, m_F = 0\rangle$). For the exper-

imental parameters, these processes are off-resonant and the two-component Bose gas model describes the physics.

In the experiment [1], the honeycomb lattice is generated by 3 lasers yielding a potential $V_i(\mathbf{r}) = V_{\rm hex}(\mathbf{r}) \pm \alpha B_{\rm eff}(\mathbf{r})$ where, state 1 sees the sign '+' and state 2 sees the sign '-' (with $\alpha = 0.13$) and

$$V_{\rm hex}(\mathbf{r}) = 2\ V_{\rm lat}(\cos[k_L\ \mathbf{b_1}.\mathbf{x}] + \cos[k_L\ \mathbf{b_2}.\mathbf{x}] + \cos[k_L\ \mathbf{b_3}.\mathbf{x}]) \tag{3.6}$$

$$B_{\rm eff}(\mathbf{r}) = 2\sqrt{3}\ V_{\rm lat}(\sin[k_L\ \mathbf{b_1}.\mathbf{x}] + \sin[k_L\ \mathbf{b_2}.\mathbf{x}] + \sin[k_L\ \mathbf{b_3}.\mathbf{x}]) \tag{3.7}$$

where, $\mathbf{b_1} = -\frac{\mathbf{1}}{\mathbf{2}}\mathbf{e_x} + \frac{\sqrt{3}}{\mathbf{2}}\mathbf{e_y}; \mathbf{b_2} = -\frac{\mathbf{1}}{\mathbf{2}}\mathbf{e_x} - \frac{\sqrt{3}}{\mathbf{2}}\mathbf{e_y}; \mathbf{b_3} = \mathbf{e_x}$ and $\mathrm{k_L} = 2\sqrt{3}\pi/\lambda_{\rm L}$ (λ_L is the laser wavelength and is 830 nm for the experiment under discussion). With these considerations $V_{\rm lat}$ is the height of the barrier between neighboring sites. The difference between the maximum and minimum values of $V_{\rm hex}(\mathbf{r})$ is $8\ V_{\rm lat}$.

The experiment uses a separate set of lasers to provide strong confinement in the third dimension, $V_{\rm conf}(\mathbf{r})$:

$$V_{\rm conf}(\mathbf{r}) = V_{\rm 1D}\ \cos[\frac{2\pi}{\lambda_{\rm 1D}}\mathrm{z}] \approx \frac{V_{\rm 1D}}{2}(\frac{2\pi}{\lambda_{\rm 1D}})^2\mathrm{z}^2. \tag{3.8}$$

This potential restricts the dynamics to two dimensions and one may take the wavefunction of the BEC in the third direction to be constant and Gaussian. Then the energy can be written as :

$$\begin{aligned} E_{\rm 2D} &= \int d^2\mathbf{r} \sum_{\sigma=1,2} [-\frac{\hbar^2}{2m}\nabla^2\psi_\sigma(\mathbf{r}) + V_\sigma(\mathbf{r})|\psi_i(\mathbf{r})|^2 \\ &+ \frac{U_{\rm 2D}}{2}|\psi_\sigma(\mathbf{r})|^4] + W_{\rm 2D}|\psi_1(\mathbf{r})|^2|\psi_2(\mathbf{r})|^2 \end{aligned} \tag{3.9}$$

where $U_{2D} = U_{3D}\sqrt{\frac{\sqrt{mV_{1D}}\ 2\pi}{\lambda_{1D}\ h}}$ and $W_{2D} = W_{3D}\sqrt{\frac{\sqrt{mV_{1D}}\ 2\pi}{\lambda_{1D}\ h}}$. In the experiment [1], $\lambda_{1D} = \lambda_L = 830$ nm and $V_{1D} = 8.8E_R$. For these parameters, the weakest lattice yielding a Mott state is $V_{lat} \approx 3.5\ E_R$ for two particles per unit cell within the Gutzwiller mean field approximation [6].

I assume a form of $\psi_1(\mathbf{r})$ and $\psi_2(\mathbf{r})$ which is consistent with the time-of-flight measurements :

$$\psi_1(\mathbf{r}) = \sum_k \psi_1(\mathbf{k}) \exp(-i\ \mathbf{k}.\mathbf{r}), \tag{3.10}$$

$$\psi_2(\mathbf{r}) = \sum_k \psi_2(\mathbf{k}) \exp(-i\ \mathbf{k}.\mathbf{r}). \tag{3.11}$$

where $\mathbf{k}$ are the reciprocal lattice vectors of a honeycomb lattice. I insert this variational ansatz into eq.(3.5) and minimize the energy with respect to the set of variational parameters $\psi_1(\mathbf{k})$ and $\psi_2(\mathbf{k})$. I find from my simulations that for all experimental parameters $\psi_1(\mathbf{k}) = \psi_2^*(\mathbf{k})$, where $\psi_2^*(\mathbf{k})$ is the complex conjugate of $\psi_2(\mathbf{k})$. This result is sensible and implies ψ_1 and ψ_2 are related by a lattice translation.

I perform the variational minimization in Fourier space rather than real space (where such minimization is usually done). This is equivalent to solving the Gross-Pitaevskii equation in real space within a single unit cell with periodic boundary conditions. Computationally, I find momentum space to be more efficient. Moreover, the experimental probes are all in momentum space. Similar approaches have been used by other authors [7, 8, 9].

3.4 Method

In k-space, the energy, eq.(3.9) becomes :

$$\begin{aligned}\frac{E_{2D}}{E_R} = \sum_{\{\mathbf{k},\mathbf{k_1},\mathbf{k_2},\mathbf{k_3}\}\epsilon\overline{\mathcal{L}}} \sum_{i=1,2} & [3\ k^2\psi_i^*(\mathbf{k})\psi_i(\mathbf{k}) + V_i(\mathbf{k_1})\psi_i^*(\mathbf{k_2})\psi_i(\mathbf{k_2}-\mathbf{k_1}) \\ & + \frac{U}{2}\psi_i^*(\mathbf{k_1})\psi_i^*(\mathbf{k_2})\psi_i(\mathbf{k_3})\psi_i(\mathbf{k_1}+\mathbf{k_2}-\mathbf{k_3})] \\ & + W\psi_1^*(\mathbf{k_1})\psi_1(\mathbf{k_2})\psi_2^*(\mathbf{k_3})\psi_2(\mathbf{k_1}+\mathbf{k_3}-\mathbf{k_2}), \end{aligned} \tag{3.12}$$

where $\overline{\mathcal{L}}$ stands for the reciprocal lattice i.e $\mathbf{k} = (a_1\mathbf{b_1} + a_2\mathbf{b_2})$, a_1 and a_2 being integers and $k = |\mathbf{k}|$. All energies (V_i, U and W) are expressed in terms of E_R.

While I carried out unrestricted minimizations, my results are best illustrated by considering an ansatz where the low momentum physics is characterized by 2 complex numbers t and z. In particular, I take $\psi_1(\mathbf{k}) = t$ and $\psi_2(\mathbf{k}) = z$ for $\mathbf{k} = \{\mathbf{b_1},\ \mathbf{b_2},\ \mathbf{b_3}\}$ and $\psi_1(\mathbf{k}) = z$ and $\psi_2(\mathbf{k}) = t$ for $\mathbf{k} = \{-\mathbf{b_1},\ -\mathbf{b_2},\ -\mathbf{b_3}\}$. In terms of their real and imaginary parts, I write

$$t = t_r + i\ t_i \text{ and} \tag{3.13}$$

$$z = z_r + i\ z_i. \tag{3.14}$$

As has been mentioned in Section 3.2.2, the order parameter (OP) for the twisted superfluid state is given by:

$$OP = |\frac{|z|^2 - |t|^2}{|z|^2 + |t|^2}| \tag{3.15}$$

For my minimization, I restrict ourselves to $|\mathbf{k}| \leq 6$ giving us 159 complex variational parameters. I find that there are no differences if I use $|\mathbf{k}| \leq 4$ instead. Therefore, I believe my results faithfully reflect what would be found if an infinite number of Brillouin zones were included. I gain further confidence in the

convergence of my results by noting that the fraction of population occupying the $|\mathbf{k}| = 4$ state when $U = 0.05E_R$ and $V_{lat} = 3.8E_R$ is about 0.0001%. It should also be noted that in the absence of interactions, at $V_{lat} = 4E_R$, the real space Wannier functions have width $\frac{1}{k_L}\sqrt{\frac{2}{3}}$ and the probability of having $|\mathbf{k}| \geq 2$ is less than 2 %. Interactions tend to spread out the wavefunction, further reducing the occupation of high $|\mathbf{k}|$ states. In my simulations, I vary U in the range $0.03E_R$ to $0.2E_R$ corresponding to various strengths of the transverse confinement. For the experiment, $U \approx 0.05E_R$. I also vary α in the range 0.08 to 0.3, corresponding to varying amounts of detuning of the laser beams.

3.5 Results

I do not find any evidence for the existence of the Twisted Superfluid state despite an extensive search of the parameter space. Since Eq.(3.12) is a quartic form, it will in general have multiple minima and a number of other stationary points. The most grave concern with my results is that I might not have found the global minimum. To some extent, I can alleviate this concern by noting that the experiment finds a continuous symmetry breaking as a function of lattice depth. It therefore suffices to establish that my solution is a dynamically stable local minimum which is continuously connected to the symmetry-unbroken ground state at $V_{lat} = 0$.

3.5.1 Local Energetic Stability

I check whether whether I have found a true minimum by looking at the eigenvalues of the Hessian H defined by :

$$H_{ij} = \frac{\partial^2 E}{\partial a_i \partial a_j}, \tag{3.16}$$

where a_i and a_j are real variational parameters (corresponding to the real and imaginary parts of $\psi(\mathbf{k})$). I find that for all parameters, the eigenvalues of H are positive. This implies that I have at least found a local minimum. In Figure 3.3, I plot the minimum eigenvalues of the Hessian for different values of the lattice depth (V_{lat}) at the illustrative interaction strength, $U = 0.05E_{\text{R}}$ and $\alpha = 0.14$, for five particles (of each species) per unit cell.

I further illustrate the stability of my theory by doing two separate numerical experiments :

(a) Fix the ratio of z_{r} (Re[z]) to t_{r} (Re[t]) and vary the remaining variational parameters to find the energy minima. I find that the minimum of the energy occurs when $z_{\text{r}} : t_{\text{r}} = 1$ and there are no other local minima. The dotted curve shows this in Figure 3.4.

(b) Fix the ratio of z_{i} (Im[z]) to t_{i} (Im[t]) and vary the remaining variational parameters to find the energy minima. I find that the minimum of the energy occurs when $z_{\text{i}} : t_{\text{i}} = 1$ and there are no other local minima. The solid curve shows this in Figure 3.4.

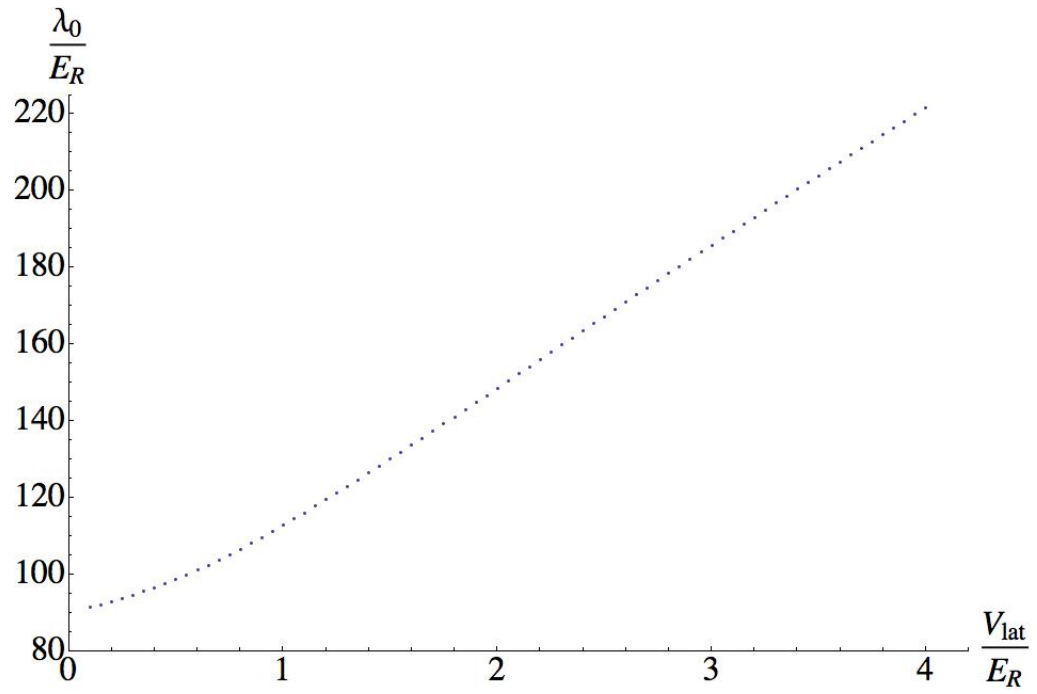

Figure 3.3: Minimum eigenvalue of the Hessian, λ_0 in the Normal superfluid phase plotted against the lattice depth, V_{lat} (in units of E_{R}) when $U = 0.05E_{\text{R}}$ and 5 particles (of each species) are present per unit cell. All the eigenvalues of the Hessian are positive, thereby showing the stability of the normal phase. I conclude that there is no Twisted superfluid state for these potential depths. This result is illustrative of all parameter ranges I explored.

I conclude that there is no second order phase transition within mean field theory.

3.5.2 Local Dynamic Stability

I also check whether the minimum found is unstable against perturbations. This is done by looking at the Gross-Pitaevskii equation :

$$i\hbar\frac{\partial\psi}{\partial t} = \frac{\partial E}{\partial\psi^*} \tag{3.17}$$

This would imply :

$$i\hbar\frac{\partial\delta a_j}{\partial t} = \frac{\delta E}{\delta a_j} \approx \sum_l \frac{\partial^2 E}{\partial a_j \partial a_l}\delta a_l \tag{3.18}$$

Taking the real and imaginary parts of both sides, I get the eigenvalue equations

$$\hbar\omega\ u = Mu \tag{3.19}$$

where,

$$M = \begin{bmatrix} \text{Re}[H] & \text{-Im}[H] \\ \text{Im}[H] & \text{Re}[H] \end{bmatrix}$$

I look at the eigenvalues of this matrix, M. A complex eigenvalue would signify the presence of a mode which will grow with time, thus rendering this ground state unstable. I find that all the eigenvalues are real. Thus, the minimum that I have found is also dynamically stable. This is a generic feature of quantum systems: Energetic stability implies dynamic stability [10].

3.6 Discussion

Given that my mean-field treatment of Eq. (3.5) fails to reproduce the experimental observations, I must now confront the question of what additional physics is needed to produce a twisted superfluid state. In this section, I present a tight-binding model which has a twisted superfluid ground state and discuss connections with my approach. Namely, consider a Hamiltonian:

$$H = \sum_{<ij>} \left(-t(\hat{a}^\dagger_{i\uparrow}\hat{a}_{j\uparrow} + \hat{a}^\dagger_{i\downarrow}\hat{a}_{i\downarrow}) + t_{cf}(\hat{a}^\dagger_{i\uparrow}\hat{a}^\dagger_{j\downarrow}\hat{a}_{j\uparrow}\hat{a}_{i\downarrow}) + h.c. \right). \tag{3.20}$$

Here, $a_{i\sigma}$ annihilates a particle labelled by the spin index σ on site i, and the sum is over all nearest neighbor sites of a honeycomb lattice. The parameters t and

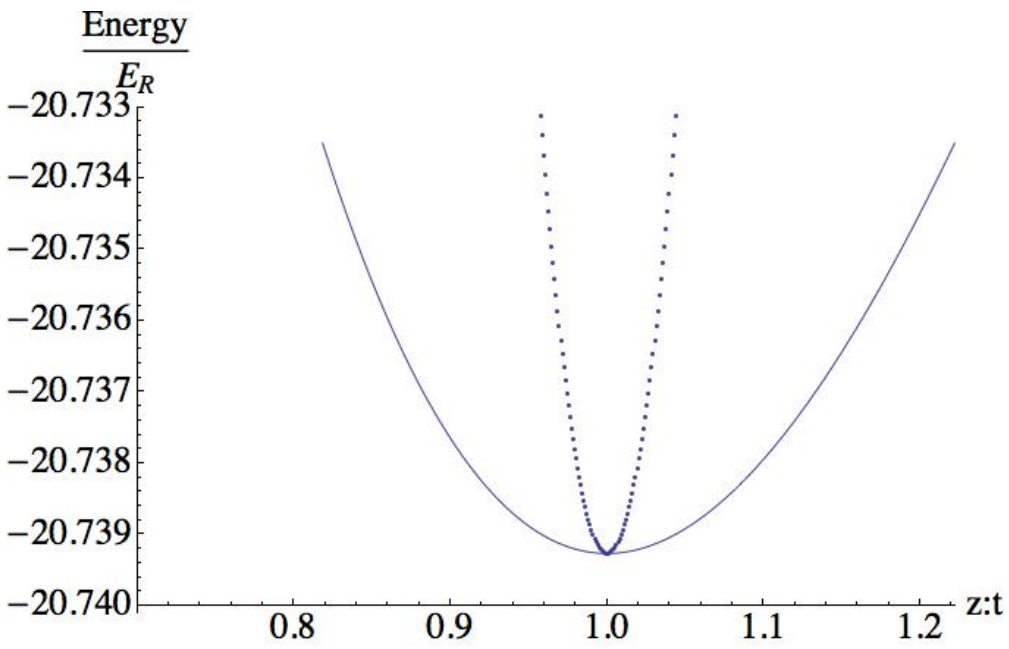

Figure 3.4: Slice through the energy landscape at $V_{\text{lat}} = 1.8E_{\text{R}}$ and $U = 0.05E_{\text{R}}$ and 5 particles (of each species) per unit cell. Dotted curve: The ratio Re[z]:Re[t]is varied and the energy is found by minimizing with respect to the other variational parameters. Solid curve: Same, but with varying Im[z]:Im[t]. I find that the overall energy minimum occurs when Re[z] = Re[t] and Im[z] = Im[t].

t_{cf} represent single particle and counter-flow hopping. I consider a mean-field ansatz where $\hat{a}_{\text{j}\sigma}$ is replaced by a c-number, which can take one of two values, depending on which sub-lattice site j belongs to (see Fig. 3.1):

$$a_{\text{j}\uparrow} = \sqrt{n_+}\ \exp(-i\ \delta/2) \quad \text{sublattice A} \tag{3.21}$$

$$a_{\text{j}\uparrow} = \sqrt{n_-}\ \exp(+i\ \delta/2) \quad \text{sublattice B} \tag{3.22}$$

and

$$a_{\text{j}\downarrow} = \sqrt{n_-}\ \exp(+i\ \delta/2) \quad \text{sublattice A} \tag{3.23}$$

$$a_{\text{j}\downarrow} = \sqrt{n_+}\ \exp(-i\ \delta/2) \quad \text{sublattice B} \tag{3.24}$$

A twisted superfluid corresponds to $\delta \neq 0$ and physically can be interpreted as a state where there are microscopic single particle single particle currents, which are precisely balanced by microscopic counterflow currents. The mean-field energy per site is :

$$E = \left(-12t\sqrt{n_+ n_-}\cos(\delta) + 6t_{\rm cf}\ n_+ n_- \cos(2\delta)\right). \tag{3.25}$$

The lowest energy state has $\delta \neq 0$ if :

$$2t_{\rm cf}(n_+ n_-) > t\sqrt{n_+ n_-} \tag{3.26}$$

My model in Eq. (3.5) contains terms of the form as those in Eq. (3.25). For deep lattices [11],

$$t \sim |a|^{-3/2}\ \exp(-\pi\sqrt{V_{\rm lat}/E_{\rm R}}/2) \tag{3.27}$$

and

$$t_{\rm cf} \sim |a|^{-3}\ \exp(-\pi\sqrt{V_{\rm lat}/E_{\rm R}}), \tag{3.28}$$

where a is the distance between nearest neighbors. The exponential suppression of $t_{\rm cf}$ means that for any reasonable particle density, Eq.(3.26) is not satisfied. On the other hand, quantum fluctuations suppress single particle hopping more than counterflow [12, 13, 14, 15, 16], and a beyond mean field theory treatment of Eq.(3.5) could yield a twisted superfluid. Thus, the observations of Soltan-Panahi *et al.* [1] may be evidence of non-mean field physics. Other explanations of non-mean field physics leading to a twisted superfluid can be found in refs.[17, 18, 19].

An alternate scenario is that once all the external potentials are turned off, interaction effects in the first milliseconds changes the momentum space wavefunction of the two component BEC and this results in the observed symmetry breaking in momentum space.

3.7 Update

In a follow up experiment, the Hamburg group performed a comprehensive study of the time-of-flight images of a single component and two-component BEC of ^{87}Rb atoms loaded in a honeycomb lattice [20]. They found that a breaking of the six-fold rotational symmetry in time-of-flight images was observed only when the different components experience different lattice potentials. For instance, a two-component BEC of ^{87}Rb atoms with atoms in the state $|2,-2\rangle$ and $|1,-1\rangle$ experience the potentials $V_{\text{hex}}(\mathbf{r}) + \alpha B_{\text{eff}}(\mathbf{r})$ and $V_{\text{hex}}(\mathbf{r}) - \alpha B_{\text{eff}}(\mathbf{r})$. When all the external potentials are turned off and the gas is allowed to expand, then the time-of-flight images of the expanding atom cloud exhibits symmetry breaking. In contrast, a 2 component BEC of atoms in non-magnetic hyperfine states (like $|1,0\rangle$ and $|2,0\rangle$) where both species experience the same potential $V_{\text{hex}}(\mathbf{r})$ does not show any symmetry breaking in time-of-flight images. Furthermore, a single component BEC never exhibits symmetry breaking in time-of-flight images.

In order to explore this issue further, the experimentalists carried out another protocol: they removed the $|2,-2\rangle$ species from the two component BEC at different times after turning off the external trapping potentials. In this case, the experimentalists observed that the symmetry breaking was not observed if one of the components was removed right after all the external potentials are turned off. However, if both components are present during the expansion, then the symmetry breaking develops over 1.2 ms and then persists upto 18 ms. All of these observations led the experimentalists to conclude that the observed symmetry breaking was a manifestation of inter-species interactions during the time-of-flight.

The experimental results can be explained theoretically by numerically integrating the Gross-Pitaevskii equation [20]. A simple model for understanding the observed momentum space symmetry breaking is illustrated in fig.. The basic idea is to consider a two-component BEC where one of the components preferentially occupy the A sub-lattice (I will label these atoms as 'A' atoms) and the other component occupies the B sub-lattice (the 'B' atoms). When the gas is expanding after all the potentials are turned off 'A' atoms interact with more 'B' atoms in the reciprocal lattice direction $\mathbf{b_1}$ than $\mathbf{b_2}$. The scenario is inverted for the 'B' atoms. This kind of momentum-dependent scattering leads to the observed breaking of the six-fold symmetry in the time-of-flight data.

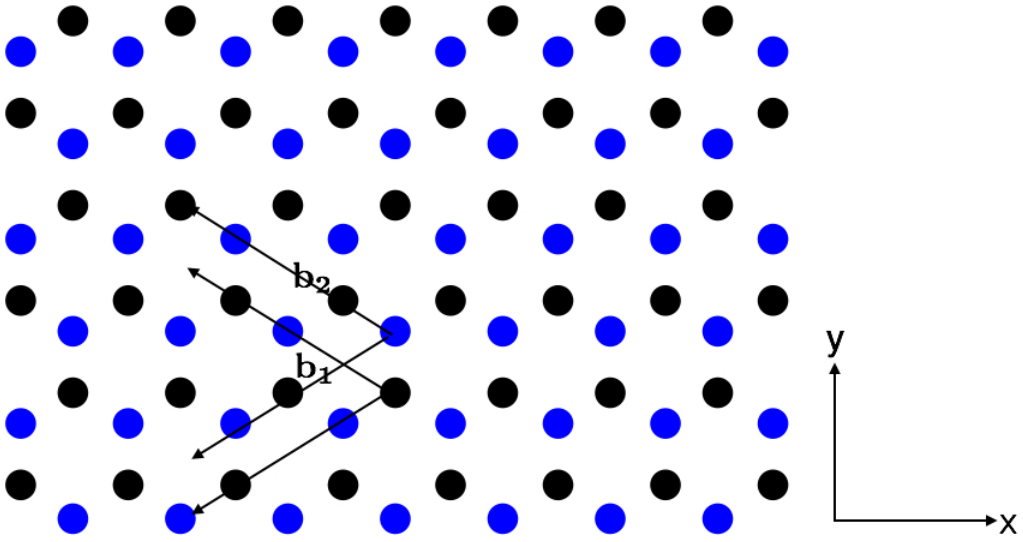

Figure 3.5: Scattering process for a 2 component BEC during time-of-flight expansion. The A sub-lattice is labelled by the color blue while the B sub-lattice is labelled by black. During time-of-flight expansion the 'A' atoms experience more lattice sites the reciprocal lattice direction $\mathbf{b_1}$ than $\mathbf{b_2}$. The effect is reversed for the'B' atoms. These scattering processes causes redistribution of the atoms and leads to the observed symmetry breaking in time-of-flight.

BIBLIOGRAPHY

[1] P. Soltan-Panahi, D.-S. Lühmann, J. Struck, P. Windpassinger and K. Sengstock, Nature Physics **8**, 71-75 (2012).

[2] J. Struck, C. Ölschläger, R. Le Targat, P. Soltan-Panahi, A. Eckardt, M. Lewenstein, P. Windpassinger and K. Sengstock, Science **333**, 996 (2011).

[3] G. Wirth, M. Ölschläger and A. Hemmerich, Nature Physics **7**, 147-153 (2011).

[4] M. Ölschläger, G. Wirth and A. Hemmerich, Phys. Rev. Lett. **106**, 015302 (2011).

[5] J. N. Kupferschmidt and E. J. Mueller, Phys. Rev. A **82**, 023618 (2010).

[6] P. Soltan-Panahi, J. Struck, P. Hauke, A. Bick, W. Plenkers, G. Meineke, C. Becker, P. Windpassinger, M. Lewenstein and Klaus Sengstock, Nature Physics **7**, 434-440 (2011).

[7] E. J. Mueller, Phys. Rev. A **66**, 063603 (2002)

[8] Z. Chen and B. Wu, Phys. Rev. Lett. **107**, 065301 (2011).

[9] H-Y Hui, R. Barnett, J. V. Porto and S. Das Sarma, Phys. Rev. A **86**, 063636 (2012).

[10] C. J. Pethick and H. Smith, *Bose-Einstein Condensation in Dilute Gases*. Cambridge University Press, Cambridge (2002).

[11] I. Bloch, J. Dalibard and W. Zwerger, Rev. Mod. Phys. **80**, 885 (2008).

[12] A. B. Kuklov and B.V. Svistunov, Phys. Rev. Lett. **90**, 100401 (2003).

[13] A. B. Kuklov, Nikolay Prokof'ev and B.V. Svistunov, Phys. Rev. Lett. **92**, 050402 (2004).

[14] E. Altman, W. Hofstetter, E. Demler and M. D. Lukin, New J. Phys. **5**, 113 (2003)

[15] A. Hu, L. Mathey, I. Danshita, E. Tiesinga, C. J. Williams, C. W. Clark, Phys. Rev. A **80**, 023619 (2009).

[16] T. Ohgoe and N. Kawashima, Phys. Rev. A **83**, 023622 (2011).

[17] O. Jürgensen, K. Sengstock, and D-S Lühmann, Scientific Reports **5**,12912 (2015).

[18] L. Cao, S. Krönke, J. Stockhofe, P. Schmelcher, J. Simonet, K. Sengstock, and D-S Lühmann, Phys. Rev. A **91**, 043639 (2015).

[19] D-S Lühmann, Phys. Rev. A 94, 011603(R) (2016).

[20] M. Weinberg, O. Jürgensen, C. Ölschlger, D-S Lühmann, K. Sengstock, and Juliette Simonet, Phys. Rev. A **93**, 033625 (2016).

CHAPTER 4

STABILITY OF A FLOQUET BOSE-EINSTEIN CONDENSATE IN A ONE-DIMENSIONAL OPTICAL LATTICE

This chapter is adapted from "Stability of a Floquet Bose-Einstein condensate in a one-dimensional optical lattice" by Sayan Choudhury and Erich J. Mueller, published in Physical Review A, **90**, *013621 (2014).*

4.1 Overview

Motivated by recent experimental observations [Parker, Ha, and Chin, Nat. Phys. 9, 769 (2013)], I analyze the stability of a Bose-Einstein condensate (BEC) in a one-dimensional lattice subjected to periodic shaking. In such a system there is no thermodynamic ground state, but there may be a long-lived steady state, described as an eigenstate of a "Floquet Hamiltonian". I calculate how scattering processes lead to a decay of the Floquet state. I map out the phase diagram of the system and find regions where the BEC is stable and regions where the BEC is unstable against atomic collisions. I show that Parker *et al.* performed their experiment in the stable region, which accounts for the long lifetime of the condensate.

4.2 Introduction

Recently there has been much interest in periodically driven quantum systems (Floquet systems), as time dependent forces provide a new knob for accessing

interesting phenomena. Some of these phenomena are analogous to physics seen in static systems (e.g edge modes in Floquet topological insulators and artificial gauge fields in cold atom systems) [1, 2, 3, 4, 5, 6, 7, 8, 9, 10, 11, 12, 13, 14, 15, 16, 17, 18, 19, 20, 21, 22, 23, 24], but other phenomena are unique to the non-equilibrium system (such as ac-induced tunneling and anamalous edge states in insulators with zero Chern number) [25, 26, 27, 28, 29]. In the cold atom context, particular interest has focussed on bosonic systems, as they are most accessible experimentally. Parker *et al.* recently observed an interesting analog of a ferromagnetic transition in a Bose gas trapped in a shaken one dimensional optical lattice [30]. Here, I theoretically analyze their experiment, studying the stability of their condensate. I find both stable and unstable regions. Consistent with the experimental observation of background gas collision limited lifetimes, I find that under the experimental conditions the condensate is stable against atomic collisions. Similar considerations will be important for any cold atom experiments on periodically driven systems.

The Schrödinger equation with periodic driving is analyzed using Floquet theory [31, 32]. Prior studies of periodically driven lattice systems have largely ignored interactions, focussing instead on how the single-particle physics is renormalized by the driving. For example, the band curvature and effective mass can be tuned with this technique [33, 34, 35]. One can even invert a band, effectively flipping the sign of the hopping matrix elements. This latter feature has been used to realize models of frustrated magnets [3, 4]. More sophisticated driving techniques can be used for engineering artificial gauge fields [5, 6]. The driving can cause band-crossing leading to non-trivial topological numbers [7, 8, 9, 10, 11, 12, 13]. Extending these results to include interactions is impor-

tant. Here, I look at atom-atom scattering. In the context of solid state physics, there has been some consideration of electron-phonon scattering [14, 15]. There also have been studies of non-dissipative interaction physics [36]. My work has connections with broader studies of heating in periodically driven systems [37, 38, 39, 40, 41, 42, 43] .

In Section 4.3, I describe the experiment and my main results about the stability of the condensate against atom-atom scattering. In section 4.4.1 and 4.4.2, I derive the Floquet spectrum and in Sec. 4.4.3, I predict the decay rate of a Floquet BEC.

4.3 Model

In Ref. [30], Parker et al. load a Bose-Einstein condensate (BEC) of 25,000 ^{133}Cs atoms into a one-dimensional optical lattice. This lattice is then shaken at a frequency ω, where $\omega \approx (7.3 \times 2\pi)$ kHz is slightly larger than $\frac{\Delta_0}{\hbar}$: Δ_0 is the energy difference between the first and the second band at $k = 0$. From the experimental parameters, I estimate $\Delta_0 \approx 4.96\ E_R$, where $E_R = \frac{h^2}{2m\lambda_L^2}$ (λ_L is the laser wavelength and is 1064 nm for this experiment). The amplitude of shaking is slowly ramped up to a final value near 15-100 nm for a time of 5-100 ms. The shaking continues for 50-100 ms before the lattice and all the confinement is turned off, allowing the condensate to expand. By looking at the time of flight expansion images, the experimentalists determine if the condensate is at zero-momentum or finite momentum. By analogy with an Ising ferromagnet, where the condensate momentum is mapped onto the magnetization, they refer to these scenarios as

paramagnetic and ferromagnetic. They also describe the finite momentum condensate as a $\mathbb{Z}_2$ condensate.

In the frame of the moving lattice, the Hamiltonian for the driven system is given by $H = H_0(t) + H_{\text{int}}$ [1], where

$$\begin{aligned} H_0(t) &= \int dx\ \Psi^\dagger(x)\left(\frac{-\hbar^2}{2m}\frac{d^2}{dx^2} + V_0\sin^2\left(\frac{2\pi x}{\lambda_L}\right)\right)\Psi(x) \\ &+ \int dx\ \Psi^\dagger(x)\left(xF_0\cos(\omega t)\right)\Psi(x), \end{aligned} \tag{4.1}$$

$$H_{\text{int}} = \frac{g}{2}\sum_{i1,i2,i3,i4}\int dx\ \Psi^\dagger_{i1}(x)\Psi^\dagger_{i2}(x)\Psi_{i3}(x)\Psi_{i4}(x). \tag{4.2}$$

The atomic mass is m, the force from the periodic shaking is $F_0\cos(\omega t)$ and $g \approx \frac{4\pi\hbar^2 a_s}{m d_\perp^2}$ is the 1-D effective interaction strength: a_s is the scattering length and $d_\perp$ is the length-scale of transverse confinement.

The most intuitive way to analyze such a periodically driven system is to imagine observing the evolution of the system stroboscopically: i.e at times $t, t+T, t+2T, \ldots t+nT$; where $T = \frac{2\pi}{\omega}$ is the time-period of the Hamiltonian and n is an integer. The time-evolution operator for n-periods is the n'th power of the time-evolution operator for one period:

$$U(nT) = \mathcal{T}\exp\left(-i\int_0^{nT} dt\ H(t)/\hbar\right) = U(T)^n \tag{4.3}$$

It is therefore natural to define an effective Hamiltonian, H_{eff}, such that

$$U(T) = \exp(-iH_{\text{eff}}T/\hbar) \tag{4.4}$$

The interested reader will find a more detailed derivation of H_{eff} in appendix A.

In analogy to describing the labeling of Bloch states as "quasi-momentum", the eigenvalues of H_{eff} are "quasi-energies". The operator H_{eff} is not unique, as its eigenvalues (i.e "quasi-energies") are only defined up to multiples of $\hbar\omega$. One can associate with each Bloch band of the undriven system, an infinite ladder of Floquet bands, separated by energies $\hbar\omega$. For the rest of the paper, I refer to the Bloch band connected adiabatically to the first (second) Bloch band in the limit of zero shaking as the ground (first excited) band.

Figure 4.1 shows typical Floquet bands for experiments analogous to Parker *et al.*'s. The ground band and the first excited band are shown by solid lines, their periodic repetitions by dashed lines. As is clear from the magnified views on the right, hybridization leads to a double well structure for the ground band. Arrows illustrate momentum and energy conserving scattering processes which can destabilize a BEC in one of the minima. In Section 4.4, I calculate the rate of scattering by Fermi's Golden rule [44]. These scatterings are made possible due to the periodicity of energy for Floquet bands.

As I explain in detail in Sec 4.4, I use phase-space arguments to construct the phase diagrams in Fig.4.3 and Fig.4.4. As already introduced, I label phases as ferromagnetic or paramagnetic, depending on the momentum of the lowest energy Bloch state in the first band. In these diagrams, I also show if a condensate in that state is stable against 2-body collisions. My model contains three relevant parameters: the detuning ($\hbar\omega - \Delta_0$), the lattice depth V_0 and the shaking amplitude F_0. Fig.4.3 shows a slice through the three dimensional phase diagram at $F_0 = 0$. I find that depending on the parameters, the paramagnet may

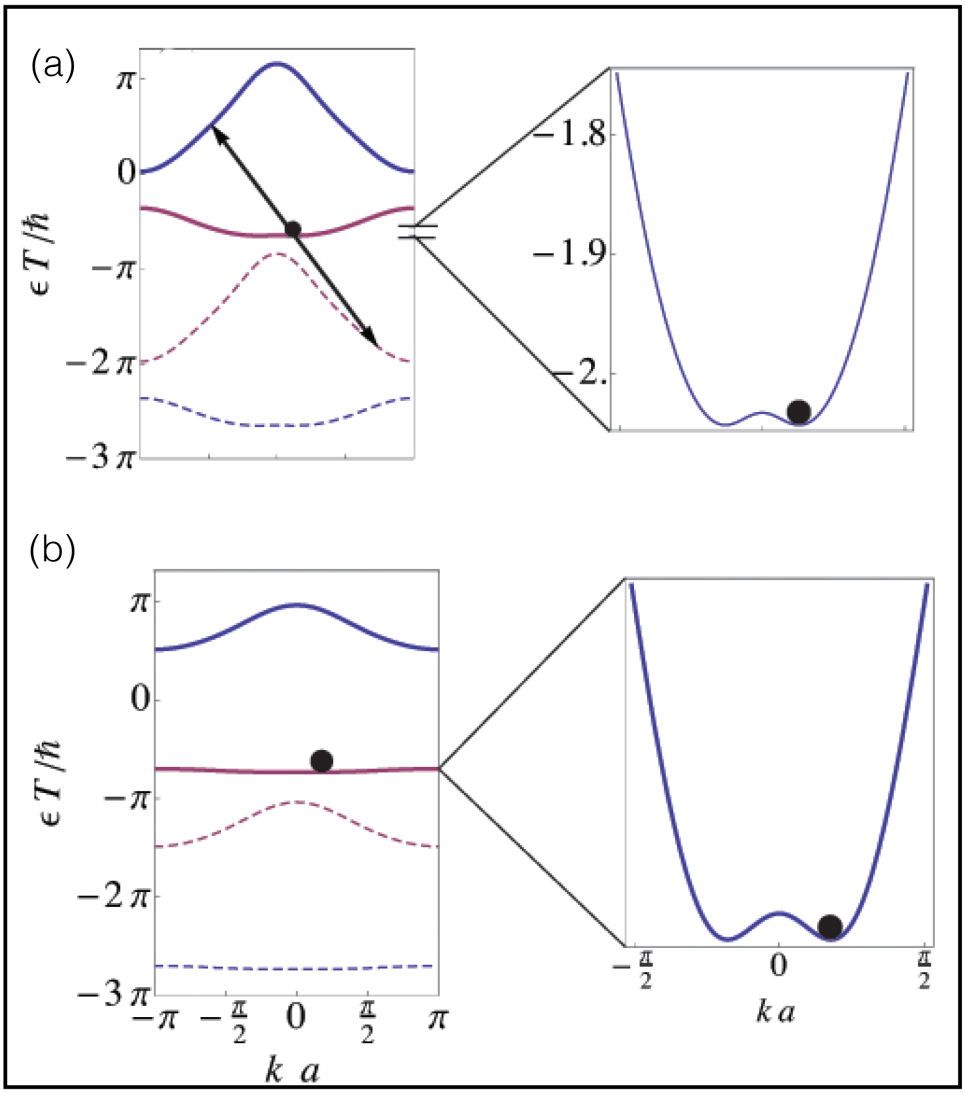

Figure 4.1: Floquet Spectra of shaken 1 D lattices for lattice depths of $V_0/E_R = 2.02$ and 7.The shaking frequency is blue detuned. The parameters in (b) are similar to those in Ref. [30]. Quasi-momentum, k and Quasi-energy, ϵ are measured in terms of the lattice spacing a and the period, $T = \frac{2\pi}{\omega}$. Solid and dashed lines represent bands and their periodic repetition and circles show location of band minima. Right panels are magnified views. Arrows represent scattering processes which cause a condensate at the band minima to decay. In (a) this is an intra-band scattering process, where the final state of the scattered particles have the same Bloch index. Case (b) is stable: there are no 2-body processes that conserve energy and momentum.

be stable or unstable. Increasing the drive strength hybridizes the bands.

In principle, there may be kinematically allowed decay channels involving higher bands, but the rates will be very low due to small matrix elements. For very strong interactions, one should also include mean-field shifts to the band-structure. These are irrelevant for Ref.[30], where the onsite interaction energy is $U_H = 0.001E_R$ and the bandwidth $4J = 0.16E_R$.

4.3.1 Floquet Spectrum

To derive the Floquet spectrum, I map the moving frame continuum Hamiltonian $H_0(t)$ onto a tight binding model. This is accomplished by expanding the field operator $\Psi(x)$ in terms of the Wannier functions for the two lowest bands of H_0 in the limit of vanishing F_0:

$$\Psi(x) = \sum_j w_1(x - x_j)a_j + w_2(x - x_j)b_j, \tag{4.5}$$

where a_j and b_j are bosonic annihilation operators and with the Wannier functions centered at the lattice site n given by:

$$w_\sigma(x - x_n) = \frac{1}{\sqrt{N}} \sum_k \exp(-inka)\psi_\sigma(x, k), \tag{4.6}$$

where N is the number of sites. The Bloch wave functions, $\psi_\sigma(x, k)$ are eigenstates of H_0 (with $F_0 = 0$) with

$$\psi_\sigma(x + a, k) = \exp(-ika)\psi_\sigma(x, k). \tag{4.7}$$

The arbitrary global phase of $\psi_\sigma(x+a,k)$ is fixed using the recipe given in Ref. [45]. The resulting tight-binding model is:

$$H_0(t) = \sum_{ij}\left(-t_{ij}^{(1)}a_i^\dagger a_j + t_{ij}^{(2)}b_i^\dagger b_j + h.c.\right) + \sum_j A_j(t), \tag{4.8}$$

where,

$$\begin{aligned} A_j(t) &= F_0\cos(\omega t)\left(x_j\left(a_j^\dagger a_j + b_j^\dagger b_j\right) + \chi_j a_j^\dagger b_j + \chi_j^* b_j^\dagger a_j\right) \\ \chi_j &= \int dx\ \ x w_1^*(x-x_j)w_2(x-x_j) \\ t_{ij}^{(1)} &= \int dx\ \ w_1^*(x-x_i)\left(\frac{-\hbar^2}{2m}\frac{d^2}{dx^2} + V(x)\right)w_1^*(x-x_j) \\ t_{ij}^{(2)} &= \int dx\ \ w_2^*(x-x_i)\left(\frac{-\hbar^2}{2m}\frac{d^2}{dx^2} + V(x)\right)w_2^*(x-x_j) \end{aligned} \tag{4.9}$$

with $V(x) = V_0\sin^2\left(\frac{2\pi x}{\lambda_L}\right)$. Equivalently, I find t_{ij}^σ by fitting the dispersion obtained from the tight-binding model to the dispersion of the Bloch bands. For the experimental lattice strength, the ground band is well approximated by a model with nearest neighbor hopping. However, to properly account for the greater curvature of the first excited band, one needs to take into account longer range hopping (up to $|i-j| \le 3$).

I now rotate my basis, taking $|\psi\rangle \to U_c(t)|\psi\rangle$ with:

$$U_c(t) = \exp\left(-\frac{i}{\hbar}\int_0^t \sum_j x_j F_0\cos(\omega t)(a_j^\dagger a_j + b_j^\dagger b_j)\right) \tag{4.10}$$

Under this unitary transformation, the Hamiltonian becomes:

$$\begin{aligned} H_0'(t) &= U_c H_0(t) U_c^{-1} - i\hbar U_c\partial_t U_c^{-1} \\ &= \sum_{ij}\left(-J_{ij}^{(1)}(t)a_i^\dagger a_j + J_{ij}^{(2)}(t)b_i^\dagger b_j + h.c.\right) + \sum_j F_0\cos(\omega t)\left(\chi_j a_j^\dagger b_j + \chi_j^* b_j^\dagger a_j\right) \\ &= \sum_k\sum_m \cos(mka)\left(-J_m^{(1)}(t)a_k^\dagger a_k - J_m^{(2)}(t)b_k^\dagger b_k\right) + \sum_k F_0\cos(\omega t)\left(\chi_j a_k^\dagger b_k + \chi_j^* b_k^\dagger a_k\right) \end{aligned} \tag{4.11}$$

where,

$$\begin{aligned} J_{ij}^{\sigma}(t) &= t_{ij}^{\sigma} \exp(-iF_0 \frac{\cos(\omega t)}{\hbar\omega}(x_i - x_j)) \\ &= t_{ij}^{\sigma} \exp(-iF_0 \frac{\cos(\omega t)}{\hbar\omega} a(i-j)), \end{aligned} \tag{4.12}$$

the lattice spacing is a and $m = |i - j| = \{1, 2, 3\}$. I numerically calculate the time evolution operator, $U(T)$ by integrating $i\hbar\partial_t U = HU$ from $t = 0$ to $t = T = \frac{2\pi}{\omega}$ with the boundary condition $U(0) = \mathbb{1}$. The "quasi-energies", ϵ are given by the eigenvalues of the matrix $(i\hbar/T)\log[U(T)]$. I stress again that since, a logarithm has an infinite number of branches, the energy spectrum is unbounded. Typical results are shown in Fig.4.1.

4.3.2 Rotating Wave Approximation

While the scattering rate may be calculated by the Floquet formalism, I can simplify the argument by making a Rotating Wave Approximation which is the leading order expansion in $F_0 a/\hbar\omega$. I will calculate the rates in the region where $\frac{F_0 a}{\hbar\omega} \approx 0.005$. In this limit, Eq.(6.24) reduces to $J_{ij}^{\sigma}(t) = t_{ij}^{\sigma}$ is time-independent. Thus, I obtain an effective Hamiltonian :

$$H_{\text{eff}}(k) = \sum_k \left(E_k^{(1)} a_k^\dagger a_k + E_k^{(2)} b_k^\dagger b_k \right) + \sum_k F_0 \left(\exp(-i\omega t)\chi_j a_k^\dagger b_k + \exp(i\omega t)\chi_j^* b_k^\dagger a_k \right),$$

where

$$\begin{aligned} E_k^{(1)} &= -\sum_m \cos(mka) t_m^0 \text{ and} \\ E_k^{(2)} &= -\sum_m \cos(mka) t_m^{(1)}, \end{aligned}$$

where $t_m^\sigma = t_{i,i+m}^\sigma$ and is the same for any site i since the system is homogenous. Further, under the canonical transformation, $U = \exp\left(i\omega t\ b_k^\dagger b_k\right)$, the Hamiltonian takes the form:

$$H_{\text{eff}}(k) = \sum_k \left(E_k^{(1)} a_k^\dagger a_k + (E_k^{(2)} - \hbar\omega) b_k^\dagger b_k\right) + \sum_k F_0 \left(\chi_j a_k^\dagger b_k + \chi_j^* b_k^\dagger a_k\right) \tag{4.13}$$

I use this Hamiltonian for calculating the scattering rate using Fermi's golden rule.

4.4 Scattering Rate

Since Eq.(4.13) is time-independent, I can use Fermi's golden rule [44] to calculate the rate for two particles to scatter from initial state $|\psi_i\rangle$ to final state $|\psi_f\rangle$ as:

$$\frac{dN}{dt} = \frac{2\pi}{\hbar} \sum_n |\langle\psi_f|H_{\text{int}}|\psi_i\rangle|^2 \delta(E_f - E_i), \tag{4.14}$$

For my calculation, $|\psi_i\rangle$ corresponds to the BEC at momentum k_0, while $|\psi_f\rangle$ has two particles outside of the condensate:

$$|\psi_i\rangle = \frac{(\Phi_1^\dagger(k_0))^N}{\sqrt{N!}}|\text{vac}\rangle$$

and

$$|\psi_f\rangle = \frac{(\Phi_{i_1}^\dagger(k_0+q))(\Phi_{i_2}^\dagger(k_0-q))(\Phi_1^\dagger(k_0))^{N-2}}{\sqrt{(N-2)!}}|\text{vac}\rangle$$

where $\Phi_i^\dagger(k)$ is the boson creator operator at momentum k is the dressed band i. Kitagawa *et al.* [14] generalize Eq.(4.14) to the situation where the rotating wave approximation breaks down.

I expand the field operator in terms of the Bloch functions in Eq. (4.7),

$$\Psi_\sigma(x) = \sum_k \overline{\Phi_\sigma}(k)\psi_\sigma(x,k). \tag{4.15}$$

This yields an interaction Hamiltonian of the form

$$\begin{aligned}\frac{H_{\rm int}}{g} &= \frac{1}{2}\left(\sum_j \int_0^L dx\ \Psi_j^\dagger(x)\Psi_j^\dagger(x)\Psi_j(x)\Psi_j(x)\right) + 2\left(\int_0^L dx\ \Psi_1^\dagger(x)\Psi_2^\dagger(x)\Psi_1(x)\Psi_2(x)\right) \\ &= \frac{1}{2}\left(\sum_{\{k\},j} \Gamma^{k_1k_2k_3k_4}_{j\ j\ j\ j}\overline{\Phi_j}^\dagger(k_1)\overline{\Phi_j}^\dagger(k_2)\overline{\Phi_j}(k_3)\overline{\Phi_j}(k_4)\right) + 2\left(\sum_{\{k\}} \Gamma^{k_1k_2k_3k_4}_{1\ 2\ 1\ 2}\overline{\Phi_1}^\dagger(k_1)\overline{\Phi_2}^\dagger(k_2)\overline{\Phi_1}(k_3)\overline{\Phi_2}(k_4)\right).\end{aligned} \tag{4.16}$$

where, the index j labels the Bloch band and $\{k\} = \{k_1, k_2, k_3, k_4\}$. The matrix elements are :

$$\Gamma^{k_1k_2k_3k_4}_{i_1i_2i_3i_4} = \int_0^L dx\ \psi^*_{i_1}(x,k_1)\psi^*_{i_2}(x,k_2)\psi_{i_3}(x,k_3)\psi_{i_4}(x,k_4).$$

$\Gamma^{k_1k_2k_3k_4}_{i_1i_2i_3i_4}$ vanishes unless $k_1 + k_2 = k_3 + k_4 + 2\pi m/a$ for some integer m.

The matrix element in Fermi's Golden rule takes the form:

$$\begin{aligned}|\langle\psi_f|H_{\rm int}|\psi_i\rangle|^2 &= N(N-1)\frac{g^2}{4}\sum_q |\sum_{i1i2} \Gamma^{k_0+qk_0-qk_0k_0}_{i_1\ i_2\ 1\ 1}|^2 \\ &\approx N^2\frac{g^2}{4}\sum_q |\sum_{i1i2} F^{qk_0}_{i_1i_2}|^2 \\ &= N^2\frac{g^2}{4}\frac{L}{2\pi}\int dq I^{qk_0}\end{aligned} \tag{4.17}$$

where,

$$I^{qk_0} = |\sum_{i1i2} F^{qk_0}_{i_1i_2}|^2$$

Hence, I see that the scattering rate is given by:

$$\begin{aligned}
\frac{dN}{dt} &= \sum_{nj_1j_2} \frac{2\pi}{\hbar}\frac{L}{2\pi}N^2\frac{g^2}{4}\int dq I^{qk_0}\delta(E_f - E_i) \\
&= \sum_{nj_1j_2} \frac{N^2g^2L}{4\hbar}\int dE_f \frac{dq}{dE_f} I^{qk_0}\delta(E_f - E_i) \\
&= \sum_{nj_1j_2} \frac{g^2}{4\hbar E_R}\frac{N^2}{La}L^2\int dE_f \frac{d(qa)}{d(E_f/E_R)} I^{qk_0}\delta(E_f - E_i) \\
&= \frac{g^2}{4\hbar E_R}\frac{N^2}{La}\Gamma, \qquad (4.18)
\end{aligned}$$

which defines the intensive dimensionless quantity Γ, which depends only on the lattice geometry, the shaking frequency and the shaking strength. All of these parameters can be tuned in the experiment The floquet BEC is stable wherever $\Gamma = 0$. One can use purely geometric arguments to find the region of phase space where the floquet BEC is stable or unstable. The crux of this geometric argument is the following. In the BEC, bosons macroscopically occupy the state with momentum k_0 (and energy $\epsilon^{(1)}_{k_0}$). Interaction drives energy-momentum conserving scattering processes that result in particles scattering out of the BEC. Each of these processes involve two particles scattering out of the BEC into a state with energy E_1 (and momentum $k_0 - k_1$) and a state with energy $2\epsilon^{(1)}_{k_0} - E_1$ (and momentum $k_0 + k_1$). The BEC is unstable wherever phase space is available for such scattering processes. I illustrate this argument in Fig.4.2.

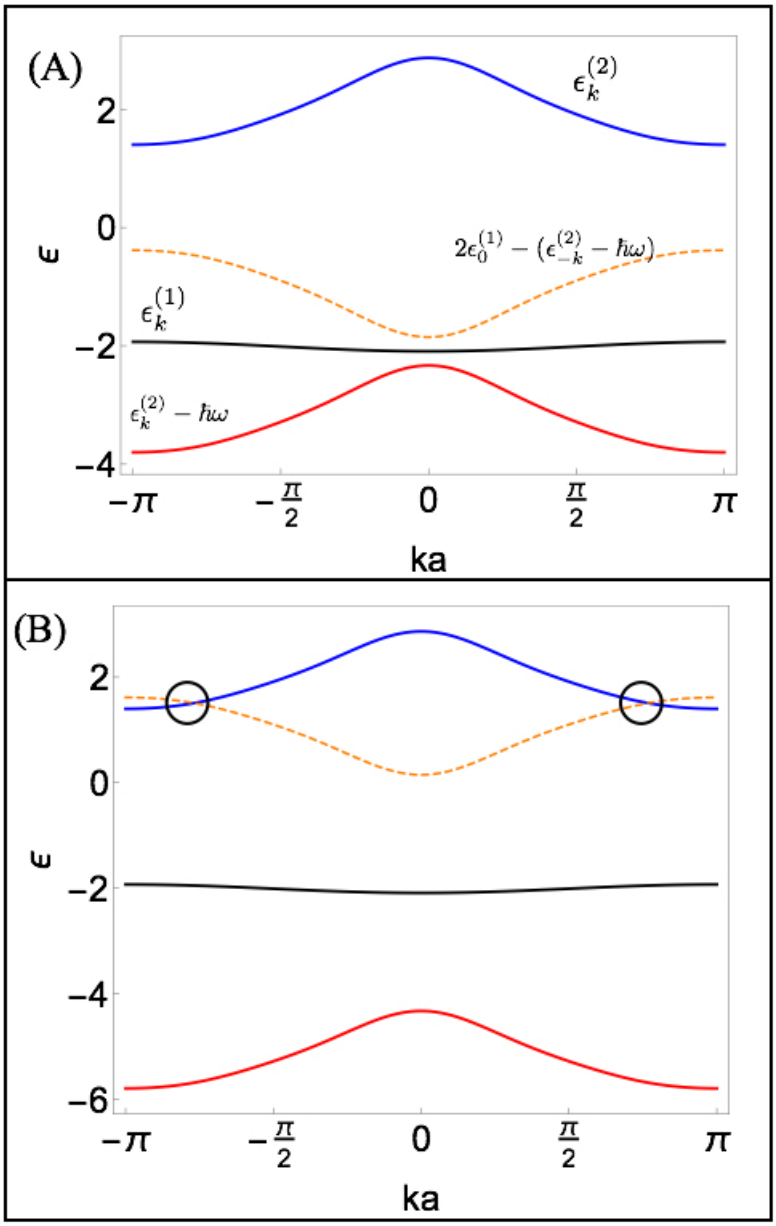

.

Figure 4.2: Geometrical construction to demonstrate when the floquet BEC is stable. Condition for the floquet BEC to be unstable: $2\epsilon_{k_0}^{(1)} - (\epsilon_{k_0-k}^{(2)} - \hbar\omega) = \epsilon_{k_0+k}^{(2)}$. Here, I illustrate the situation when $k_0 = 0$. (A) illustrates the situation where the floquet BEC is stable while (B) illustrates the situation where the floquet BEC is unstable. The BEC is unstable wherever the blue line (representing $\epsilon_k^{(2)}$) and the orange line (representing $2\epsilon_0^{(1)} - (\epsilon_{-k}^{(2)} - \hbar\omega)$) cross. I have marked the crossing points with circles.

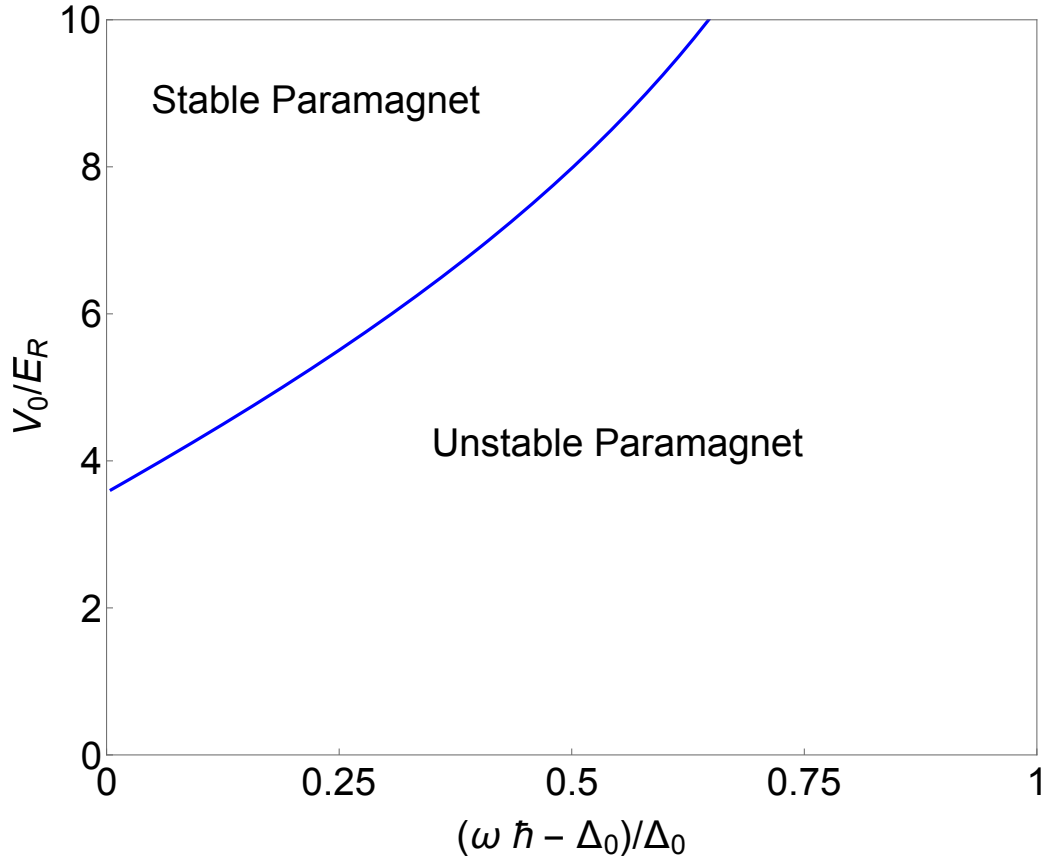

.

Figure 4.3: Phase diagram of the floquet BEC for a variety of lattice depths and detunings in the limit of infinitesimal driving.

In order to analyze the stability of the floquet BEC, I look at two slices through parameter space. Figure 4.3 shows the stability phase diagram of the periodically driven BEC for a variety of lattice depths and detunings in the limit of infinitesimal driving.

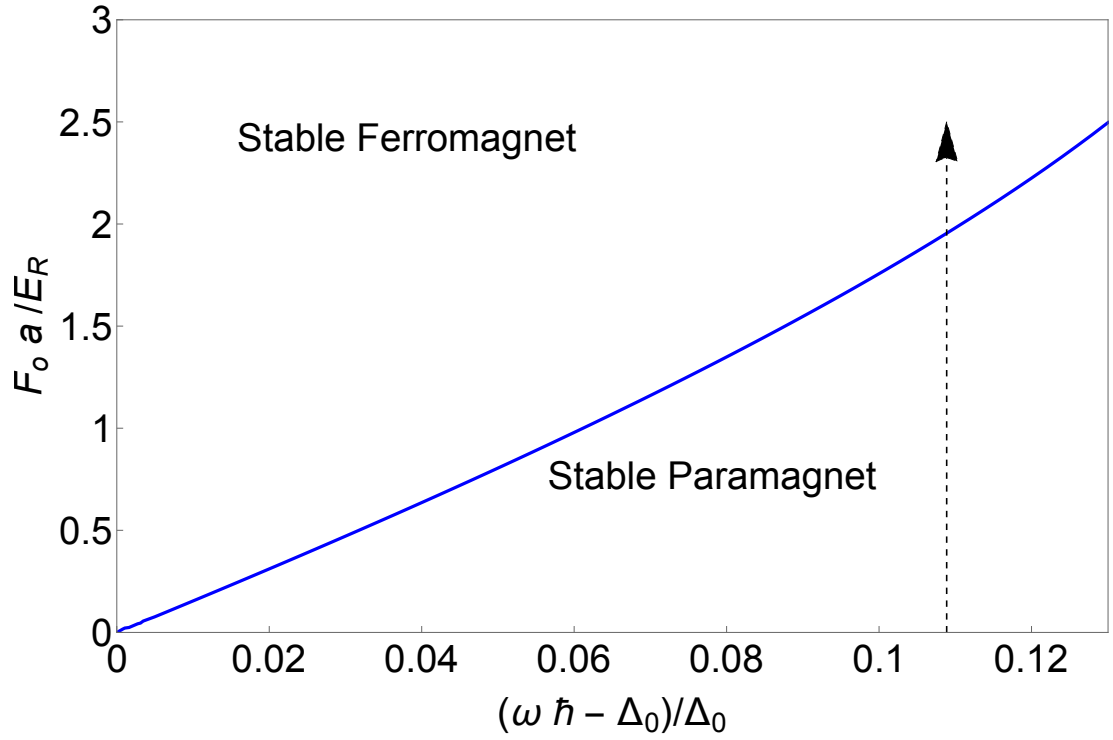

.

Figure 4.4: (Color Online) Phase Diagram of the Floquet BEC in a shaken one-dimensional lattice of depth $V_0 = 7.0\ E_R$. The zero-momentum bandgap, Δ_0 is 4.96 E_R. The vertical arrow shows the parameters of Ref.[30]. The BEC is stable in the blue detuned regime. In the red detuned regime, the BEC is unstable below a critical driving strength and stable above it. The thick black line shows the critical driving strength.

Figure 4.4 shows the stability phase diagram of the floquet BEC for typical experimental parameters of $V_0 = 7E_R$, (where $\Delta_0 = 4.96E_R$). I find that there is a large region of parameter space where the floquet BEC is stable ($\Gamma = 0$).

4.5 Conclusion

In this chapter, I analyzed the stability of a one dimensional Floquet BEC. I identified a large parameter regime where the BEC is stable. The experiment in ref.[30] was done in the regime where the BEC should be stable. The experimentalists observe "moderate heating" and they find that the condensate has a lifetime of about 1 second. In chapter 5, I show how the geometry of the experiment can lead to the observed moderate heating. Finally, in chapter 6, I will show how the heating rate of a Floquet BEC can be reduced by changing the transverse confinement.

BIBLIOGRAPHY

[1] E. Arimondo, D. Ciampini, A. Eckardt, M. Holthaus and O. Morsch, Advances in Atomic Molecular and Optical Physics, **61**, 515 (2012).

[2] A. Alberti, V. V. Ivanov, G. M. Tino, and G. Ferrari, Nature Phys. **5**, 547 (2009);

[3] J. Struck, C. Ölschläger, R. Le Targat, P. Soltan-Panahi, A. Eckardt, M. Lewenstein, P. Windpassinger and K. Sengstock, Science **333**, 996 (2011).

[4] J. Struck, M. Weinberg, C. Olschlager, P. Windpassinger, J. Simonet, K. Sengstock, R. Hoppner, P. Hauke, A. Eckardt, M. Lewenstein, and L. Mathey Nature Phys. **9**, 738 (2013)

[5] J. Struck, C. Olschlager, M. Weinberg, P. Hauke, J. Simonet, A. Eckardt, M. Lewenstein, K. Sengstock, and P. Windpassinger, Phys. Rev. Lett. **108**, 225304 (2012)

[6] P. Hauke, O. Tieleman, A. Celi, C. Olschlager, J. Simonet, J. Struck, M. Weinberg, P. Windpassinger, K. Sengstock, M. Lewenstein, and A. Eckardt Phys. Rev. Lett. **109**, 145301 (2012)

[7] N. H. Lindner, G. Refael, V. Galitski, Nature Phys. **7**, 490 (2011).

[8] M. C. Rechtsman, J. M. Zeuner, Y. Plotnik, Y. Lumer, D. Podolsky, F. Dreisow, S. Nolte, M. Segev, and A. Szameit, Nature (London) **496**, 196 (2013).

[9] W. Zheng and H. Zhai, Phys. Rev. A **89**, 061603 (2014)

[10] N. H. Lindner, D. L. Bergman, G. Refael and V. Galitski, Phys. Rev. B **87**, 235131 (2013).

[11] Y. H. Wang, H. Steinberg, P. Jarillo-Herrero and N. Gedik, Science **342**, 453 (2013).

[12] B. M. Fregoso, Y. H. Wang, N. Gedik, and V. Galitski Phys. Rev. B **88**, 155129 (2013)

[13] Á. Gómez-León, P. Delplace and G. Platero, Phys. Rev. B 89, 205408 (2014).

[14] T. Kitagawa, T. Oka, A. Brataas, L. Fu, and E. Demler, Phys. Rev. B 84, 235108 (2011).

[15] M. Thakurathi, A. A. Patel, D. Sen, and A. Dutta Phys. Rev. B **88**, 155133 (2013).

[16] Y. T. Katan and D. Podolsky Phys. Rev. Lett. **110**, 016802 (2013)

[17] D. E. Liu, A. Levchenko and H. U. Baranger,Phys. Rev. Lett. **111**, 047002 (2013)

[18] L. Jiang, T. Kitagawa, J. Alicea, A.R. Akhmerov, D. Pekker, G. Refael, J. I. Cirac, E. Demler, M. D. Lukin, and P. Zoller, Phys. Rev. Lett. **106**, 220402 (2011).

[19] A. Kundu and B. Seradjeh, Phys. Rev. Lett. **111**, 136402 (2013).

[20] Q-J. Tong, J-H. An, J. Gong, H-G. Luo, C. H. Oh, Phys. Rev. B **87**, 201109(R) (2013)

[21] S. K. Baur, M. H. Schleier-Smith, and N. R. Cooper, Phys. Rev. A **89**, 051605(R) (2014)

[22] A. Grushin, T. Neupert and Á. Gómez-León Phys. Rev. Lett. **112**, 156801 (2014).

[23] E. S. Morell and L. E. F. Torres, Phys. Rev. B **86**, 125449 (2012).

[24] P.M. Perez-Piskunow, G. Usaj, C. A. Balseiro and L. E. F. Foa Torres, Phys. Rev. B **89**, 121401(R), (2014).

[25] A. Eckardt and M. Holthaus, Europhys. Lett. **80**, 50 004 (2007).

[26] T. Kitagawa, E. Berg, M. Rudner, and E. Demler, Phys. Rev. B **82**, 235114 (2010).

[27] M. S. Rudner, and N. H. Lindner, E. Berg and M. Levin, Phys. Rev. X **3**, 033105, (2013).

[28] M. Lababidi, I. Satija and E. Zhao, Phys. Rev. Lett. **026805**, 026805 (2014).

[29] M. Reichl and E. J. Mueller, Phys. Rev. A **89**, 063628 (2014)

[30] C. V. Parker, L-C. Ha and C. Chin, Nature Phys. **9**,769 (2013).

[31] Á. Gómez-León and G. Platero, Phys. Rev. Lett. **110**, 200403 (2013).

[32] P. Hänggi, Chapter 5 in T. Dittrich, P. Hänggi, G.-L. Ingold, B. Kramer, G. Schön and W. Zwerger ed. *Quantum Transport and Dissipation*, Wiley-VCH, Weinheim 1998.

[33] A. Eckardt, C. Weiss, and M. Holthaus, Phys. Rev. Lett. **95**, 260404 (2005)

[34] H. Lignier, C. Sias, D. Ciampini, Y. Singh, A. Zenesini, O. Morsch, and E. Arimondo, Phys. Rev. Lett. **99**, 220403 (2007).

[35] N. Tsuji, T. Oka, P. Werner and H. Aoki, Phys. Rev. Lett. **106**, 236401 (2011)

[36] W. Zheng, B. Liu, J. Miao, C. Chin,and H. Zhai, Phys. Rev. Lett. **113**, 155303 (2014)

[37] L. D'Alessio and A. Polkovnikov, Annals of Physics, **33**,19 (2013).

[38] L. D'Alessio and M. Rigol, Phys. Rev. X **4**, 041048 (2014).

[39] D. Vorberg, W. Wustmann, R. Ketzmerick and A. Eckardt, Phys. Rev. Lett. **111**, 240405 (2013).

[40] A. Lazarides, A. Das, R. Moessner, Phys. Rev. Lett. **112**, 150401 (2014).

[41] A. Lazarides, A. Das, R. Moessner, Phys. Rev. E **90**, 012110 (2014).

[42] S. De Sarkar, R. Sensarma and K. Sengupta, Journal of Physics: Condensed Matter, **26**, 325602 (2014).

[43] P. Ponte, A. Chandran, Z. Papić, D. A. Abanin Annals of Physics **353**, 196 (2015)

[44] J. J. Sakurai and S. F. Tuan, *Modern Quantum Mechanics* Vol. 104. Reading (Mass.): Addison-Wesley, 1994.

[45] J. Zak, Phys. Rev. B **20**, 2228 (1979).

CHAPTER 5

TRANSVERSE COLLISIONAL INSTABILITIES OF A BOSE-EINSTEIN CONDENSATE IN A DRIVEN ONE-DIMENSIONAL LATTICE

This chapter is adapted from "Transverse collisional instabilities of a Bose-Einstein condensate in a driven one-dimensional lattice" by Sayan Choudhury and Erich J. Mueller, published in Physical Review A, **91**, *023624 (2015)"*

5.1 Overview

Motivated by recent experiments, I analyze the stability of a three-dimensional Bose-Einstein condensate (BEC) loaded in a periodically driven one-dimensional optical lattice. Such periodically driven systems do not have a thermodynamic ground state, but may have a long-lived steady state which is an eigenstate of a "Floquet Hamiltonian". I explore collisional instabilities of the Floquet ground state which transfer energy into the transverse modes. I calculate decay rates, finding that the lifetime scales as the inverse square of the scattering length and inverse of the peak three- dimensional density. These rates can be controlled by adding additional transverse potentials.

5.2 Introduction

In the previous chapter, I discussed how periodically driven cold atom systems has been used to emulate models of frustrated quantum magnetism [1, 2, 3, 4] and models of topological matter [5, 6, 7, 8, 9, 10]. However, some of these ex-

periments have unexpected heating [10, 11]. In the last chapter, I began addressing the sources of this heating by studying collisions within a one-dimensional Bose-Einstein condensate (BEC) in a shaken optical lattice. I found that in the presence of strong transverse confinement, there were large parameter ranges where the system was stable. Here, I extend that work to the regime where there is no transverse confinement. The additional decay channels generally lead to more dissipation and diffusive dynamics.

In this chapter, I consider two paradigmatic examples of Floquet systems in which a three dimensional BEC is loaded into an a modulated one-dimensional lattice. The difference lies in the nature of the drive: I consider (a) amplitude modulation of lattice depth (similar to the setup in Refs. [12, 13, 14]) and (b) lattice shaking (similar to the setup in Ref. [15, 16]). These two protocols are illustrated schematically in Fig. 5.1. I solve the Schrödinger equation for both systems and treat the inter-atomic interactions perturbatively. My analysis is along the lines of the last chapter, where I used Fermi's golden rule to study the tight confinement limit. This kinetic approach can be contrasted with quantum coherent arguments such as those used by Creffield in Ref. [17]. Creffield used the Bogoliubov equations to look at a dynamical instability of a BEC in a shaken one dimensional optical lattice. These decay channels are important when the interactions are strong. I consider a different limit: for most recent experiments, the interaction strengths are too low for the interaction-driven modification of the dispersion to be relevant, rather the physics is dominated by the energy and momentum conserving scattering processes which are accounted for through my kinetic equations. In a field-theoretic formulation this corresponds to only keeping the imaginary part of the self-energy.

In section 5.3, I analyze the stability of a BEC in an amplitude modulated tilted optical lattice. A similar analysis can be used for Raman-driven lattices, such as those used to realize the Harper Hamiltonian [10, 14]. It is also related to earlier studies of Bloch oscillations [18]. In section 5.4, I study the stability of a BEC loaded in a shaken optical lattice. This system can be mapped onto a classical spin model which exhibits a paramagnetic-ferromagnetic phase transition as well as a roton-maxon excitation spectrum [15, 16]. In both section 5.3 and section 5.4, I obtain analytical results for the lifetime of the BEC. Finally, in section 5.4, I discuss the general form of the dissipation rate in driven systems.

5.3 Amplitude Modulated Lattice

In this section, I consider a BEC in a deep tilted one dimensional optical lattice. Adjacent sites are offset by an energy $\Delta \gg J$, suppressing tunneling (J being the nearest neighbor tunnelling matrix element). There is no transverse confinement, yielding a one-dimensional array of pancakes. The lattice depth is then modulated at a frequency $\omega(\approx \Delta)$ so that tunnelling is restored between the pancakes. The Hamiltonian describing this system is :

$$\begin{aligned} H &= \int d^2 r_\perp \sum_j -(J + 2\Omega\cos(\omega t))\left(a_{j+1}^\dagger a_j + a_j^\dagger a_{j+1}\right) \\ &+ \Delta j a_j^\dagger a_j + \frac{\overline{g}}{2} a_j^\dagger a_j^\dagger a_j a_j + \frac{\hbar^2}{2m}\nabla_\perp a_j^\dagger \nabla_\perp a_j, \end{aligned} \tag{5.1}$$

The constant Ω parameterizes the modulation of the hopping matrix element. The transverse spatial components are suppressed : $a_j = a_j(r_\perp)$ where $r_\perp = (x, y)$

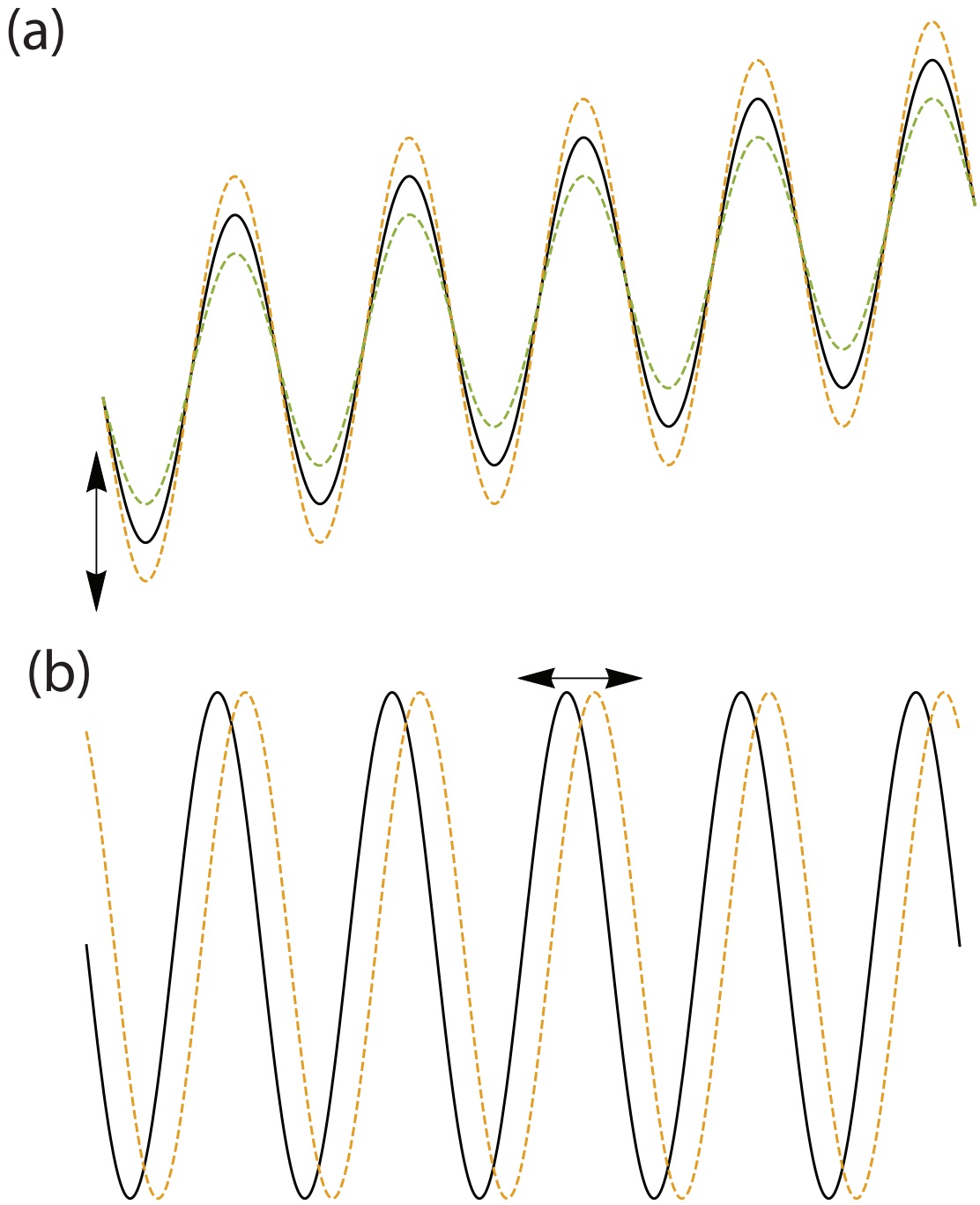

Figure 5.1: The two protocols of lattice driving (a) An amplitude modulated tilted lattice and (b) A shaken lattice

and $\nabla_\perp = \hat{x}\partial_x + \hat{y}\partial_y$. The coupling constant is

$$\begin{aligned} \overline{g} &= \frac{4\pi\hbar^2 a_s}{m}\int dz\,\phi(z)^4 \\ &= \frac{4\pi\hbar^2 a_s}{md} \end{aligned} \tag{5.2}$$

where $\phi(z)$ is the Wannier wavefunction in the z direction, normalized so that $\int |\phi|^2 dz = 1$. This equation defines d, the size of the Wannier state and is valid if $d \gg a_s$ [19].

Depending on how one sets up the problem the $\phi(z)$ used in Eq.(5.2) will be either the Wannier states of the static lattice, some time average of the instantaneous eigenstates or even some time-dependent function which yields an oscillating $\overline{g}$. The distinction will be important if the drive frequency is resonant with a band changing collision or if the modulation amplitude is large. Similarly, the relationship between J, Ω and the lattice parameters may be renormalized by large amplitude driving and the time-dependence of the parameters may not be sinusoidal. For most present experiments, where the amplitude of oscillations is small, these effects can be ignored.

As in [20], I now perform a gauge transformation to replace the tilt with a time dependent phase :

$$a_j = b_j e^{-i\Delta j t}. \tag{5.3}$$

The operators b_j will evolve with a new Hamiltonian H', chosen so that

$$i\partial_t b_j = [b_j, H']. \tag{5.4}$$

Specializing to the resonant case $\omega = \Delta$, I Fourier transform this equation yield-

ing

$$H' = \sum_k \epsilon_{\mathbf{k}}(t) b^\dagger_{\mathbf{k}} b_{\mathbf{k}} + \frac{g}{2V} \sum_{\mathbf{k_1},\mathbf{k_2},\mathbf{k_3}} b^\dagger_{\mathbf{k_1}} b^\dagger_{\mathbf{k_2}} b_{\mathbf{k_3}} b_{\mathbf{k_4}}, \tag{5.5}$$

where $\mathbf{k_4} = \mathbf{k_1} + \mathbf{k_2} - \mathbf{k_3}$, $\mathbf{k} = \{k_z, k_\perp\}$ and $g = \overline{g}a$, where a is the lattice spacing. The instantaneous single-particle dispersion is given by:

$$\epsilon_{\mathbf{k}}(t) = -2\Omega\cos(k_z) - 2\Omega\cos(k_z - 2\Delta t) - 2J\cos(k_z - \Delta t) + \frac{\hbar^2 k_\perp^2}{2m} \tag{5.6}$$

where V is the system volume and $b_{\mathbf{k}} = \sum_j b_j \exp(i\mathbf{k}j)$. The best interpretation of this dispersion comes from looking at the group velocity of a wave-packet, $\partial\epsilon/\partial k$. There is a drift term, $v_d = \partial\epsilon/\partial k_z = 2\Omega\sin(k_z)$ and an oscillating part $v_m = \partial\epsilon/\partial k_z = -4\Omega\Delta\sin(k_z - 2\Delta t) - 2J\sin(k_z - \Delta t)$ which is analogous to micro motion in ion traps [21].

I wish to explore the behaviour of a condensate at $\mathbf{k} = 0$. To this end, I break my Hamiltonian into three terms $H' = H_0 + H_1 + H_2$,

$$H_0 = \sum_{\mathbf{k}} \epsilon_{\mathbf{k}}(t) b^\dagger_{\mathbf{k}} b_{\mathbf{k}} + \frac{g}{2V} b^\dagger_0 b^\dagger_0 b_0 b_0 + \frac{2g}{V} \sum_{\mathbf{k}\neq\mathbf{0}} b^\dagger_0 b^\dagger_{\mathbf{k}} b_{\mathbf{k}} b_0, \tag{5.7}$$

$$H_1 = \alpha\frac{g}{2V} \sum_{\mathbf{k}\neq\mathbf{0}} b^\dagger_{-\mathbf{k}} b^\dagger_{\mathbf{k}} b_0 b_0 + \text{H.C.}, \tag{5.8}$$

$$H_2 = H - H_1 - H_0 \tag{5.9}$$

where $\alpha = 1$ is a formal parameter I will use for perturbation theory. As α is accompanied by a factor of the interaction strength gN/V, this expansion is equivalent to perturbation theory in g. Here H_0 contains the single-particle physics and the Hartree-Fock terms, H_1 contains interaction terms corresponding to atoms scattering from the condensate to finite momentum states and H_2 contains terms where a condensed and a non-condensed atom scatter or two non-condensed atoms scatter. H_2 does not contribute at lowest order in perturbation theory, as

there are initially no non-condensed atoms.

I will imagine that at time $t = 0$, the state of the system is:

$$|0\rangle = \frac{\left(b_0^\dagger\right)^N}{\sqrt{N!}}|\text{vac}\rangle, \tag{5.10}$$

which is an eigenstate of H_0. I will perturbatively calculate how $|\psi(t)\rangle$ evolves. To lowest order,

$$|\psi(t)\rangle \quad = \quad e^{-i\frac{E_0 t}{\hbar}}\left[|0\rangle + \sum_{\mathbf{k}} c_{\mathbf{k}}(t)|\mathbf{k}\rangle + \cdots\right] \tag{5.11}$$

where the state $|\mathbf{k}\rangle$ is given by :

$$|\mathbf{k}\rangle = b_{\mathbf{k}}^\dagger b_{-\mathbf{k}}^\dagger \frac{\left(b_0^\dagger\right)^{N-2}}{\sqrt{(N-2)!}}|\text{vac}\rangle. \tag{5.12}$$

and the coefficient is

$$c_{\mathbf{k}}(t) = \frac{\Lambda_k}{i\hbar}\int_0^t d\tau\, \exp\left[-i\int_\tau^t 2\frac{E_k(s)}{\hbar}\, ds\right]. \tag{5.13}$$

whose amplitude is given by

$$\Lambda_k = \langle \mathbf{k}|H_1|0\rangle/\alpha = \frac{gn}{2} \tag{5.14}$$

In Eq.(5.13), the (Hartee-Fock) excitation energy is

$$E_k(t) = \epsilon_{\mathbf{k}}(t) + gn - \epsilon_0(t). \tag{5.15}$$

Performing the integral in the exponent yields

$$\begin{aligned}\int_\tau^t E_k(s)\, ds \quad &= \quad E_k^{(0)} \times (t-\tau) \\ &+ \quad \frac{\Omega}{\Delta}\left(\sin(k_z - 2\Delta\tau) - \sin(k_z - 2\Delta t)\right) \\ &+ \quad \frac{2J}{\Delta}\left(\sin(k_z - \Delta\tau) - \sin(k_z - \Delta t)\right)\end{aligned} \tag{5.16}$$

where the "effective dispersion" is

$$E_k^{(0)} = 2\Omega[1-\cos(k_z)] + gn + \frac{k_\perp^2}{2m}. \tag{5.17}$$

This energy corresponds to the spectrum one would obtain from Floquet theory. It takes the form of a tight-binding model along z with a nearest-neighbor hopping of strength Ω. The resonant modulation has restored hopping. I now expand Eq. (5.13) in powers of J/Δ and Ω/Δ. Neglecting off-resonant terms and making the standard approximation $\sin^2(xt)/(xt)^2 \approx 2\pi t\delta(x)$, finding

$$\begin{aligned} |c_{\mathbf{k}}|^2 &\approx \frac{|\Lambda_k|^2}{\hbar}\frac{\Omega^2}{\Delta^2} t\, 2\pi\delta(E_k^{(0)}-\Delta) \\ &+ \frac{|\Lambda_k|^2}{\hbar}\frac{4J^2}{\Delta^2} t\, 2\pi\delta(E_k^{(0)}-\Delta/2), \end{aligned} \tag{5.18}$$

which is analogous to Fermi's golden rule. The result can also be derived using the formulation in Ref. [22]. The first term proportional to Ω^2 is naturally interpreted as coming from a pair of particles absorbing a lattice vibration. The second term involves one particle "hopping downhill" with the potential energy converted to transverse motion.

I now calculate the total rate of scattering out of the condensate. The relevant

timescale is

$$\begin{aligned}
\frac{1}{\tau} &= \frac{1}{N_0}\partial_t N_0 = \frac{2}{N}\partial_t \sum_k |c_{\mathbf{k}}|^2 = \frac{1}{\tau_2} + \frac{1}{\tau_1} \\
\frac{1}{\tau_2} &= \frac{2|\Lambda_k|^2}{N\hbar}\frac{\Omega^2}{\Delta^2}\sum_k 2\pi\delta(E_k^{(0)} - \Delta) \qquad (5.19) \\
\frac{1}{\tau_1} &= \frac{2|\Lambda_k|^2}{N\hbar}\frac{4J^2}{\Delta^2}\sum_k 2\pi\delta(E_k^{(0)} - \Delta/2). \qquad (5.20)
\end{aligned}$$

The sums over k are straightforward. I first note that that because Ω is small, the dependence of $E_k^{(0)}$ on k_z is weak, and can be neglected. Thus the sum over k just yields a constant

$$\begin{aligned}
\rho(\nu) &= \sum_k 2\pi\delta(E_k^{(0)} - \nu) \\
&\approx \frac{V}{a}\int \frac{d^2k_\perp}{(2\pi)^2} 2\pi\delta\left(\frac{k_\perp^2}{2m} + gn - \nu\right) \\
&= \frac{Vm}{a}. \qquad (5.21)
\end{aligned}$$

Putting in the factors of $\hbar$ the total rate of scattering out of the condensate is

$$\begin{aligned}
\frac{1}{\tau} &= \frac{g^2 nm}{2a\hbar^3}\frac{\Omega^2 + 4J^2}{\Delta^2} \\
&= gn\frac{2\pi a_s}{\hbar d}\frac{\Omega^2 + 4J^2}{\Delta^2} \qquad (5.22)
\end{aligned}$$

Some typical numbers are $gn/h \sim 300\text{Hz}, \Omega \sim 40\text{Hz}, J \sim 5\text{Hz}, \Delta \sim 1\text{kHz}$ and $d \sim 75\text{nm}$. For ^{87}Rb, the scattering length is $a_s \sim 5\text{nm}$. Thus the lifetime of the BEC is about 750ms.

5.4 Shaken Lattice

In this section, I look at the stability of a three-dimensional BEC loaded into a shaken one-dimensional optical lattice. I considered the strictly one-dimensional version in the last chapter. I are motivated by the set-up in Ref.

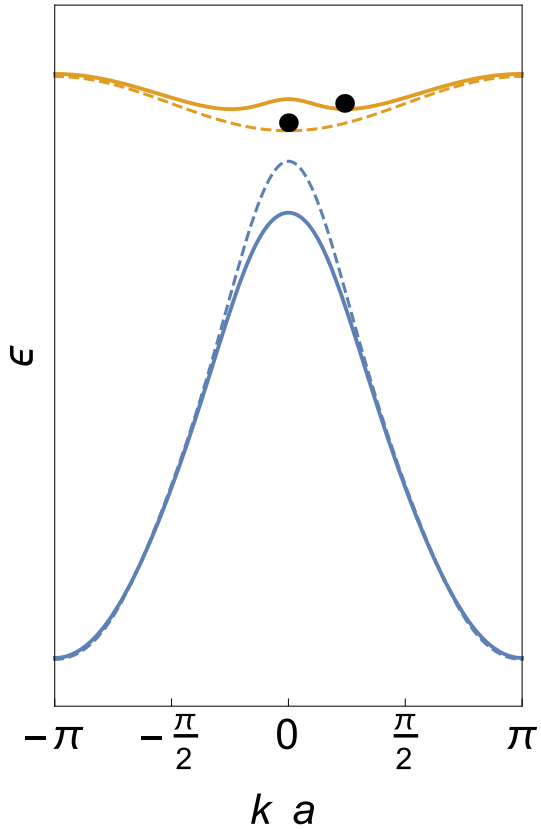

Figure 5.2: Schematic showing first (top) and second (bottom) Floquet quasi-energy bands of an optical lattice: ϵ is the single-particle energy, k is the quasi-momentum and a is the lattice spacing. Since Floquet energies are only defined modulo the shaking quanta $\hbar\omega$, the energy of the second band has been shifted down by $\hbar\omega$. Alternatively, this shift can be interpreted as working in a dressed basis, where the energy includes a contribution from the phonons. The mixing between the bands depends on the shaking amplitude. Dashed curves correspond to weak shaking, where the first band has its minimum at $k = 0$. Solid curves correspond to strong shaking, where there are two minima at $k = \pm k_0 \neq 0$.

[15] where Parker *et al.* load a three-dimensional BEC of ^{133}Cs atoms in a one-dimensional lattice and then shake the lattice at a frequency resonant with the zero-energy bandgap of the first two bands. This results in a strong mixing of the first two bands (schematically illustrated in Fig. 6.2). For my analysis, I label the Bloch band connected adiabatically to the first Bloch band in the limit of zero shaking as the ground band. As is evident from Fig. 6.2, due to level repulsion between the Bloch bands, the ground band exhibits a bifurcation from having one minimum at $\{\mathbf{k} = 0\}$ to two minima at $\{\mathbf{k}_\perp = 0, k = k_0 \neq 0\}$. This is analogous to the paramagnetic-ferromagnetic phase transition in Landau theory for classical spin models. In the paramagnetic regime the bosons always condense at $\mathbf{k} = 0$, while in the ferromagnetic regime, the bosons condense at some finite momentum $\{\mathbf{k}_\perp = 0, k \neq 0\}$. Here, I first perturbatively analyze the stability of a BEC against collisions in the limit of weak forcing amplitude. This gives an intuitive picture about how the scattering rate varies with amplitude. I then numerically calculate collision rates for larger shaking amplitudes spanning the experimentally interesting critical region. I find that the linearized theory overestimates the damping, but gives the correct order of magnitude.

5.4.1 Model

In the frame co-moving with the lattice, the tight-binding Hamiltonian describing the system can be written as $H_0(t) + H_{\rm int}$:

$$\begin{aligned} H_0(t) &= \int d^2r_\perp \sum_{ij} \left(-t_{ij}^{(1)} a_i^\dagger a_j + t_{ij}^{(2)} b_i^\dagger b_j + h.c.\right) \\ &+ \sum_j F_0 \cos(\omega t) \left(z_j \left(a_j^\dagger a_j + b_j^\dagger b_j\right) + \chi_j a_j^\dagger b_j + \chi_j^* b_j^\dagger a_j\right) \\ &+ \frac{\hbar^2}{2m} \left(\nabla_\perp a_j^\dagger \nabla_\perp a_j + \nabla_\perp b_j^\dagger \nabla_\perp b_j\right) \qquad (5.23) \\ H_{\rm int} &= \int d^2r_\perp \sum_i \frac{\overline{g}_1}{2} a_i^\dagger a_i^\dagger a_i a_i + \frac{\overline{g}_2}{2} b_i^\dagger b_i^\dagger b_i b_i + 2\overline{g}_{12} a_i^\dagger b_i^\dagger a_i b_i + H' \qquad (5.24) \end{aligned}$$

where,

$$\begin{aligned} \chi_j &= \int dz\ z w_1^*(z - z_j) w_2(z - z_j) \\ t_{ij}^{(1)} &= \int dz\ w_1^*(z - z_i) \left(\frac{-\hbar^2}{2m} \frac{d^2}{dz^2} + V(z)\right) w_1^*(z - z_j) \\ t_{ij}^{(2)} &= \int dz\ w_2^*(z - z_i) \left(\frac{-\hbar^2}{2m} \frac{d^2}{dx^2} + V(z)\right) w_2^*(z - z_j) \end{aligned}$$

with $V(z) = V_0 \sin^2\left(\frac{2\pi z}{\lambda_L}\right)$ and H' is off-resonant. It should also be noted that χ_j is independent of j and so I can call it χ. If necessary more bands can be included.

I now perform a basis rotation : $|\psi\rangle \rightarrow U_c(t)|\psi\rangle$ with:

$$U_c(t) = \exp\left(-\frac{i}{\hbar} \int_0^t \sum_j z_j F_0 \cos(\omega t)(a_j^\dagger a_j + b_j^\dagger b_j)\right) \qquad (5.25)$$

Under this unitary transformation, the Hamiltonian becomes:

$$\begin{aligned} H_0'(t) &= U_c H_0(t) U_c^{-1} - i\hbar U_c \partial_t U_c^{-1} \\ &= \sum_{ij} \left(-J_{ij}^{(1)}(t) a_i^\dagger a_j + J_{ij}^{(2)}(t) b_i^\dagger b_j + h.c. \right) + F\cos(\omega t) \left(\chi a_j^\dagger b_j + \chi^* b_j^\dagger a_j \right) + \sum_{k_\perp} \frac{\hbar^2 k_\perp^2}{2m} \\ &= \sum_k \sum_m \cos(mka) \left(-J_m^{(1)}(t) a_{\mathbf{k}}^\dagger a_{\mathbf{k}} - J_m^{(2)}(t) b_{\mathbf{k}}^\dagger b_{\mathbf{k}} \right) + \sum_k F_0 \cos(\omega t) \left(\chi a_{\mathbf{k}}^\dagger b_{\mathbf{k}} + \chi^* b_{\mathbf{k}}^\dagger a_{\mathbf{k}} \right) \\ &+ \sum_{k_\perp} \frac{\hbar^2 k_\perp^2}{2m} \end{aligned} \tag{5.26}$$

where,

$$\begin{aligned} J_{ij}^\sigma(t) &= t_{ij}^\sigma \exp(-iF_0 \frac{\cos(\omega t)}{\hbar\omega}(z_i - z_j)) \\ &= t_{ij}^\sigma \exp(-iF_0 \frac{\cos(\omega t)}{\hbar\omega} a(i-j)), \end{aligned} \tag{5.27}$$

$a = \lambda_L/2$ is the lattice spacing and $\chi = \chi^*$ for a suitable choice of phase for a_k and b_k.

Thus, in the limit of $F/(\hbar\omega) \ll 1$, the Hamiltonian describing the system is : $H = H_{\text{sp}} + H_{\text{int}}$, where

$$\begin{aligned} H_{\text{sp}} &= \sum_{\mathbf{k}} \epsilon_{\mathbf{k}}^{(1)} a_{\mathbf{k}}^\dagger a_{\mathbf{k}} + \epsilon_{\mathbf{k}}^{(2)} b_{\mathbf{k}}^\dagger b_{\mathbf{k}} + \chi F_0 \cos(\omega t) \left(a_{\mathbf{k}}^\dagger b_{\mathbf{k}} + b_{\mathbf{k}}^\dagger a_{\mathbf{k}} \right) \\ H_{\text{int}} &= \int d^2 r_\perp \sum_i \frac{\overline{g}_1}{2} a_i^\dagger a_i^\dagger a_i a_i + \frac{\overline{g}_2}{2} b_i^\dagger b_i^\dagger b_i b_i + 2\overline{g}_{12} a_i^\dagger b_i^\dagger a_i b_i + H' \end{aligned} \tag{5.28}$$

Here, $\epsilon_{\mathbf{k}}^{(1)}(\epsilon_{\mathbf{k}}^{(2)})$ is the dispersion of the first (second) band and $a_{\mathbf{k}}(b_{\mathbf{k}})$ is the annihilation operator for particles in the first (second band).

I make the transformation $b_{\mathbf{k}} \rightarrow \exp(-i\omega t) b_{\mathbf{k}}$ and discard far off-resonant terms (making the rotating wave approximation) to simplify the single-particle

terms :

$$H^{(\mathrm{sp})}_{\mathrm{RWA}} = \sum_{\mathbf{k}} \epsilon^{(1)}_{\mathbf{k}} a^{\dagger}_{\mathbf{k}} a_{\mathbf{k}} + \epsilon^{(2)}_{\mathbf{k}} b^{\dagger}_{\mathbf{k}} b_{\mathbf{k}} + \chi F_0 \left(a^{\dagger}_{\mathbf{k}} b_{\mathbf{k}} + b^{\dagger}_{\mathbf{k}} a_{\mathbf{k}} \right),$$

Here $\mathbf{k} = \{k, \mathbf{k}_{\perp}\}$, $\epsilon^{(1)}_{\mathbf{k}} = \epsilon^{(1)}_{k} + (\hbar k_{\perp})^2/(2m)$, $\epsilon^{(2)}_{k} = \epsilon^{(2)}_{\mathbf{k}} + (\hbar k_{\perp})^2/(2m) - \hbar\omega$. I diagonalise this quadratic form writing

$$H^{(\mathrm{sp})}_{\mathrm{RWA}} = \sum_{\mathbf{k}} \overline{\epsilon}^{(1)}_{\mathbf{k}} \overline{a}^{\dagger}_{\mathbf{k}} \overline{a}_{\mathbf{k}} + \overline{\epsilon}^{(2)}_{\mathbf{k}} \overline{b}^{\dagger}_{\mathbf{k}} \overline{b}_{\mathbf{k}} \tag{5.29}$$

The dressed dispersions $\overline{\epsilon}^{(1)}_{\mathbf{k}}$ and $\overline{\epsilon}^{(2)}_{\mathbf{k}}$ are shown as solid lines in Fig.(6.2). The bare dispersions $\epsilon^{(1)}_{\mathbf{k}}$ and $\epsilon^{(2)}_{\mathbf{k}}$ are shown as dashed lines. I treat $H^{(\mathrm{sp})}_{\mathrm{RWA}}$ both perturbatively and non-perturbatively to obtain scattering rates in the next two subsections.

5.4.2 Perturbation Theory

For small forcing amplitudes, I gain insight by a perturbative expansion in F_0. To linear order in F_0, the dressed operators are

$$\overline{a}^{\dagger}_{\mathbf{k}} = a^{\dagger}_{\mathbf{k}} - (\chi F_0)/(\epsilon^{(2)}_{\mathbf{k}} - \epsilon^{(1)}_{\mathbf{k}}) b^{\dagger}_{\mathbf{k}} \tag{5.30}$$

$$\overline{b}^{\dagger}_{\mathbf{k}} = b^{\dagger}_{\mathbf{k}} + (\chi F_0)/(\epsilon^{(2)}_{\mathbf{k}} - \epsilon^{(1)}_{\mathbf{k}}) a^{\dagger}_{\mathbf{k}} \tag{5.31}$$

Because I have made the rotating wave approximation, I have a time-independent problem and I can simply apply Fermi's Golden Rule to calculate the lifetime of the BEC, treating the interaction term as a perturbation. The standard procedure yields a scattering rate:

$$\frac{dN}{dt} = \int \frac{dk}{2\pi} \int \frac{d^2 k_{\perp}}{(2\pi)^2} |\langle \psi_f | H_{\mathrm{int}} | \psi_i \rangle|^2 \sigma \tag{5.32}$$

$$\sigma = \frac{2\pi}{\hbar} \delta(\overline{\epsilon}^{(1)}_{\mathbf{k}} + \overline{\epsilon}^{(2)}_{\mathbf{k}} + \frac{(\hbar k_{\perp})^2}{m} - 2\overline{\epsilon}^{(1)}_{0})$$

The initial and final states are

$$|\psi_i\rangle = \frac{(\overline{a}_0^\dagger)^N}{\sqrt{N!}}|0\rangle$$
$$|\psi_f\rangle = \overline{b}_{\mathbf{k}}^\dagger \overline{a}_{-\mathbf{k}}^\dagger \frac{(\overline{a}_0^\dagger)^{(N-2)}}{\sqrt{N-2!}}|0\rangle \tag{5.33}$$

$|\psi_i\rangle$ represents all particles in the condensate, while $|\psi_f\rangle$ has one particle with momentum $\mathbf{k}$ in the dressed b band and one with momentum $-\mathbf{k}$ in the ground band.

The transverse integrals are elementary and yield

$$\frac{dN}{dt} = \frac{m}{2\hbar^3} n^2 \int \frac{dk}{2\pi} (\frac{g_1}{\Delta_k} - 2\frac{g_{12}}{\Delta_0})^2 (\chi F_0)^2, \tag{5.34}$$

where $\Delta_k = \left(\epsilon_k^{(2)} - \epsilon_k^{(1)}\right)$, $\Delta_0 = \left(\epsilon_0^{(2)} - \epsilon_0^{(1)}\right)$ and $g = \overline{g}a$. While Eq.(5.34) can always be integrated numerically, I have found a sequence of approximations which let us analytically estimate the scattering rate. First, I approximate the Wannier functions as $w_1(x) = (\frac{1}{d_1^2\pi})^{1/4} \exp(-x^2/2d_1^2)$ and $w_2(x) = (\frac{1}{\pi d_1^2})^{3/4} x \exp(-x^2/2d_1^2)$, where $d_1 = a/(\pi(V_0)^{1/4})$ (V_0 being the lattice depth expressed in units of E_R). Within this approximation, $g_1 \approx 2g_{12}$, where $g_1 = (4\pi\hbar^2 a_s a)/(md)$, $d = d_1\sqrt{2\pi}$ ie the size of the Wannier state, a is the lattice spacing, and a_s is the scattering length . This is a good approximation as a numerical calculation using the exact Wannier states for the lattice in Ref. [15, 16] yields $g_1 = (1/0.41)\, g_{12}$.

As a second approximation, I note that except for k near 0, $\Delta_k \gg \Delta_0$. The contribution of those parts to the integral in Eq.(5.34) is small, allowing us to neglect the k dependence of the integrand. Hence, I see that the rate of scattering is approximately:

$$\frac{dN}{dt} \approx (g_1 n)^2 (\frac{\chi F_0}{\Delta_0})^2 \frac{Vm}{2a\hbar^3} \tag{5.35}$$

This gives the timescale for the scattering to be:

$$\tau = \frac{N}{\frac{dN}{dt}} \approx \frac{2\hbar^3 a}{m g_1^2 n}(\frac{\Delta_0}{\chi F_0})^2. \tag{5.36}$$

Stronger interactions, higher density and larger forcing amplitudes all increase the scattering rate.

5.4.3 Beyond Perturbation Theory

In this section, I extend my results to larger F_0. This allows us to probe the critical and ferromagnetic region. Generically, I write

$$\overline{a}_{\mathbf{k}}^{\dagger} = u_k a_{\mathbf{k}}^{\dagger} + v_k b_{\mathbf{k}}^{\dagger} \tag{5.37}$$

$$\overline{b}_{\mathbf{k}}^{\dagger} = -v_k a_{\mathbf{k}}^{\dagger} + u_k b_{\mathbf{k}}^{\dagger} \tag{5.38}$$

with $|u_k|^2 + |v_k|^2 = 1$. In particular,

$$\begin{aligned} u_k &= \frac{1}{\sqrt{1+|\gamma_k|^2}};\ v_k = \frac{\gamma_k}{\sqrt{1+|\gamma_k|^2}} \\ \frac{1}{\gamma_k} &= \frac{\sqrt{4F_0^2\chi^2 + \delta\epsilon_k^2} + \delta\epsilon_k}{2\chi F_0} \\ \delta\epsilon_k &= \epsilon_k^{(1)} - \epsilon_k^{(2)} \end{aligned}$$

One can invert the above relationships to obtain:

$$a_{\mathbf{k}}^{\dagger} = u_k \overline{a}_{\mathbf{k}}^{\dagger} - v_k \overline{b}_{\mathbf{k}}^{\dagger} \tag{5.39}$$

$$b_{\mathbf{k}}^{\dagger} = v_k \overline{a}_{\mathbf{k}}^{\dagger} + u_k \overline{b}_{\mathbf{k}}^{\dagger} \tag{5.40}$$

For $F_0 < F_c$ (F_c being the critical shaking force), I use Eq. (5.33) as my initial and final states. For $F_0 > F_c$, I use

$$\begin{aligned} |\psi_i\rangle &= \frac{(\overline{a}^\dagger_{\mathbf{k_0}})^N}{\sqrt{N!}}|0\rangle \\ |\psi_f^{(1)}\rangle &= \overline{b}^\dagger_{\mathbf{k_0}+\mathbf{k}}\overline{a}^\dagger_{\mathbf{k_0}-\mathbf{k}}\frac{(\overline{a}^\dagger_{\mathbf{k_0}})^{(N-2)}}{\sqrt{N-2!}}|0\rangle \\ |\psi_f^{(2)}\rangle &= \overline{b}^\dagger_{\mathbf{k_0}+\mathbf{k}}\overline{b}^\dagger_{\mathbf{k_0}-\mathbf{k}}\frac{(\overline{a}^\dagger_{\mathbf{k_0}})^{(N-2)}}{\sqrt{N-2!}}|0\rangle \end{aligned} \tag{5.41}$$

The states are analogous to those in eq.(5.33). In particular, $|\psi_i\rangle$ has all particles in a finite momentum condensate ($\mathbf{k_0} = \{k = k_0, \mathbf{k}_\perp = 0\}$).

The scattering rate is then:

$$\begin{aligned} \frac{dN}{dt} &= \int \frac{dk}{2\pi}\int \frac{d^2k_\perp}{(2\pi)^2}|\langle\psi_f^{(1)}|H_{\rm int}|\psi_i\rangle|^2\sigma_{12} \\ &+ \int \frac{dk}{2\pi}\int \frac{d^2k_\perp}{(2\pi)^2}|\langle\psi_f^{(2)}|H_{\rm int}|\psi_i\rangle|^2\sigma_{22} \end{aligned} \tag{5.42}$$

where

$$\begin{aligned} \sigma_{12} &= \frac{2\pi}{\hbar}\delta(\overline{\epsilon}^{(1)}_{k_0-k} + \overline{\epsilon}^{(2)}_{k_0+k} + \frac{(\hbar k_\perp)^2}{m} - 2\overline{\epsilon}^{(1)}_{k_0}) \\ \sigma_{22} &= \frac{2\pi}{\hbar}\delta(\overline{\epsilon}^{(2)}_{k_0-k} + \overline{\epsilon}^{(2)}_{k_0+k} + \frac{(\hbar k_\perp)^2}{m} - 2\overline{\epsilon}^{(1)}_{k_0}) \end{aligned}$$

In general $g_{12} = \alpha g_1$ and $g_2 = \beta g_1$. Approximating the Wannier functions with the harmonic oscillator wave functions would yield $\alpha = 1/2$ and $\beta = 3/4$. Rather than using this approximation, I numerically calculate the maximally localised Wannier functions for the experimental lattice depth of $V = 7E_R$ and find that $\alpha = 0.41$ and $\beta = 0.6$.

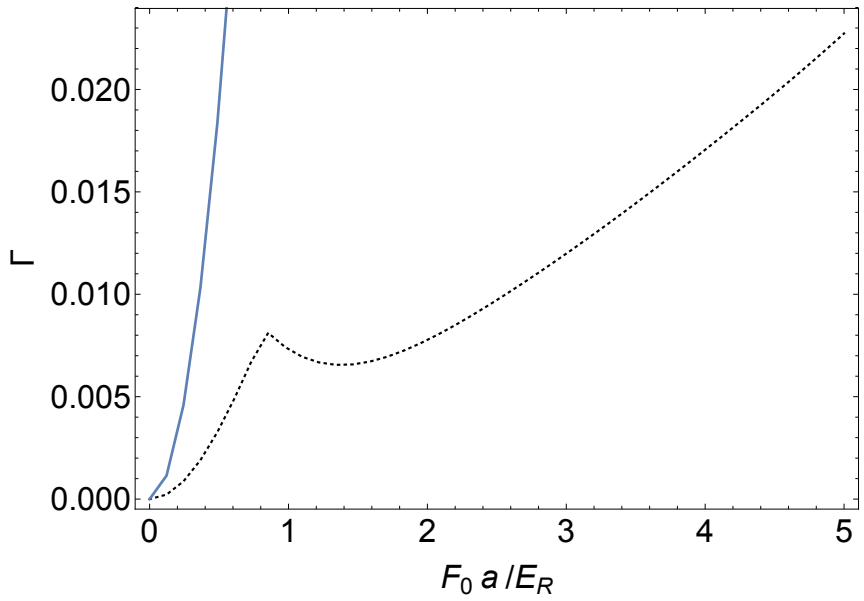

Figure 5.3: Plot of dimensionless decay rate Γ as a function of amplitude of shaking, F_0 for $\omega = 5.5\ E_R/\hbar$ and $V_0 = 7.0E_R$. The dotted line shows Γ calculated using Eq.(5.44), while the thick line shows the function $(\frac{\chi F_0}{\Delta_0})^2$ corresponding to the rate in Eq.(5.36). The kink shows the paramagnetic-ferromagnetic phase transition.

Extracting the dimensional factors ,

$$\tau = \frac{N}{\frac{dN}{dt}} = \frac{2\hbar^3 a}{m g_1^2 n \Gamma} \tag{5.43}$$

where the dimensionless parameter Γ depends on the forcing strength and can be expressed as

$$\begin{aligned}\Gamma &= \int \frac{dk}{2\pi}(|-u_{k_0-k}v_{k_0+k}u_{k_0}u_{k_0} + \alpha\, u_{k_0+k}v_{k_0-k}v_{k_0}v_{k_0} + 2\beta(u_{k_0+k}u_{k_0-k}u_{k_0}v_{k_0} - v_{k_0+k}v_{k_0-k}u_{k_0}v_{k_0})|^2) \\ &+ (|v_{k_0-k}v_{k_0+k}u_{k_0}u_{k_0} + \alpha\, u_{k_0+k}u_{k_0-k}v_{k_0}v_{k_0} - 2\beta(v_{k_0+k}u_{k_0-k}u_{k_0}v_{k_0} + u_{k_0+k}v_{k_0-k}u_{k_0}v_{k_0})|^2)\end{aligned} \tag{5.44}$$

The dotted line in Fig.(5.3) shows Γ using $\alpha = 0.41$ and $\beta = 0.6$ corresponding to a lattice depth of $V = 7E_R$ There is a distinct kink in the Γ vs F_0 plot which

shows the paramagnetic-ferromagnetic phase transition. For all F_0, the numerical calculation gives a smaller Γ than the perturbative estimate in Eq.(5.35). For the experimental lattice depths, $d \sim 100$nm, $gn/h \sim 150$Hz, $a_s \sim 1.5$nm yielding $\tau \sim 1$s which matches experimental observations [15].

5.5 General Conclusions

5.5.1 Form of the scattering rate

Generically two-particle scattering will give a rate proportional to $g^2 n$. The instabilities studied here relied upon scattering into transverse modes. These rates can be modified by tuning the density of these modes. For example, one could imagine engineering band gaps with transverse optical lattices. Note, such lattices may provide additional confinement and increase the effective g, inadvertently increasing the decay rate.

5.5.2 Diffusive Dynamics

The same dissipation which causes the condensate to decay can also lead to diffusive motion. Such diffusion may provide another way to study this physics. I model the kinetics by a Boltzmann equation:

$$\frac{\partial n(z,p)}{\partial t} + v(p)\frac{\partial n(z,p)}{\partial z} = \frac{n(z,p) - (n(z)/2\pi)}{\tau} \tag{5.45}$$

Here $n(z,p)$ is the coarse-grained number of particles whose position along the lattice direction is z and whose quasi-momentum in that direction is p, while

$n(z) = \int dp\, n(z,p)$ is the linear density and the group velocity is $v(p) = \partial\epsilon/\partial p$. I have integrated over the transverse directions. The τ appearing here is exactly the same as in Eqs.(5.22), (5.36) and (5.43). The collision term takes this simple form because atoms are scattered to random values of momentum in the lattice direction after a collision. Taking the zeroth and first moments of the Boltzmann equation yields typical hydrodynamic equations

$$\frac{\partial n(z)}{\partial t} + \frac{\partial J}{\partial z} = 0 \tag{5.46}$$

$$\frac{\partial J}{\partial t} + \frac{\partial}{\partial z}(\langle v^2\rangle n(z)) = \frac{J}{\tau} \tag{5.47}$$

where the current J is defined by $J = \int dv\, v(p) n(z,p)$. In the over damped limit, these can be rewritten as a diffusion equation with diffusion constant $D = \langle v^2\rangle\tau \propto J_{\rm eff}^2\tau$, where $J_{\rm eff}$ is the effective tunnelling coefficient (cf. Eq.(5.17)). Observing the diffusive motion may be one way of experimentally measuring τ, complementing more direct methods [23, 24].

5.6 Summary and Outlook

In this chapter, I analyzed the stability of a BEC in a driven one-dimensional optical lattice with no transverse confinement. I found that due to the presence of transverse modes, the BEC would always be unstable and I calculated the decay rates. Experimentally, this instability would be manifest in many forms, including heating and diffusive dynamics. In chapter 4, I had found that in the limit of extremely tight transverse confinement the BEC has regimes of stability.

Generally, experiments are neither in the tight binding limit, nor in the limit with no transverse confinement. The results in the present paper are applicable

as long as the level spacing of the quantum modes in the transverse direction ($\sim$ 100 Hz for Ref.[15]) are small as compared to the drive frequency ω ($\sim$ 7.3 KHz for Ref.[15]). The results from the previous chapter apply in the opposite limit. In the next chapter, I study the heating rates of a Floquet BEC in the crossover from weak to strong transverse confinement. This study will provide insight about how the heating rate of a Floquet BEC can be controlled by suitably designing the transverse confinement.

BIBLIOGRAPHY

[1] E. Arimondo, D. Ciampini, A. Eckardt, M. Holthaus and O. Morsch, Advances in Atomic Molecular and Optical Physics, **61**, 515 (2012).

[2] A. Alberti, V. V. Ivanov, G. M. Tino, and G. Ferrari, Nature Phys. **5**, 547 (2009).

[3] J. Struck, C. Ölschläger, R. Le Targat, P. Soltan-Panahi, A. Eckardt, M. LeInstein, P. Windpassinger and K. Sengstock, Science **333**, 996 (2011).

[4] J. Struck, M. Iinberg, C. Olschlager, P. Windpassinger, J. Simonet, K. Sengstock, R. Hoppner, P. Hauke, A. Eckardt, M. LeInstein, and L. Mathey Nature Phys. **9**, 738 (2013)

[5] J. Struck, C. Olschlager, M. Iinberg, P. Hauke, J. Simonet, A. Eckardt, M. LeInstein, K. Sengstock, and P. Windpassinger, Phys. Rev. Lett. **108**, 225304 (2012)

[6] G. Jotzu, M. Messer, R. Desbuquois, M. Lebrat, T. Uehlinger, D. Greif and T. Esslinger, Nature **515**, 237-240 (2014)

[7] M. Aidelsburger, M. Lohse, C. SchIizer, M. Atala, J. T. Barreiro, S. Nascimbéne, N. R. Cooper, I. Bloch, and N. Goldman, Nature Physics **11**, 162-166 (2015).

[8] C. J. Kennedy, G. A. Siviloglou, H. Miyake, W. C. Burton and W. Ketterle Phys. Rev. Lett. **111**, 225301 (2013).

[9] M. Aidelsburger, M. Atala, M. Lohse, J. T. Barreiro, B. Paredes, and I. Bloch, Phys. Rev. Lett. **111**, 185301 (2013).

[10] H. Miyake, G. A. Siviloglou, C. J. Kennedy, W. C. Burton and W. Ketterle Phys. Rev. Lett. **111**, 185302 (2013).

[11] C. Chin, Private Communication

[12] A. Alberti, G. Ferrari, V. V. Ivanov, M. L. Chiofalo, and G. M. Tino, New J. Phys. **12**, 065037 (2010).

[13] V. V. Ivanov, A. Alberti, M. Schioppo, G. Ferrari, M. Artoni, M. L. Chiofalo, and G. M. Tino, Phys. Rev. Lett. **100**, 043602 (2008).

[14] H. Miyake, Ph.D. Thesis, Massachusetts Institute of Technology, October 2013.

[15] C. V. Parker, L-C. Ha and C. Chin, Nature Phys. **9**,769 (2013).

[16] L-C. Ha, L. Clark, C. V. Parker, B. M. Anderson and C. Chin, Phys. Rev. Lett. **114**, 055301 (2015)

[17] C. E. Creffield, Phys. Rev. A **79**, 063612 (2009).

[18] O. Morsch, J. H. Müller, M. Cristiani, D. Ciampini and E. Arimondo, Phys. Rev. Lett. **87**, 140402 (2001).

[19] K. R. A. Hazzard and E. J. Mueller, Phys. Rev. A **81**, 033404 (2010).

[20] A. R. Kolovsky, H. J. Korsch, and E-M Graefe, Phys. Rev. A **80**, 023617 (2009).

[21] D. J. Berkeland, J. D. Miller, J. C. Bergquist, W. M. Itano and D. J. Wineland, J. App. Phys. **83**, 5025 (1998).

[22] A. Verdeny, A. Mielke and F. Mintert, Phys. Rev. Lett. **111**, 175301 (2013).

[23] U. Schneider, L. Hackermüller, J. P. Ronzheimer, S. Will, S. Braun, T. Best, I. Bloch, E. Demler, S. Mandt, D. Rasch and A. Rosch, Nature Phys. **8**, 213-218 (2012).

[24] J. P. Ronzheimer, M. Schreiber, S. Braun, S. S. Hodgman, S. Langer, I. P. McCulloch, F. Heidrich-Meisner, I. Bloch and U. Schneider, Phys. Rev. Lett. **110**, 205301 (2013).

CHAPTER 6

STABILITY OF A BOSE-EINSTEIN CONDENSATE IN A DRIVEN OPTICAL LATTICE: CROSSOVER BETWEEN WEAK AND TIGHT TRANSVERSE CONFINEMENT

This chapter is adapted from "Stability of a Bose-Einstein condensate in a driven optical lattice: Crossover between weak and tight transverse confinement" by Sayan Choudhury and Erich J. Mueller, published in Physical Review A **92**, *063639 (2015)*

6.1 Overview

In this chapter, I explore the effect of transverse confinement on the stability of a Bose-Einstein condensate loaded in a shaken one-dimensional or two-dimensional square lattice. I calculate the decay rate from two-particle collisions. I predict that if the transverse confinement exceeds a critical value, then, for appropriate shaking frequencies, the condensate is stable against scattering into transverse directions. I explore the confinement dependence of the loss rate, explaining the rich structure in terms of resonances.

6.2 Introduction

In the last two chapters, I have discussed some conceptual and practical issues with using periodic driving to control a cold atom system. A driven system has neither a "ground state" nor a well-defined thermodynamic temperature. Furthermore, nearly all successful examples of this technique study non-interacting or very weakly interacting particles, and one almost always sees strong heating

effects when moderate or strong interactions are introduced. In this chapter, I model some simple examples where these fundamental and practical issues are transparent. I make a series of predictions which are readily verifiable using techniques demonstrated in recent experiments [1, 2], and which will enable the experimental study of interacting Floquet systems with cold atoms.

These chapter builds on the last two chapters where I studied the heating rates of a periodically driven (Floquet) Bose-Einstein condensate (BEC) in two different geometries. In chapter 4, I considered a 1D gas of atoms trapped in a shaken 1D lattice. There I found large parameter regions where a Floquet BEC is stable against 2-body collisions. In chapter 5, I considered a 3D gas of atoms trapped in a shaken 1D lattice, making an array of "pancakes". I found that two-body collisions allowed energy to be taken from the shaking and transferred to transverse motion. The heating rates were consistent with those observed in experiment. In this setting, there is no steady state: the energy increases monotonically with time. The natural question is how these limits are connected. A 3D gas with harmonic transverse confinement should interpolate between these behaviors. In this chapter, I calculate heating rates in this crossover.

I find a rich structure. First, there is a critical strength of the transverse confinement beyond which two-body collisions are unable to deplete the condensate. Second, as a function of the transverse confinement, the dimensionless loss rate is non-monotonic, displaying drops and jumps characteristic of resonances. I explain this behavior in terms of the opening and closing of transverse decay channels. My results will be crucial to the next generation of experi-

ments. For example, one will be unable to observe a Floquet fractional quantum Hall effect without tuning to parameters where losses are negligible. While other authors have conducted related studies of the stability of driven systems [3, 4, 5, 6, 7, 8, 9, 10, 11, 12], the question of collisional loss into transverse channels is relatively unexplored. While I focus on a particular model, the loss into transverse modes is quite generic in cold atoms.

Figure 6.1(a) depicts a 1-D lattice with weak transverse confinement yielding an array of pancake traps. I consider driving the system by moving the lattice sites back-and-forth in the lattice direction. Figure 6.1(b) illustrate the tight confinement limit. Figure 6.1(c) illustrates a 2D lattice in the weak confinement limit, where one has an array of cigar shaped traps. I consider square arrays, with the shaking oriented 45^o from a lattice direction. These geometries are motivated by the experiments performed at Chicago [1, 2]. Using a kinetic model, I predict the scattering rate of bosons from a BEC as a function of the transverse confinement. Bilitewski and Cooper have performed a related study of the population dynamics in the Floquet realization of the Harper-Hofstader model [10]. In places where our studies overlap our results agree.

In section 6.3, I introduce my model for analyzing the shaken lattice experiments. I also discuss the general formalism for obtaining the Floquet band structure. In section 6.4, I use Fermi's golden rule to predict the scattering rate for bosons out of the BEC and obtain the stability phase diagram for a BEC loaded in a one-dimensional shaken lattice and in a shaken square lattice. Finally, I conclude with directions for future experiments.

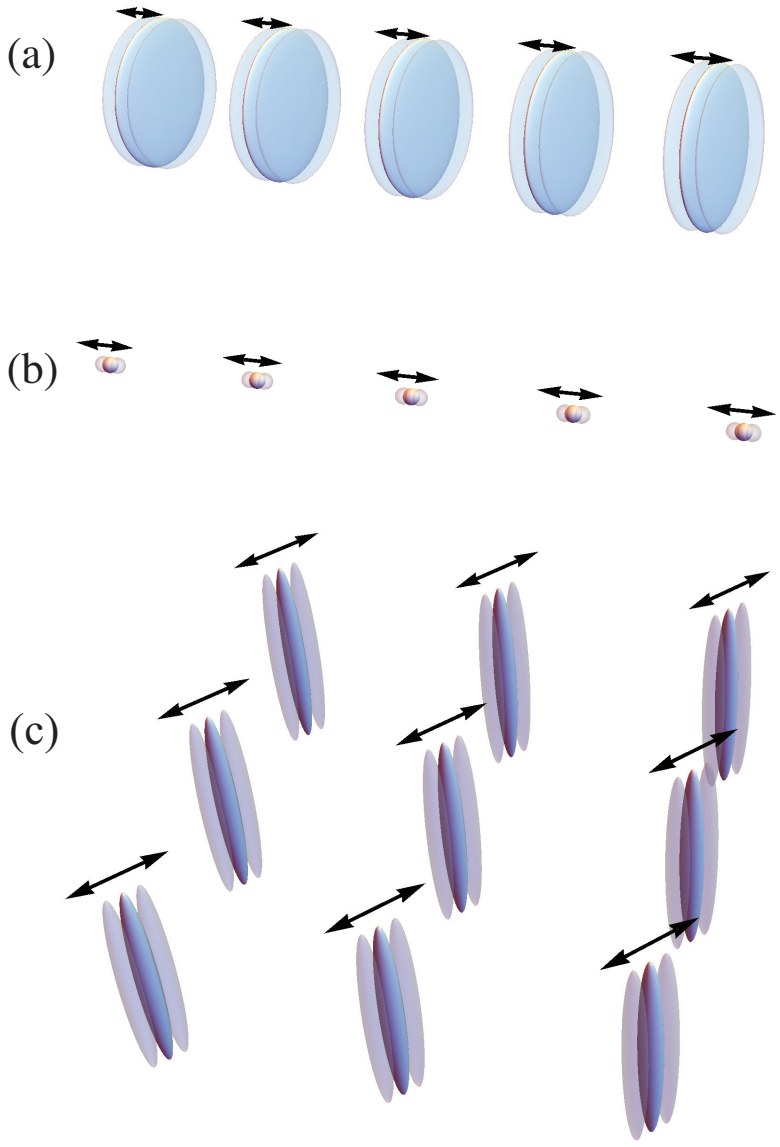

Figure 6.1: Schematic of shaken optical lattices: (a)1D lattice with weak transverse confinement; (b) 1D Lattice with tight transverse confinement; (c) 2D lattice with weak transverse confinement. Ellipsoids represent edges of cloud in each well of the optical lattice sites and arrows illustrate motion of trap. A typical spacing between lattice sites is 532 nm (half the laser wavelength λ_L = 1064 nm) and a typical shaking amplitude is 15 nm.

6.3 Model

6.3.1 One-Dimensional Shaken Lattice

The starting point of my modeling is the set-up in [1] where a BEC of ^{133}Cs atoms is trapped in a one-dimensional shaken optical lattice (with weak transverse confinement). When the shaking amplitude exceeds a certain critical value, the BEC undergoes a phase transition to a $\mathbb{Z}_2$ superfluid (where condensation occurs at finite momentum $k = \pm k_0 \neq 0$). A schematic of the dispersion is shown in Fig. 6.2. For modeling this physics, it is sufficient to consider the first two Bloch bands and ignore the remaining bands (see supplement of [1]).

In the frame of the moving lattice, the Hamiltonian for the driven system is given by $H = H_0(t) + H_{\text{int}}$, where [1],

$$\begin{aligned} H_0(t) &= \int d^3\mathbf{r}\ \Psi^\dagger(\mathbf{r})\left(\frac{-\hbar^2}{2m}\frac{d^2}{dz^2} + V_0\sin^2\left(\frac{2\pi z}{\lambda_L}\right) + zF_0\cos(\omega t) + \left(\frac{-\hbar^2}{2m}\nabla_\perp^2 + m\Omega^2(x^2+y^2)\right)\right)\Psi(\mathbf{r}) \\ H_{\text{int}} &= \frac{g}{2}\int d^3\mathbf{r}\ \Psi^\dagger(\mathbf{r})\Psi^\dagger(\mathbf{r})\Psi(\mathbf{r})\Psi(\mathbf{r}). \end{aligned} \tag{6.1}$$

The atomic mass is m, the wavelength of the laser forming the optical lattice is λ_L, the force from the periodic shaking is $F_0\cos(\omega t)$ and $g \approx \frac{4\pi\hbar^2 a_s}{m}$ is the interaction strength, a_s being the scattering length. The transverse trap frequency is Ω.

As is detailed in in the appendix at the end of this chapter, the single particle part of the Hamiltonian describing the system H_{sp} can be written as

$$H_{\text{sp}} = \sum_{\mathbf{n},k} \epsilon^{(1)}_{\mathbf{n}k} a_k^{\mathbf{n}\dagger} a_k^{\mathbf{n}} + \epsilon^{(2)}_{\mathbf{n}k} b_k^{\mathbf{n}\dagger} b_k^{\mathbf{n}} + F_0\cos(\omega t)\left(\chi a_k^{\mathbf{n}\dagger} b_k^{\mathbf{n}} + \chi^* b_k^{\mathbf{n}\dagger} a_k^{\mathbf{n}}\right) \tag{6.2}$$

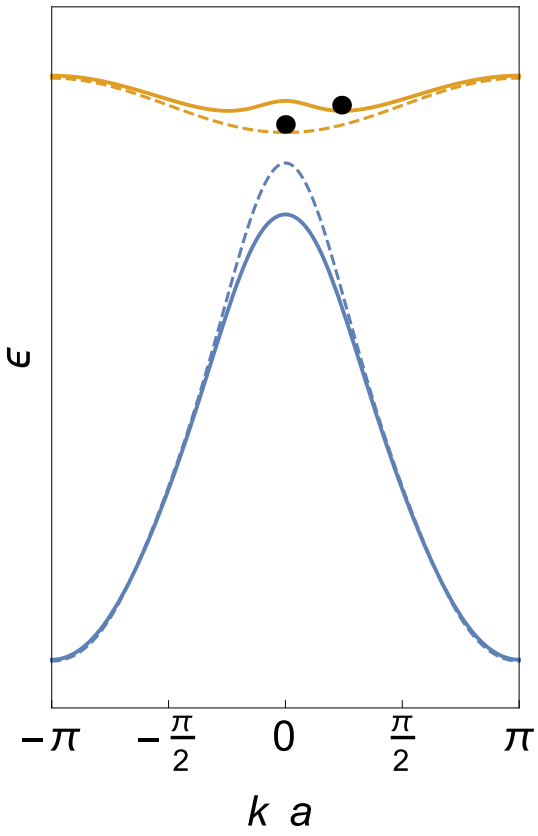

Figure 6.2: Schematic showing first (top) and second (bottom) Floquet quasi-energy bands of an optical lattice: ϵ is the single-particle energy (arbitrary units used for schematic), k is the quasi-momentum and a is the lattice spacing. Since Floquet energies are only defined modulo the shaking quanta $\hbar\omega$, the energy of the second band has been shifted down by $\hbar\omega$ so that it lies below the first band. Alternatively, this shift can be interpreted as working in a dressed basis, where the energy includes a contribution from the phonons. The mixing between the bands depends on the shaking amplitude. Dashed curves correspond to weak shaking, where the first band has its minimum at $k = 0$. Solid curves correspond to strong shaking, where there are two minima at $k = \pm k_0 \neq 0$.

Here, $\epsilon^{(1)}_{\mathbf{n}k}(\epsilon^{(2)}_{\mathbf{n}k})$ is the dispersion of the first (second) band, $a^{\mathbf{n}}_k(b^{\mathbf{n}}_k)$ is the annihilation operator for particles in the first (second) band with the harmonic oscillator level being $\mathbf{n}$ and χ is dipole matrix element between the first and the second band. As described in in the appendix at the end of this chapter, $\epsilon_{\mathbf{n}k}$ is generally time-dependent. However, when $F_0 a/(\hbar\omega) \ll 1$, $\epsilon_{\mathbf{n}k}$ can be taken to be time-independent.

I make the transformation $b_{\mathbf{k}} \rightarrow \exp(-i\omega t)b_{\mathbf{k}}$ and discard far off-resonant terms (making the rotating wave approximation) to simplify the single-particle Hamiltonian :

$$H^{(\mathrm{sp})}_{\mathrm{RWA}} = \sum_{\mathbf{n},k} \epsilon^{(1)}_{\mathbf{n}k} a^{\mathbf{n}\dagger}_k a^{\mathbf{n}}_k + \epsilon^{(2)}_{\mathbf{n}k} b^{\mathbf{n}\dagger}_k b^{\mathbf{n}}_k + \chi F\left(a^{\mathbf{n}\dagger}_k b^{\mathbf{n}}_k + b^{\mathbf{n}\dagger}_k a^{\mathbf{n}}_k\right), \tag{6.3}$$

Here $\epsilon^{(1)}_{\mathbf{n}k} = \epsilon^{(1)}_k + (n_x + n_y + 1)\hbar\Omega$, $\epsilon^{(2)}_{\mathbf{n}k} = \epsilon^{(2)}_k + (n_x + n_y + 1)\hbar\Omega - \hbar\omega$. I diagonalize this quadratic form writing

$$H^{(\mathrm{sp})}_{\mathrm{RWA}} = \sum_{\mathbf{n}k} \overline{\epsilon}^{(1)}_{\mathbf{n}k} \overline{a}^{\mathbf{n}\dagger}_k \overline{a}^{\mathbf{n}}_k + \overline{\epsilon}^{(2)}_{\mathbf{n}k} \overline{b}^{\mathbf{n}\dagger}_k \overline{b}^{\mathbf{n}}_k \tag{6.4}$$

For a particular value of $\mathbf{n} = \{n_x, n_y\}$, the dressed dispersions $\overline{\epsilon}^{(1)}_{\mathbf{n}k}$ and $\overline{\epsilon}^{(2)}_{\mathbf{n}k}$ are shown as solid lines in Fig. 6.2. The bare dispersions $\epsilon^{(1)}_{\mathbf{n}k}$ and $\epsilon^{(2)}_{\mathbf{n}k}$ are shown as dashed lines.

6.3.2 Shaken Square Lattice

I can easily extend the analysis of the previous section to the case of the square lattice. Since the shaken square lattice is separable and equivalent to two shaken one-dimensional lattices, one can write down the single-particle part of the

Hamiltonian, H_{2D} in the frame of the optical lattice as :

$$H_{2D} = \int d^3\mathbf{r}\, \Psi(\mathbf{r})^\dagger (H_{1D}(z) + H_{1D}(y))\Psi(\mathbf{r}) + \left(-\frac{\hbar^2}{2m}\frac{d^2}{dx^2} + m\Omega^2 x^2\right)\Psi(\mathbf{r})^\dagger\Psi(\mathbf{r}) \qquad (6.5)$$

where,

$$\begin{aligned} H_{1D}(z) &= -\frac{\hbar^2}{2m}\frac{d^2}{dz^2} + V_0 \sin^2\left(\frac{2\pi z}{\lambda_L}\right) + zF_0\cos(\omega t) \\ H_{1D}(y) &= -\frac{\hbar^2}{2m}\frac{d^2}{dy^2} + V_0 \sin^2\left(\frac{2\pi y}{\lambda_L}\right) + yF_0\cos(\omega t) \end{aligned}$$

Performing the same manipulations as in the last section, I end up with the following single particle Hamiltonian :

$$H_{2D}^{RWA} = \sum_{n,\mathbf{k}} \overline{\epsilon}^{(1,1)}_{n,\mathbf{k}} \overline{a}^{n\dagger}_{\mathbf{k}} \overline{a}^{n}_{\mathbf{k}} + \overline{\epsilon}^{(1,2)}_{n,\mathbf{k}} \overline{b}^{n\dagger}_{\mathbf{k}} \overline{b}^{n}_{\mathbf{k}} + \overline{\epsilon}^{(2,1)}_{n,\mathbf{k}} \overline{c}^{n\dagger}_{\mathbf{k}} \overline{c}^{n}_{\mathbf{k}} + \overline{\epsilon}^{(2,2)}_{n,\mathbf{k}} \overline{d}^{n\dagger}_{\mathbf{k}} \overline{d}^{n}_{\mathbf{k}} \qquad (6.6)$$

where $\overline{\epsilon}^{(i,j)}_{n,\mathbf{k}} = \overline{\epsilon}^{(i)}_{n=0,k_z} + \overline{\epsilon}^{(j)}_{n=0,k_y} + (n+1/2)\hbar\Omega$.

Due to the separability of the square lattice, instead of the $\mathbb{Z}_2$ reflection symmetry, the ground band develops a D_4 symmetry for shaking beyond a critical force. I show this schematically in Fig. 6.3.

6.4 Stability Analysis

In this section, I use a kinetic approach to investigate the stability of a Floquet BEC as a function of transverse confinement. Just like the treatment in chapters 4 and 5, I use Fermi's golden rule, treating the interaction term as a perturbation. An equivalent approach is to calculate the self-energy of the Floquet BEC. The imaginary part of the self-energy then gives the decay rate of the BEC.

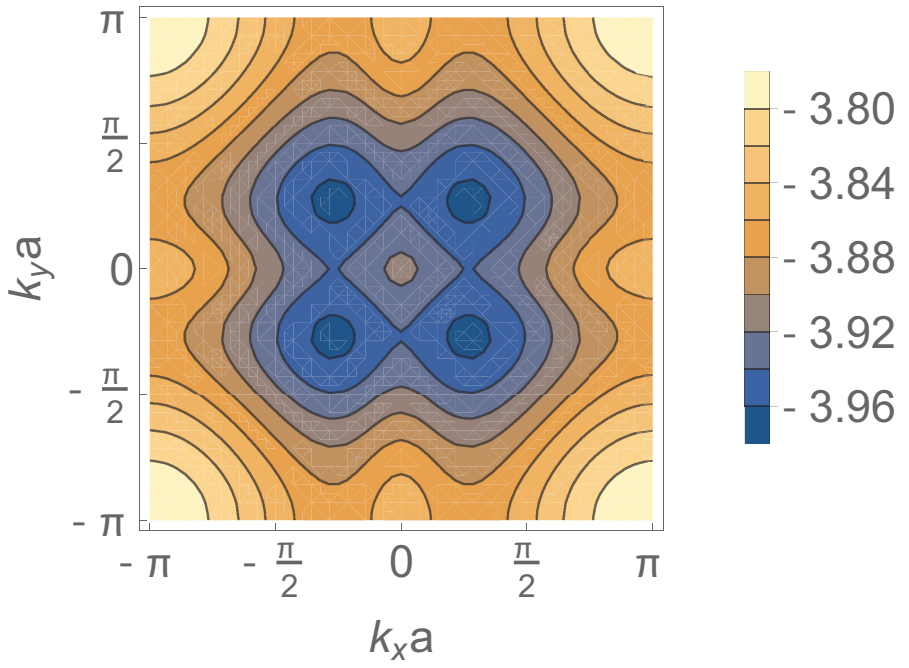

Figure 6.3: Schematic showing the dispersion of the first Floquet band of a shaken square lattice beyond a critical amplitude. Color represents energy in units of the recoil energy, E_R (see scale). I see that the superfluid order parameter develops a D_4 symmetry in momentum space.

Based on my results in chapters 4 and 5, one would expect that the Floquet BEC would be unstable when the transverse confinement is weak. However, a stable Floquet BEC can be realized if the transverse confinement exceeds a critical value. I find this critical transverse confinement strength for both the 1D shaken lattice and the shaken square lattice. For tighter potentials, the condensate is truly stable against energy-momentum conserving two-body collisions. I also identify several distinct signatures of interaction-driven scattering.

Within the rotating wave approximation, the rate of scattering of two atoms out of the BEC is then given by:

$$\frac{dN}{dt} = \frac{2\pi}{\hbar}\sum_f |\langle\psi_f|H_{\rm int}|\psi_i\rangle|^2\delta(\epsilon_f - \epsilon_i) \tag{6.7}$$

where

$$\begin{aligned} |\psi_i\rangle &= \frac{(\overline{a}^{\mathbf{0}\dagger}_{k_0})^N}{\sqrt{N!}}|0\rangle \\ |\psi_f\rangle &= \overline{\Psi}^\dagger_{k_0+k}\overline{\Psi}^\dagger_{k_0-k}\frac{(\overline{a}^{\mathbf{0}\dagger}_{k_0})^{(N-2)}}{\sqrt{N-2!}}|0\rangle \end{aligned} \tag{6.8}$$

where, $\overline{\Psi}_k$ is a shorthand for representing $\{\overline{a}_k, \overline{b}_k, \overline{c}_k, \overline{d}_k\}$, the state $|\psi_i\rangle$ denotes the BEC where the bosons have condensed at momentum k_0, while $|\psi_f\rangle$ denotes a state where two bosons have scattered out of the condensate to momenta $k_0 + k$ and $k_0 - k$ respectively. The energies of the final states are ϵ_f and ϵ_i respectively. If I did not use the Rotating Wave Approximation, a more complicated expression is necessary [14]. Using Eq.(6.7) I investigate the stability of a Floquet BEC. All my calculations are done for the experimental parameters of Ref.[1] a lattice depth of $7E_R$, where the recoil energy, $E_R = h^2/(2m\lambda_L^2)$ where $\lambda_L = 1064$ nm and $m = 133$ amu. For these units, the zero-momentum bandgap for the 1D optical lattice is is 4.96 E_R and the lattice is shaken at the blue detuned frequency of 5.5 E_R. It is reasonable to assume that loss is exponential. If not, Eq.(6.7) only describes the short-time behavior. At finite temperature, there are also heating processes involving one condensed atom and non-condensed atoms, or two non-condensed atoms. At typical BEC temperatures, these are negligible.

6.4.1 One-Dimensional Shaken Lattice

I first consider the case of a Floquet BEC loaded in a shaken 1D lattice. For this case, the boson scattering rate in Eq.(6.7) can be expressed as :

$$\frac{dN}{dt} = \frac{2\pi}{\hbar}\frac{g^2}{4}\frac{N^2}{Ll_\perp^2}\frac{1}{E_R a^3}\Gamma == \frac{2\pi}{\hbar}(\frac{gn}{2})^2\frac{V}{E_R a^3}\Gamma \tag{6.9}$$

where Γ is the adimensional scattering rate, L is the linear system size, $l_\perp = \sqrt{\hbar/(m\Omega)}$, and n is the density. This is of the same form as eq.(5.35). The detailed derivation and the expression for Γ are given in the appendix at the end of this chapter. Γ depends on the lattice depth, shaking frequency, shaking force and transverse confinement. It does not depend on the scattering length or the density.

Figure 6.4 shows Γ vs F_0 for weak transverse confinement ($\hbar\Omega/E_R = 0.04 \text{ and } 0.08$). As is expected from my results in chapter 5, for small F_0, Γ rises quadratically and is roughly independent of Ω. For large F_0, a series of resonances are visible. The lifetime of the condensate is given by :

$$\tau = \frac{N}{dN/dt} = \frac{mLl_\perp^2 a}{8ha_s^2 N\Gamma} = \frac{ma}{8ha_s^2 n\Gamma} \tag{6.10}$$

Taking typical experimental parameters from the experiment in ref.[1], $m = 133\,\text{amu}$, $L = 30000\,\text{nm}$, $l_\perp = 1000\,\text{nm}$ $a_s = 1.5\,\text{nm}$, $N = 30,000$ and $\Gamma = 0.01$, I get $\tau \sim 1\,\text{s}$.

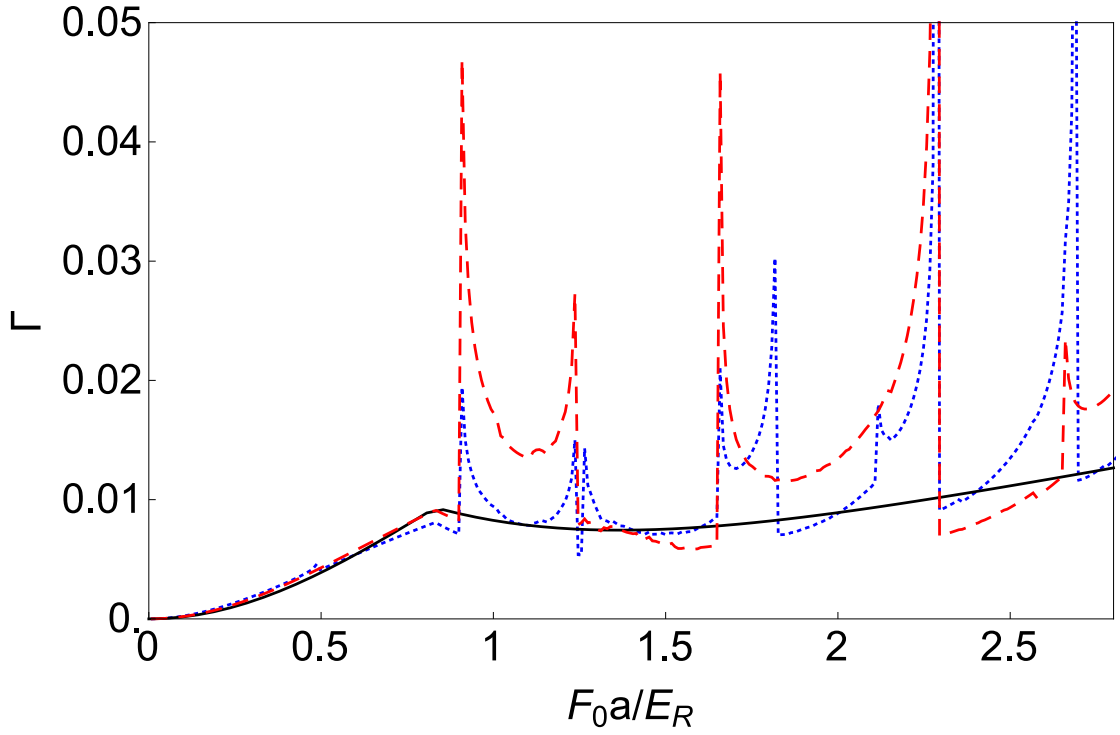

Figure 6.4: Adimensional scattering rate Γ as a function of the forcing amplitude, F_0 in the limit of weak confinement into a 1D lattice [Fig. 6.1(a)]. Blue, Dotted : $\hbar\Omega/E_R = 0.04$, Red, Dashed : $\hbar\Omega/E_R = 0.08$, Black, Solid: Analytic result from Chapter 5.

To better understand the structure of resonances in Fig. 6.4, I plot Γ on a log scale as a function of the transverse confinement frequency, Ω in Fig. 6.5. The set of vertical lines are given by the formulae:

$$\begin{aligned} \hbar\Omega_n^{(a)} &= E_{12}/(2n) = \left(\epsilon_\pi^{(1)} + \epsilon_{-\pi}^{(2)} - 2\epsilon_0^{(1)}\right)/(2n) \quad \text{and} \\ \hbar\Omega_n^{(b)} &= E_{22}/(2n) = \left(\epsilon_\pi^{(2)} + \epsilon_{-\pi}^{(2)} - 2\epsilon_0^{(1)}\right)/2n \end{aligned} \tag{6.11}$$

$$\tag{6.12}$$

These energy values, E_{12} and E_{22} correspond to the maximum longitudinal energy transfer in two different scattering channels and the resonance structure in Fig. 6.5 corresponds to the closing of scattering channels. The factor of $2n$ corresponds to the spacing of parity allowed states. This structure can be understood by considering the energy and momentum conserving scattering processes in Fig.(6.6). Whenever a scattering channel closes, the available phase space for energy-momentum conserving scattering processes suddenly reduces leading to a sudden drop in the scattering rate.

As explained in the appendix of this chapter (eqns.6.23 and 6.25), the scattering rate of atoms out of the floquet BEC is proportional to the overlap of the square of the excited state oscillator wave function with the square of the ground state oscillator wave function and a density of states factor, dk/dE_f where k is the crystal momentum and E_f is the energy of the final state that the bosons scatter to. There are two primary types of scattering channels: (a) when two bosons from the condensate scatter into the the first excited band (i.e band 2) and (b) when one boson from the condensate goes to some higher energy state in the ground band (band 1) and the other boson goes to the first excited band (band 2). The density of states factor is much higher for the latter type of chan-

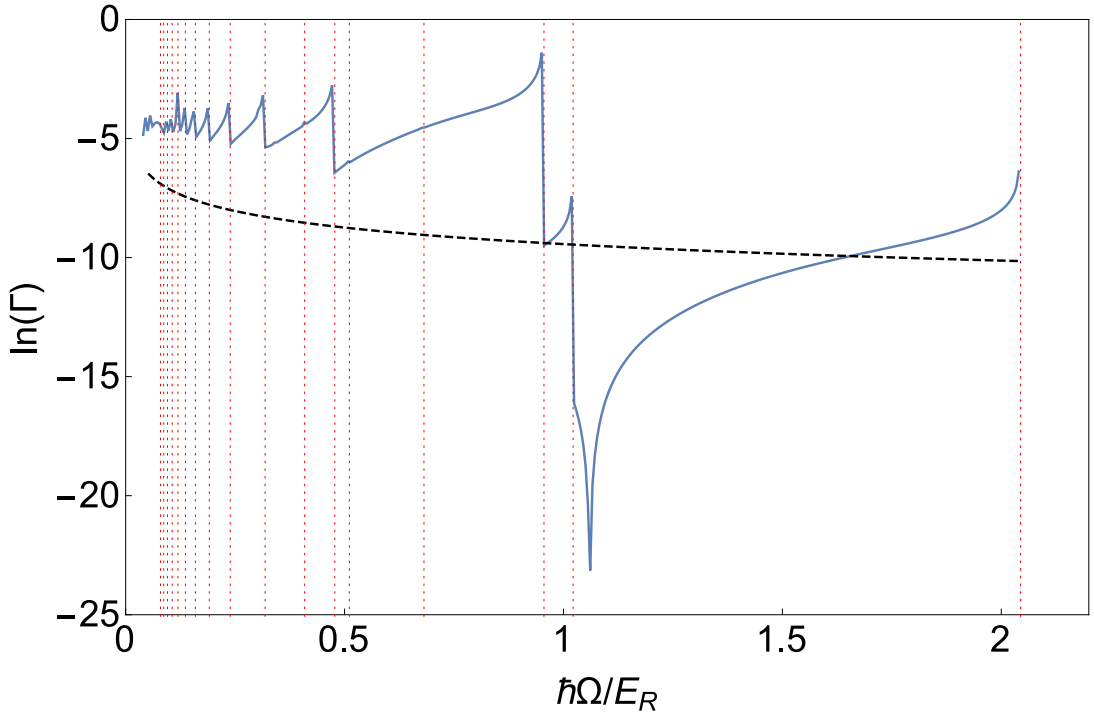

Figure 6.5: Logarithm of the adimensional scattering rate, Γ in a 1D lattice [Fig. 6.1(a),(b)] as a function of the transverse trapping frequency, Ω for a fixed value of the forcing amplitude, $F_0 = F_c$, where F_c is the amplitude where the dispersion of the ground band is quartic near $k = 0$. Red vertical lines denote resonances at $\Omega = \Omega_n^{(a)}, \Omega_n^{(b)}$ corresponding to the closing of scattering channels (see text).The black dashed line shows the value of $\ln(\Gamma)$ for different values of the transverse confinement for which the BEC lifetime is greater than 10 s (assuming the parameters quoted after Eq.(6.10)).

nel. Thus, the drop in scattering rate is bigger when a channel of type (b) closes compared to the situation when a channel of type (a) closes. The wavefunction overlap is also larger for large Ω leading to greater drops in the scattering rate when the transverse confinement is tighter.

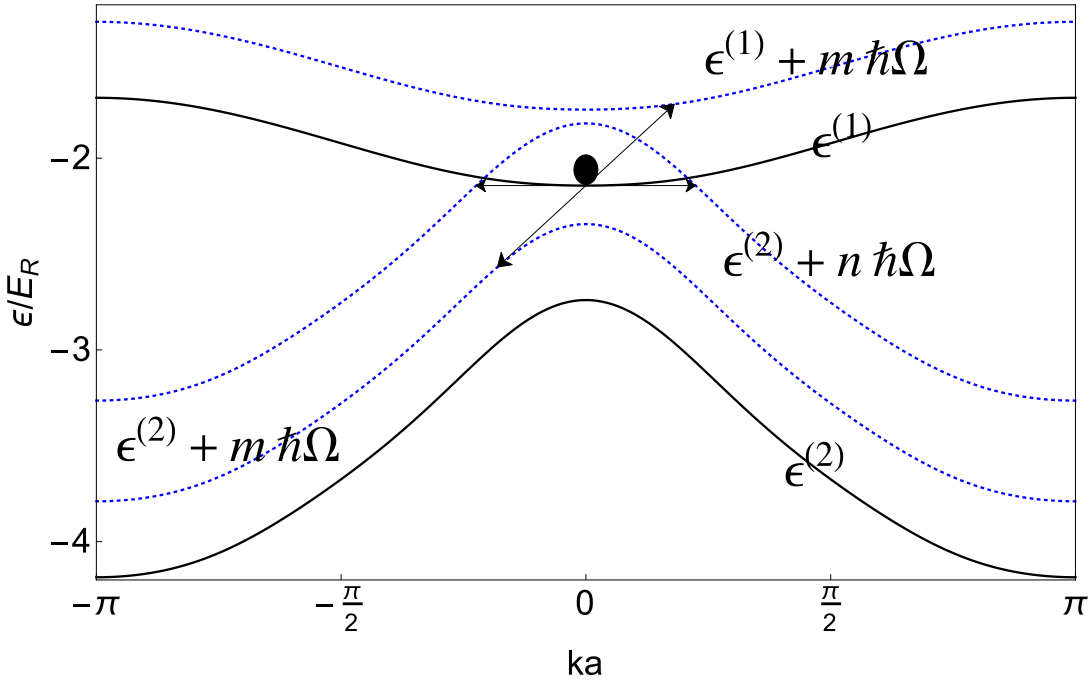

Figure 6.6: Schematic illustrating conservation of energy and momentum in two-body collisions in a shaken pancake lattice. Black dot denotes condensate in first band at $k = 0$. Solid lines show first and second with no transverse excitations. Arrows denote an energy and momentum conserving collision. The resonances in Figs. (6.4) and (6.5) correspond to the situation where the final states have $|ka| = \pi$

This resonance structure leads to special parameters where the BEC would be particularly stable or unstable. These resonances are a useful fingerprint of the loss mechanism and can be used in an experiment to test my model of interaction-driven instability. The dashed line in Fig.6.5 corresponds to a life-time of $\tau \approx 10$s (using the parameters below Eq.(6.10)). There is a large window around $\hbar\Omega \sim 1.1E_R$, where the lifetime exceeds 10 s.

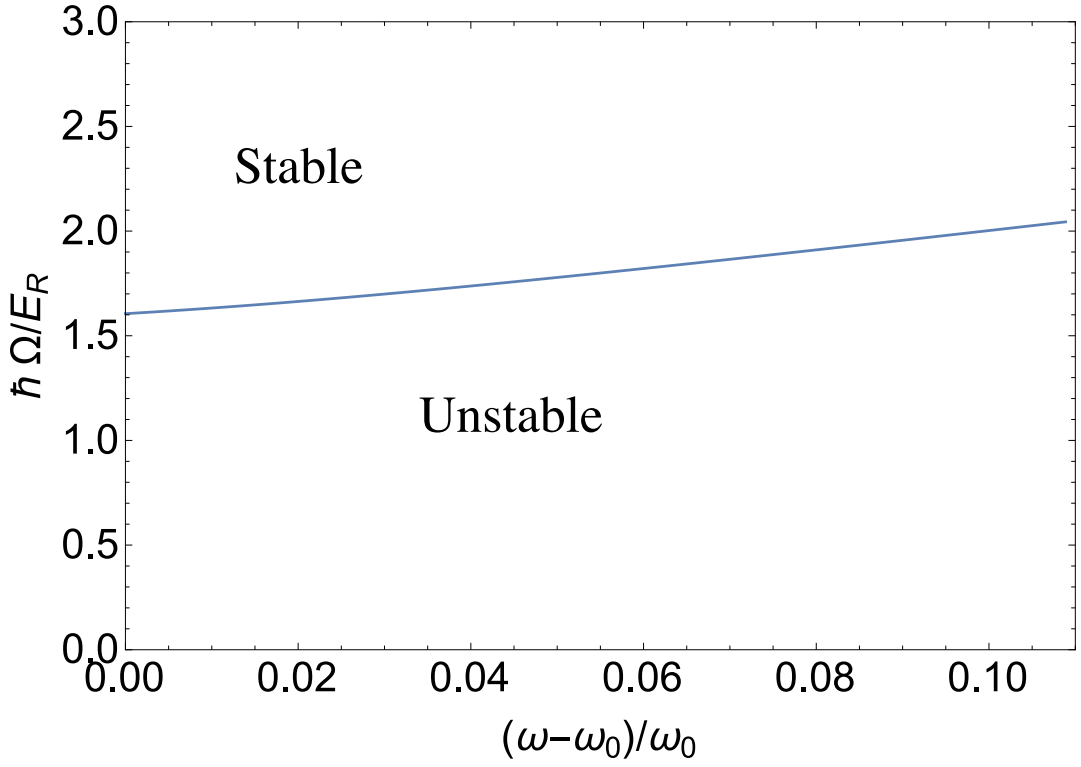

Figure 6.7: Stability phase diagram for a BEC in a driven 1D lattice for a fixed value of the forcing amplitude, $F_0 = F_c$. Here $\omega - \omega_0$ is the detuning of the shaking frequency ω from the zero-momentum bandgap ω_0.

The BEC is completely stable against collisions $\hbar\Omega > 2.05E_R$. In Fig. 6.7, I show how the stability boundary varies with drive frequency. In terms of the dispersions of the two bands, the critical confinement is given by :

$$\hbar\Omega = \epsilon_{\pi}^{(2)} + \epsilon_{-\pi}^{(2)} - 2\epsilon_{0}^{(1)} \tag{6.13}$$

For larger Ω, energy and momentum can't be conserved in 2-body collisions.

One concern with my analysis is that the optical dipole traps used in experiments are not completely harmonic. The anharmonicity of the traps imply that the different energy levels in the transverse directions are not equally spaced :

the energy levels are placed more closely together for higher values of energy [13, 14]. From eq.6.12, this implies that for small values of Ω, the resonances will be very closely spaced making it difficult to detect them [13, 14]. For larger values of Ω, however the shift is much smaller, making the resonances detectable. Another consequence of the anharmonicty of the trapping potential is the gas atoms at the edge of the trap experience a different trapping frequency than the atoms at the center. Thus, the anharmonicity will also lead to a broadening of the resonances. To make a quantitative estimate for the resonance broadening, I consider a trapping potential of the form [13] :

$$V_{\text{trap}} = U_0 \left(1 - \cos(k_L.x)\right) \tag{6.14}$$

The oscillator frequency at the center of the trap is $\Omega_0 = V_0 k_L^2/m$. This is the value of Ω that I use for my calculations. The spread in position for the gas cloud, Δx is given by :

$$U_0 \left(1 - \cos(k_L \frac{\Delta x}{2})\right) = k_B T. \tag{6.15}$$

The frequency at the edge of the trap is given by $\Omega' = \Omega_0 \sqrt{\cos(k_L \frac{\Delta x}{2})}$. Thus, the range of frequencies experienced by the gas in the trap is then given by:

$$\Delta\Omega = \Omega_0 \left(1 - \sqrt{\cos(k_L \frac{\Delta x}{2})}\right) = \Omega_0 \left(1 - \sqrt{\frac{U_0 - k_B T}{U_0}}\right) \tag{6.16}$$

Taking $U_0 = 10\hbar\Omega_0$ [13], and $T = 7nK$, I get that $\frac{\Delta\Omega}{\Omega_0}$ can vary between 0.16 (for the weakly confined case, $\Omega = 0.04E_R$) to 0.005 (for the tightly confined case, $\Omega = 1.1E_R$).

Thus, it will be difficult to observe the resonances for small Ω since these resonances are closely spaced and also broadened more. However, the resonances at large Ω should be observable. Moreover, I expect my analysis for the stability

boundary for the Floquet BEC to be robust because it only involves the lowest energy levels of the transverse traps.

6.4.2 Two Dimensional Shaken Lattice

In this section, I explore the stability of a Bose-Einstein condensate loaded in a two-dimensional optical lattice. The stability analysis is very similar to that of the shaken 1D lattice. The scattering rate of bosons can be written down as :

$$\frac{dN}{dt} = \frac{2\pi}{\hbar}\frac{g^2}{4}\frac{N^2}{L_y L_z l_\perp}\frac{1}{E_R a^3}\Gamma = \frac{2\pi}{\hbar}(\frac{gn}{2})^2\frac{V}{E_R a^3}\Gamma \tag{6.17}$$

where Γ is the adimensional scattering rate and L_z and L_y denotes the linear system size in the z and y directions. This is again of the form of eq.6.9. The detailed derivation and the expression for Γ are given in in the appendix at the end of this chapter.

I show Γ for a relatively weak value of transverse confinement ($\hbar\Omega/E_R$ = 0.08) in Fig. 6.8. The adimensional scattering rate, Γ is higher for the shaken two-dimensional square lattice when compared to the one-dimensional lattice.

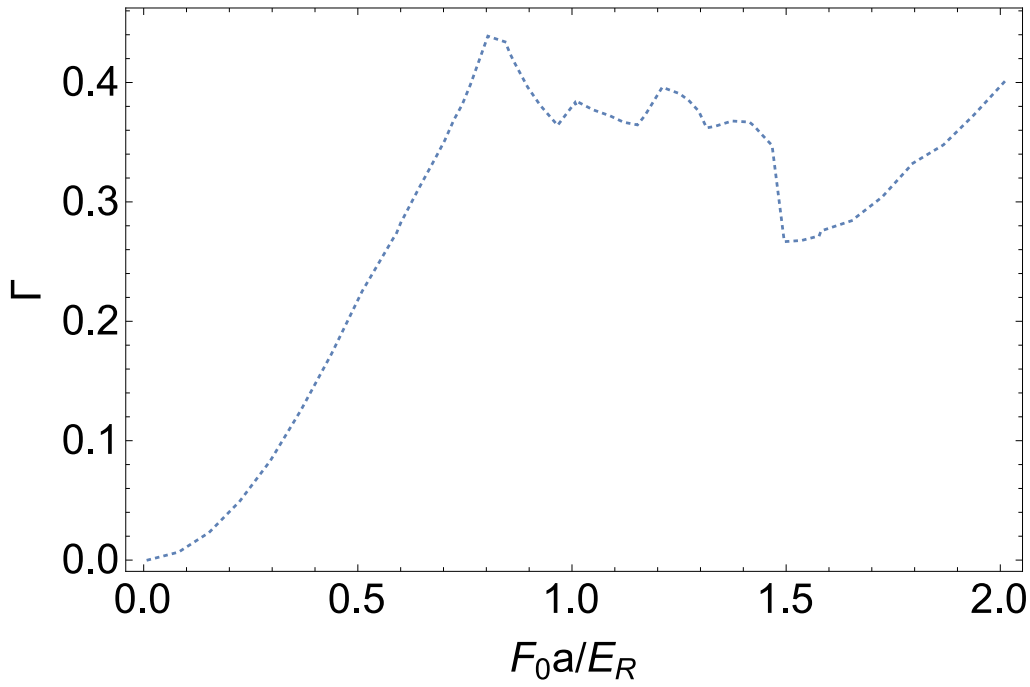

Figure 6.8: Adimensional scattering rate Γ as a function of the forcing amplitude, F_0 in the limit of weak confinement ($\hbar\Omega = 0.08E_R$) for a 2D lattice [Fig. 6.1(c)]

The lifetime of the condensate is given by :

$$\tau = \frac{N}{dN/dt} = \frac{mL_yL_zl_\perp a}{8ha_s^2N\Gamma} \tag{6.18}$$

Now, taking typical experimental parameters from the experiment in ref.[1], $m = 133$ amu, $L_y = 30000$ nm, $L_z = 30000$ nm, $l_\perp = 1000$ nm $a_s = 1.5$ nm, $N = 30,000$ and $\Gamma = 0.4$, I get $\tau \sim 0.73$ s.

The scatter of points in Fig. 6.8 is related to the resonances. Again, these can be explored by fixing F_0 to some value (here, F_c) and then plotting the scattering rate, Γ as a function of the transverse confinement, Ω as shown in Fig. 6.9. The black dashed line again corresponds to a lifetime of 10 s. There are specific value of Ω at which the scattering rate drops significantly.

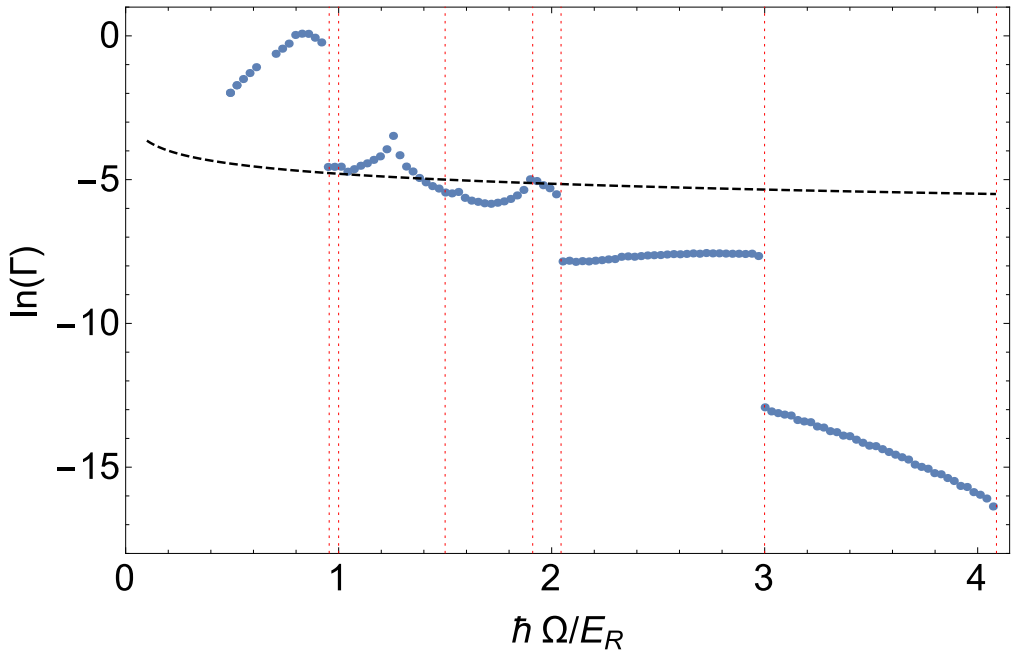

Figure 6.9: Logarithm of the adimensional scattering rate Γ in a 2D lattice as a function of the transverse confinement, Ω for a fixed value of the forcing amplitude, $F_0 = F_c$. The black dashed line shows the value of ln(Γ) for different values of the transverse confinement for which the BEC lifetime is greater than 10 s (assuming the parameters quoted after Eq.(6.18)).

These values of Ω are shown as vertical lines in Fig. 6.9 and correspond to $\hbar\Omega = (E_{12} + E_{22})/(2n), (E_{12} + E_{12})/(2n), (E_{22} + E_{22})/(2n)$. As in the 1D case, these frequencies correspond to the closing of scattering channels. There is also structure related to the van Hove singularities in the density of states, but for clarity, I do not mark them with vertical lines. Beyond a transverse confinement of 1.4 E_R, the BEC will almost always have a lifetime $\tau > 10$s.

Due to the separability of the Hamiltonian, the critical transverse confinement for the 2D square lattice is exactly twice that of the one-dimensional lattice, so the stability phase diagram is readily inferred from Fig.6.7.

6.5 Conclusion

In this chapter, I have studied the effect of transverse confinement on the stability of a Floquet BEC for both a shaken 1D lattice and a shaken 2D square lattice. I obtained scattering rates as well as the stability phase diagrams for both systems. The scattering rate shows a resonant structure and fine tuning parameters can drastically reduce the loss rate. This structure arises from the opening and closing of loss channels corresponding to the quantized transverse modes. It provides a fingerprint of the loss mechanism and could be a valuable tool for minimizing loss. I find a critical value of transverse confinement, beyond which there are no allowed 2-body scattering processes which can deplete the condensate. Well before this point however, the scattering rate drops to extremely small values, making the BEC stable for the time-scales of the experiment.

The loss mechanism that I study has another distinct signature - namely that energy is converted from the time-dependent potential into transverse motion of the atoms. This transverse motion can be directly probed in time-of-flight experiments. With this chapter, I conclude my studies on the stability of a periodically driven BEC.

6.6 Appendix

6.6.1 Derivation of the 1D Hamiltonian

In a tight-binding prescription, the single-particle Hamiltonian describing the system in the frame co-moving with the lattice can be written as $H_0(t)$:

$$\begin{aligned} H_0(t) &= \int d^2r_\perp \sum_{ij} \left(-t_{ij}^{(1)} a_i^\dagger a_j + t_{ij}^{(2)} b_i^\dagger b_j + h.c.\right) \\ &+ \sum_j F(t)\left(z_j\left(a_j^\dagger a_j + b_j^\dagger b_j\right) + \chi_j a_j^\dagger b_j + \chi_j^* b_j^\dagger a_j\right) \\ &+ \frac{\hbar^2}{2m}\left(\nabla_\perp a_j^\dagger \nabla_\perp a_j + \nabla_\perp b_j^\dagger \nabla_\perp b_j\right) + m\Omega^2(x^2+y^2)\left(a_j^\dagger a_j + b_j^\dagger b_j\right) \end{aligned} \tag{6.19}$$

where,

$$\begin{aligned} \chi_j &= \int dz\ z w_1^*(z-z_j) w_2(z-z_j) \\ t_{ij}^{(1)} &= \int dz\ w_1^*(z-z_i)\left(\frac{-\hbar^2}{2m}\frac{d^2}{dz^2} + V(z)\right) w_1^*(z-z_j) \\ t_{ij}^{(2)} &= \int dz\ w_2^*(z-z_i)\left(\frac{-\hbar^2}{2m}\frac{d^2}{dx^2} + V(z)\right) w_2^*(z-z_j) \\ F(t) &= F_0\cos(\omega t) \end{aligned} \tag{6.20}$$

Here, w_i is the Wannier function for the ith band. It should be noted that χ_j is independent of j and so I can call it χ. The operators a_j and b_j annihilate particles in the two bands. If necessary more bands can be included.

Performing a basis rotation : $|\psi\rangle \rightarrow U_c(t)|\psi\rangle$ where

$$U_c(t) = \exp\left(-\frac{i}{\hbar}\int_0^t \sum_j z_j F_0\cos(\omega t)(a_j^\dagger a_j + b_j^\dagger b_j)\right), \tag{6.21}$$

I transform the Hamiltonian as:

$$\begin{aligned} H_0'(t) &= U_c H_0(t) U_c^{-1} - i\hbar U_c \partial_t U_c^{-1} \\ &= \sum_{n_x,n_y} H_{\mathbf{n}} \end{aligned} \tag{6.22}$$

with

$$\begin{aligned} H_{\mathbf{n}} &= \sum_{ij} \left(-J_{ij}^{(1)}(t) a_i^{\mathbf{n}\dagger} a_j^{\mathbf{n}} + J_{ij}^{(2)}(t) b_i^{\mathbf{n}\dagger} b_j^{\mathbf{n}} + h.c.\right) + F_0 \cos(\omega t)\left(\chi a_j^{\mathbf{n}\dagger} b_j^{\mathbf{n}} + \chi^* b_j^{\mathbf{n}\dagger} a_j^{\mathbf{n}}\right) \\ &+ \sum_{\mathbf{n}} \hbar\Omega(n_x + n_y + 1)\left(a_j^{\mathbf{n}\dagger} a_j^{\mathbf{n}} + b_j^{\mathbf{n}\dagger} b_j^{\mathbf{n}}\right) \\ &= \sum_k \sum_m \cos(mka)\left(-J_m^{(1)}(t) a_k^{\mathbf{n}\dagger} a_k^{\mathbf{n}} - J_m^{(2)}(t) b_k^{\mathbf{n}\dagger} b_k^{\mathbf{n}}\right) + \sum_k F_0 \cos(\omega t)\left(\chi a_k^{\mathbf{n}\dagger} b_k^{\mathbf{n}} + \chi^* b_k^{\mathbf{n}\dagger} a_k^{\mathbf{n}}\right) \\ &+ \sum_{\mathbf{n}} \hbar\Omega(n_x + n_y + 1)\left(a_k^{\mathbf{n}\dagger} a_k^{\mathbf{n}} + b_k^{\mathbf{n}\dagger} b_k^{\mathbf{n}}\right) \end{aligned} \tag{6.23}$$

where,

$$J_{ij}^{\sigma}(t) = t_{ij}^{\sigma} \exp(-iF_0 \frac{\sin(\omega t)}{\hbar\omega}(z_i - z_j)) = t_{ij}^{\sigma} \exp(-iF_0 \frac{\sin(\omega t)}{\hbar\omega} a(i-j)), \tag{6.24}$$

$a = \lambda_L/2$ is the lattice spacing and $\chi = \chi^*$ for a suitable choice of phase for a_k and b_k. I use $\mathbf{n}$ as a shorthand for denoting $\{n_x, n_y\}$.

In the limit of $F_0 a/(\hbar\omega) \ll 1$, $J_{ij}^{\sigma}(t) = t_{ij}^{\sigma}$. Hence, I can write down the Hamiltonian as :

$$H_{\text{sp}} = \sum_{\mathbf{n},k} \epsilon_{\mathbf{n}k}^{(1)} a_k^{\mathbf{n}\dagger} a_k^{\mathbf{n}} + \epsilon_{\mathbf{n}k}^{(2)} b_k^{\mathbf{n}\dagger} b_k^{\mathbf{n}} + F_0 \cos(\omega t)\left(\chi a_k^{\mathbf{n}\dagger} b_k^{\mathbf{n}} + \chi^* b_k^{\mathbf{n}\dagger} a_k^{\mathbf{n}}\right) \tag{6.25}$$

where,

$$\begin{aligned} \epsilon_{\mathbf{n}k}^{(1)} &= \sum_k \sum_m -t_m^{(1)} \cos(mka) + \hbar\Omega(n_x + n_y + 1) \\ \epsilon_{\mathbf{n}k}^{(2)} &= \sum_k \sum_m t_m^{(2)} \cos(mka) + \hbar\Omega(n_x + n_y + 1) \end{aligned} \tag{6.26}$$

6.6.2 Derivation of the scattering rate

1D Lattice

For the case of the 1D optical lattice, the scattering rate in Eq.(6.7) can be written down as

$$\frac{dN}{dt} = \frac{2\pi}{\hbar}\frac{g^2}{4}N^2\frac{L}{2\pi}\sum_{\mathbf{n}_a,\mathbf{n}_b}\int dk\Gamma_k^{\mathbf{n}_a,\mathbf{n}_b}\delta(\epsilon_f-\epsilon_i) \tag{6.27}$$

where

$$\Gamma_k^{\mathbf{n}_a,\mathbf{n}_b} = \left|\frac{I_x^{\mathbf{n}_a,\mathbf{n}_b}I_y^{\mathbf{n}_a,\mathbf{n}_b}\langle\psi_f|\int dk\Psi^\dagger_{k_0-k}\Psi^\dagger_{k_0+k}\Psi_{k_0}\Psi_{k_0}|\psi_i\rangle}{Ll_\perp^2}\right|^2$$

and

$$I_x^{\mathbf{n}_a,\mathbf{n}_b} = \int dx\phi^{(n_a^x)}(x)\phi^{(n_b^x)}(x)\phi^{(0)}(x)\phi^{(0)}(x) \tag{6.28}$$

with $\mathbf{n}_a(\mathbf{n}_b) = \{n_a^x, n_a^y\}(\{n_b^x, n_b^y\})$, $\phi^{(n)}(x) = H_n(x)\exp(-x^2/2)$, $H_n(x)$ being the Hermite polynomial of order n. An important consequence of the form of 6.28 is that $I_x^{\mathbf{n}_a,\mathbf{n}_b} = 0$ unless n_a^x and n_b^x (as well as n_a^y and n_b^y) have the same parity. Finally, Eq.(6.27) can be simplified to write

$$\frac{dN}{dt} = \frac{2\pi}{\hbar}\frac{g^2}{4}\frac{N^2}{Ll_\perp^2}\frac{1}{E_Ra^3}\Gamma \tag{6.29}$$

with

$$\begin{aligned}\Gamma &= \frac{L^2l_\perp^2E_Ra^3}{2\pi}\sum_{\mathbf{n}_a,\mathbf{n}_b}\int dk\Gamma_k^{\mathbf{n}_a,\mathbf{n}_b}\delta(\epsilon_f-\epsilon_i)\\ &= \frac{L^2l_\perp^2E_Ra^3}{2\pi}\sum_{\mathbf{n}_a,\mathbf{n}_b}\int d\epsilon_f\frac{dk}{d\epsilon_f}\Gamma_k^{\mathbf{n}_a,\mathbf{n}_b}\delta(\epsilon_f-\epsilon_i)\end{aligned} \tag{6.30}$$

This is Eq.(6.9).

2D Square Lattice

For the case of the 2D square lattice, the scattering rate in Eq.(6.7) can be written down as

$$\frac{dN}{dt} = \frac{2\pi}{\hbar}\frac{g^2}{4}N^2\frac{L_yL_z}{(2\pi)^2}\sum_{n_a,n_b}\int d^2\mathbf{k}\Gamma_{\mathbf{k}}^{n_a,n_b}\delta(\epsilon_f-\epsilon_i) \tag{6.31}$$

where

$$\Gamma_{\mathbf{k}}^{n_a,n_b} = \left|\frac{I^{n_a,n_b}\langle\psi_f|\int d^2\mathbf{k}\Psi^\dagger_{\mathbf{k_0}-\mathbf{k}}\Psi^\dagger_{\mathbf{k_0}+\mathbf{k}}\Psi_{\mathbf{k_0}}\Psi_{\mathbf{k_0}}|\psi_i\rangle}{L_yL_zl_\perp}\right|^2$$

and

$$I^{n_a,n_b} = \int dx\phi^{(n_a)}(x)\phi^{(n_b)}(x)\phi^{(0)}(x)\phi^{(0)}(x) \tag{6.32}$$

with $l_\perp = \sqrt{\hbar/(m\Omega)}$ just as in the case of the 1D shaken lattice. An important consequence of the form of 6.32 is that I^{n_a,n_b} is 0 unless n_a and n_b have the same priority. Eqn.(6.31) simplifies to give :

$$\frac{dN}{dt} = \frac{2\pi}{\hbar}\frac{g^2}{4}\frac{N^2}{L_yL_zl_\perp}\frac{1}{E_Ra^3}\Gamma \tag{6.33}$$

with

$$\Gamma = \frac{L_y^2L_z^2l_\perp E_Ra^3}{(2\pi)^2}\sum_{n_a,n_b}\int d^2\mathbf{k}\Gamma_{\mathbf{k}}^{n_a,n_b}\delta(\epsilon_f-\epsilon_i)$$

This is Eq.(6.17).

BIBLIOGRAPHY

[1] C. V. Parker, L-C. Ha and C. Chin, Nature Phys. **9**,769 (2013).

[2] L-C. Ha, L. W. Clark, C. V. Parker, B. M. Anderson and C. Chin, Phys. Rev. Lett. **114**, 055301 (2015).

[3] D. Abanin, W. De Roeck, F. Huveneers, Phys. Rev. Lett. **95**, 014112 (2017)

[4] L. D'Alessio and M. Rigol, Phys. Rev. X **4**, 041048 (2014).

[5] D. Vorberg, W. Wustmann, R. Ketzmerick and A. Eckardt, Phys. Rev. Lett. **111**, 240405 (2013).

[6] K. I. Seetharam, C.-E Bardyn, N. H. Lindner, M. S. Rudner, and G. Refael, Phys. Rev. X **5**, 041050 (2015).

[7] J. Knebel, M F. Weber, T. Krüger, and E. Frey Nature Commun. **6**, 6977 (2015).

[8] M. Genske and A. Rosch, Phys. Rev. A **92**, 062108 (2015).

[9] T. Bilitewski and N. R. Cooper, Phys. Rev. A **91**, 033601 (2015).

[10] T. Bilitewski and N. R. Cooper, Phys. Rev. A **91**, 063611 (2015).

[11] C. E. Creffield, Phys. Rev. A **79**, 063612 (2009).

[12] M. Bukov, S. Gopalakrishnan, M. Knap, and E. Demler, Phys. Rev. Lett. **115**, 205301 (2015)

[13] R. Jáuregui, N. Poli, G. Roati, and G. Modugno, Phys. Rev. A **64**, 033403 (2001).

[14] S. Balik, A.L. Win, and M.D. Havey, Phys. Rev. A **80**, 023404 (2009)

CHAPTER 7

CONCLUSION

In this thesis, I have explored a variety of aspects of quantum simulation using Bose-Einstein condensates in optical lattices. This thesis can be divided into two broad themes:

Realization of novel quantum states in cold atom systems : I have explored this theme in chapter 3. In this chapter, motivated by the observation of an exotic "twisted superfluid phase" in Prof. Klaus Sengstock's group (Soltan-Panahi *et al.*, Nat. Phys. 8, 71 (2012)), I have studied the stability of a Bose-Einstein condensate towards forming a twisted superfluid within the framework of mean field theory. I found that the twisted superfluid state is absent in mean field theory thus pointing to either beyond mean-field correlations or interaction effects during time of flight.

My results are presented in :

Sayan Choudhury and Erich J Mueller, Phys. Rev. A **87**, 033621 (2013).

Stability of driven quantum systems : Chapters 4,5 and 6 are devoted to this theme. In these chapters, I have explored the stability of a periodically driven (Floquet) Bose-Einstein condensate to interactions. My work was primarily motivated by observations in Prof. Cheng Chin's group [Parker, Ha, and Chin, Nat. Phys. 9, 769 (2013)]. I found that a Floquet BEC loaded in a low dimensional optical lattice is generically unstable in the absence of transverse confinement. However, by suitably adjusting the transverse confinement, the BEC can be stabilized.

My results are presented in:

1. Sayan Choudhury and Erich J. Mueller, Phys. Rev. A **92**, 063639 (2015).
2. Sayan Choudhury and Erich J. Mueller, Phys. Rev. A **91**, 023624 (2015).
3. Sayan Choudhury and Erich J. Mueller, Phys. Rev. A **90**, 013621 (2014).

APPENDIX A

FLOQUET THEORY

In this appendix, I give a more detailed derivation of the effective Hamiltonian of a periodically driven system. I set $\hbar = 1$ for my analysis. The starting point of my analysis is the Schrödinger equation for a periodically driven system:

$$i\frac{\partial}{\partial t}|\psi(t)\rangle = H(t)|\psi(t)\rangle, \tag{A.1}$$

where $H(t+T) = H(t)$.

This equation was first solved by Gaston Floquet and he found that the solutions to this equation had the form:

$$|\psi_\alpha(x,t)\rangle = \exp(-i\epsilon_\alpha t)|\phi_\alpha(x,t)\rangle \tag{A.2}$$

where $|\phi_\alpha(x,t+T)\rangle = |\phi_\alpha(x,t)\rangle$. In the context of Floquet systems, ϵ_α is called the quasi-energy and the quantum states described by $|\psi_\alpha(x,t)\rangle$ are known as Floquet states. Floquet states satisfy the Schrödinger equation:

$$\mathcal{H}|\phi_\alpha(x,t)\rangle = \epsilon_\alpha|\phi_\alpha(x,t)\rangle, \tag{A.3}$$

where $\mathcal{H} = (H(t) - i\frac{\partial}{\partial t})$. Fourier transforming both sides of eq.(A.3) leads to a matrix equation whose eigenvalues are ϵ_α. An important property of $\mathcal{H}$ that if $|\phi_\alpha(x,t)\rangle$ is an eigenstate of $\mathcal{H}$ with eigenvalue ϵ_α, then $|\phi_\alpha(x,t)\rangle \exp(-in\Omega t)$ is also an eigenstate with the eigenvalue $\epsilon_\alpha + n\Omega$, where $\Omega = \frac{2\pi}{T}$. This means that the quasi-energies of a Floquet system is unbounded.

To compute ϵ_α, I use the observation that over the course of one drive period, a Floquet state evolves as

$$|\psi_\alpha(x,T)\rangle = \exp(-i\epsilon_\alpha T)|\phi_\alpha(x,T)\rangle = \exp(-i\epsilon_\alpha T)|\phi_\alpha(x,0)\rangle = U(0,T)|\phi_\alpha(x,0)\rangle \tag{A.4}$$

Thus, the quasi-energies can be obtained as eigenvalues of the operator $\log(U(0,T))$. Moreover, I can now define an effective Hamiltonian, H_{eff} that captures the stroboscopic dynamics by the following equation:

$$H_{\text{eff}} = \frac{i}{T}\log(U(0,T)) \tag{A.5}$$